

This document has been digitized by the Oil Sands Research and Information Network, University of Alberta with permission of Alberta Environment.

MODELLING TOPOGRAPHIC EFFECTS ON WINDS
IN THE ALBERTA OIL SANDS AREA

by

MAURICE DANARD

MARK GRAY

Atmospheric Dynamics Corporation

for

RESEARCH MANAGEMENT DIVISION AND
POLLUTION CONTROL DIVISION
ALBERTA ENVIRONMENT

AOSERP Report 126

March 1982

TABLE OF CONTENTS

	Page
LIST OF TABLES	viii
LIST OF FIGURES	ix
ABSTRACT	xiii
ACKNOWLEDGEMENTS	xiv
1. INTRODUCTION	1
2. THE STONEY MOUNTAIN MODEL	6
2.1 Description of the Model	6
2.2 Verification of Results	11
3. THE MILDRED LAKE MODEL	36
3.1 Description of the Model	36
3.2 Preparation of Input Data	37
3.3 Verification of Results	61
4. MODEL SENSITIVITY AND APPLICATION TO OTHER AREAS	74
4.1 General Guidelines for New Applications	75
4.2 Sensitivity Tests	75
5. CONCLUSIONS AND RECOMMENDATIONS	81
6. REFERENCES CITED	82
7. LIST OF AOSERP RESEARCH REPORTS	83

LIST OF TABLES

	Page
1. Cases to which the Stoney Mountain model was Applied.....	13
2. Reported and Stoney Mountain Model Computed Winds at Fort McMurray	34
3. Reported and Stoney Mountain Model Computed Winds at Stoney Mountain	35
4. Median of the Absolute Value of the Vector, Speed and Angle Differences between Stoney Mountain Model Computed and Reported Winds	35
5. Cases to which the Mildred Lake Model was Applied	39
6. Reported and Mildred Lake Model Computed Winds at Thickwood Hills	68
7. Reported and Mildred Lake Model Computed Winds at Mildred Lake	69
8. Reported and Mildred Lake Model Computed Winds at Muskeg Mountain	70
9. Reported and Mildred Lake Model Computed Winds at Bitumount	71
10. Reported and Mildred Lake Model Computed Winds at Ells	72
11. Reported and Mildred Lake Model Computed Winds at Fort McMurray	73
12. Median of the Absolute Value of the Vector, Speed, and Angle Differences between Mildred Lake Model Computed and Reported Winds for All Stations	73
13. Sensitivity of Wind Speed to Changes in Input Data, Computed at Fort McMurray by the Stoney Mountain Model	77
14. Sensitivity of Wind Speed to Changes in Input Data, Computed at Stoney Mountain by the Stoney Mountain Model ..	78
15. Sensitivity of Wind Angle(^o) to Changes in Input Data, Computed at Fort McMurray by the Stoney Mountain Model	79
16. Sensitivity of Wind Angle(^o) to Changes in Input Data, Computed at Stoney Mountain by the Stoney Mountain Model ..	80

LIST OF FIGURES

	Page
1. Map of the AOSERP Study Area	2
2. Area for which Topographic Effects on Winds are Computed by the Stoney Mountain Model Showing Smoothed Terrain Heights in hundreds of m	4
3. Area for which Topographic Effects on Winds are Computed by the Mildred Lake Model	5
4. Sea-level Pressure (mb) for 1200 GMT 17 October 77	14
5. Sea-level Pressure (mb) for 1800 GMT 17 October 77	15
6. Sea-level Pressure (mb) for 1200 GMT 23 October 77	16
7. Sea-level Pressure (mb) for 1800 GMT 23 October 77	17
8. Sea-level Pressure (mb) for 1200 GMT 8 February 78	18
9. Sea-level Pressure (mb) for 0000 GMT 9 February 78	19
10. Sea-level Pressure (mb) for 0000 GMT 11 May 78	20
11. Sea-level Pressure (mb) for 1200 GMT 23 July 78	21
12. Sea-level Pressure (mb) for 0000 GMT 26 July 78	22
13. Sea-level Pressure (mb) for 0000 GMT 26 August 78	23
14. Winds Computed by the Stoney Mountain Model for Case 1 1400 GMT 17 October 77	24
15. Winds Computed by the Stoney Mountain Model for Case 2 1809 GMT 17 October 77	25
16. Winds Computed by the Stoney Mountain Model for Case 3 1411 GMT 23 October 77	26
17. Winds Computed by the Stoney mountain Model for Case 4 0000 GMT 24 October 77	27
18. Winds Computed by the Stoney Mountain Model fo Case 5 1200 GMT 8 February 78	28
19. Winds Computed by the Stoney Mountain Model for Case 6 0000 GMT 9 February 78	29

LIST OF FIGURES (CONTINUED)

	Page
20. Winds Computed by the Stoney Mountain Model for Case 7 0000 GMT 11 May 78	30
21. Winds Computed by the Stoney Mountain Model for Case 8 1200 GMT 25 July 78	31
22. Winds Computed by the Stoney Mountain Model for Case 9 0000 GMT 26 July 78	32
23. Winds Computed by the Stoney Mountain Model for Case 10 0000 GMT 26 August 78	33
24. Sea-level Pressure (mb) for 1200 GMT 27 January 77	40
25. Sea-level Pressure (mb) for 1800 GMT 23 March 77	41
26. Sea-level Pressure (mb) for 1200 GMT 12 July 77	42
27. Temperature Profile at Mildred Lake for 1550 GMT 27 January 77	43
28. Temperature Profile at Mildred Lake for 2100 GMT 23 March 77	44
29. Temperature Profile at Mildred Lake for 1435 GMT 12 July 77	45
30. Temperature Profile at Mildred Lake for 1400 GMT 17 October 77	46
31. Temperature Profile at Mildred Lake for 1809 GMT 17 October 77	47
32. Temperature Profile at Mildred Lake for 1411 GMT 23 October 77	48
33. Wind Hodograph at Mildred Lake for 1550 GMT 27 January 77	49
34. Wind Hodograph at Mildred Lake for 2100 GMT 23 March 77	50
35. Wind Hodograph at Mildred Lake for 1435 GMT 12 July 77	51

LIST OF FIGURES (CONCLUDED)

	Page
36. Wind Hodograph at Mildred Lake for 1400 GMT 17 October 77	52
37. Wind Hodograph at Mildred Lake for 1809 GMT 17 October 77	53
38. Wind Hodograph at Mildred Lake for 1411 GMT 23 October 77	54
39. Profile of Wind Components at Mildred Lake for 1550 GMT 27 January 77	55
40. Profile of Wind Components at Mildred Lake for 2100 GMT 23 March 77	56
41. Profile of Wind Components at Mildred Lake for 1435 GMT 12 July 77	57
42. Profile of Wind Components at Mildred Lake for 1400 GMT 17 October 77	58
43. Profile of Wind Components at Mildred Lake for 1809 GMT 17 October 77	59
44. Profile of Wind Components at Mildred Lake for 1411 GMT 23 October 77	60
45. Winds Computed by the Mildred Lake Model for 1550 GMT 27 January 77	62
46. Winds Computed by the Mildred Lake Model for 2100 GMT 23 March 77	63
47. Winds Computed by the Mildred Lake Model for 1435 GMT 12 July 77	64
48. Winds Computed by the Mildred Lake Model for 1400 GMT 17 October 77	65
49. Winds Computed by the Mildred Lake Model for 1809 GMT 17 October 77	66
50. Winds Computed by the Mildred Lake Model for 1411 GMT 23 October 77	67

ABSTRACT

Two versions of the mesoscale, one-level, primitive equations wind model of Danard (1977) have been adapted to northeastern Alberta. The model starts from a surface wind obtained from a balance between large-scale pressure gradient, Coriolis, and frictional forces. The surface temperatures and pressures are changed by adiabatic flow over varying terrain and non-adiabatic heating. The changes in horizontal pressure gradient force then modify the surface winds to account for small-scale topographic effects. This is referred to as dynamical adjustment.

In one version of the model, the Stoney Mountain model, geostrophic winds are obtained from Atmospheric Environment Service (AES) sea-level and 850 mb charts. In the other application, the Mildred Lake model, the thermal and momentum boundary layers are estimated directly from high-resolution vertical profiles of temperatures and winds provided by minisondes. Geostrophic winds and isobaric temperature gradients are obtained from observed minisonde winds above the momentum boundary layer.

The Stoney Mountain model is applied to ten cases and the Mildred Lake version to six. The cases were chosen because good data were available and because they provided variety in wind direction, season, and synoptic conditions. In the Stoney Mountain model, 50% of the time, the difference between reported and computed speeds is less than 2.8 km/h in magnitude. The fiftieth percentile for angle difference is only 9° . For the Mildred Lake version, fiftieth percentiles for the magnitude of the speed and angle differences are 2.7 km/h and 19° , respectively.

ACKNOWLEDGEMENTS

This research project was funded by the Alberta Oil Sands Environmental Research Program, established to fund, direct, and coordinate environmental research in the Athabasca oil sands area of northeastern Alberta.

The authors wish to thank Goz Lyv for assisting with the computer calculations and Georgina Smith for typing the report.

1. INTRODUCTION

Orographic channeling effects on winds are commonly observed. In a stable atmosphere, upslope motion produces local cooling and surface pressure rise. Conversely, downslope motion results in a fall in pressure. If the wind blows at an angle to a valley, the resulting horizontal pressure gradient force will be directed across the valley from the upslope side to the downslope side. This tends to deflect the wind to blow parallel to the valley. The greater the atmospheric stability, the greater this channeling effect will be.

Wind speeds at night are usually lighter than during the day. This means that although the frictional stress (force per unit area) decreases at night, the frictional force per unit mass (proportional to the vertical stress gradient) must increase. This apparent contradiction may be explained by a reduction in height of the planetary boundary layer.

Land and lake breezes are caused by differential heating over land and water. In the morning, pressure first rises at higher elevations over land due to heating near the surface. The resulting upper-level offshore pressure gradient force transfers mass from land to water, lowering surface pressure over land and raising surface pressure over water. The low-level onshore pressure gradient force then drives the cooler air over water onto land. At night the circulation normally reverses if the land becomes colder than the water. Coriolis deflections contribute to a clockwise wind rotation during the day in the northern hemisphere.

Diurnal variations in winds also occur over sloping terrain even in the absence of a land-water contrast. At night a point on an inclined surface cools, acquiring a lower temperature and higher pressure than at the same elevation in the free atmosphere. The resulting horizontal pressure gradient force drives the air downhill. The reverse process occurs during the day.

This report is concerned with the adaptation of a mesoscale model for surface winds to the oil sands area of northeastern Alberta. The model was created in its original form by Danard (1977).

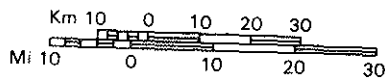
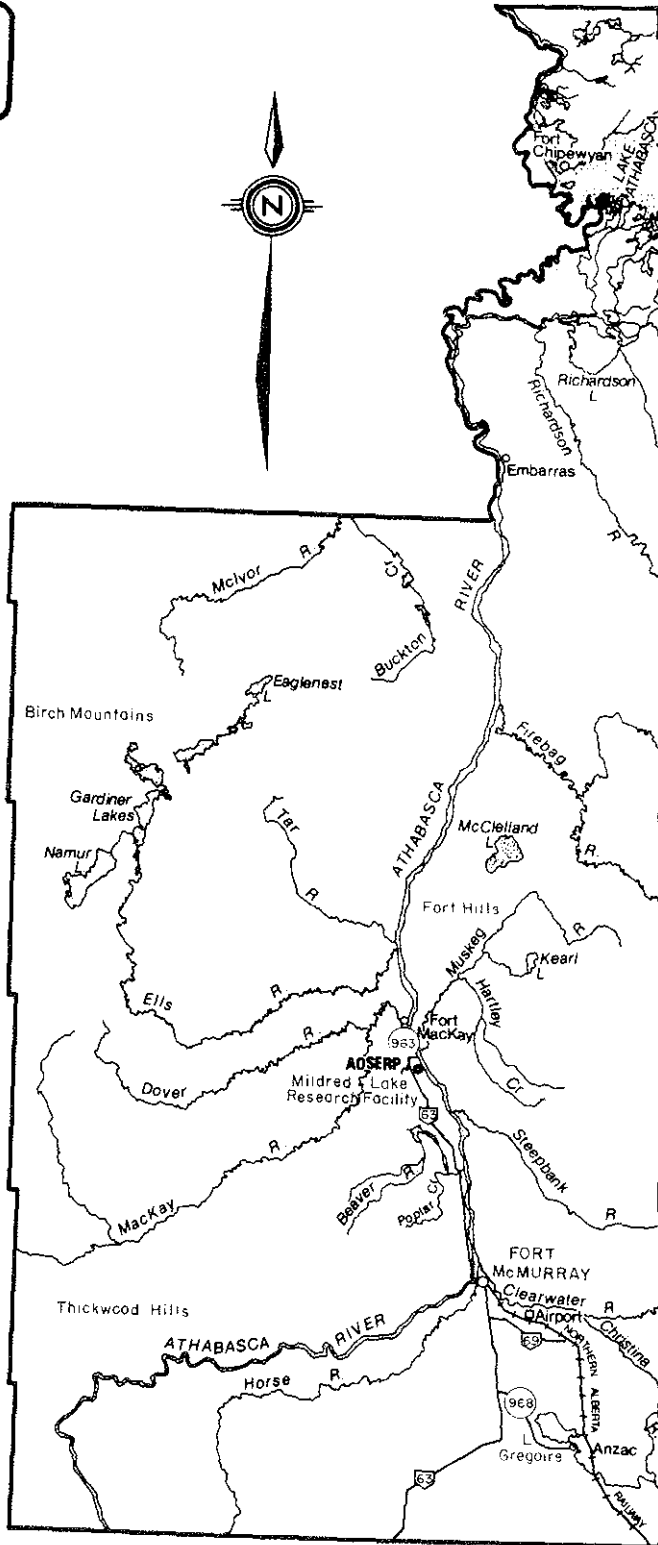


Figure 1. Map of the AOSERP Study Area.

Two versions of the model have been designed. The first uses only data readily available from AES. It is applied to the Stoney Mountain area and will be referred to as the Stoney Mountain model. The second version uses upper air winds and temperatures measured by minisondes at Mildred Lake, and surface winds and temperatures at the AOSERP stations. It will be termed the Mildred Lake model.

The regions to which the two versions of the model are applied are shown in Figures 1 and 2. In both cases the grid size is 2.5 km. The number of points for which terrain heights are needed is 25 x 25 for the Stoney Mountain model and 44 x 44 for the Mildred Lake version. Topographical effects on winds are calculated for 21 x 21 and 40 x 40 points, respectively (the areas shown in the figures).

The Stoney Mountain model has the following advantages:

1. It can be used with forecast data. In general, it is not possible to predict 24 h or more in advance detailed temperature and pressure fields in the lower troposphere. The model needs only the following meteorological data at one point: sea-level and 850-mb geostrophic winds, 850-mb height and temperature, and surface temperature.
2. It can be used in data-sparse areas.
3. It can be used historically (e.g., to study a past air pollution episode in which wind data were inadequate or non-existent).
4. It can be easily adapted to different areas (i.e., it is "portable").
5. It is economical. No special data are needed and computing costs are small.

The Mildred Lake model is less flexible but has the potential for more accurate wind computations. Computing costs are comparable to those for the Stoney Mountain model for similar array sizes.

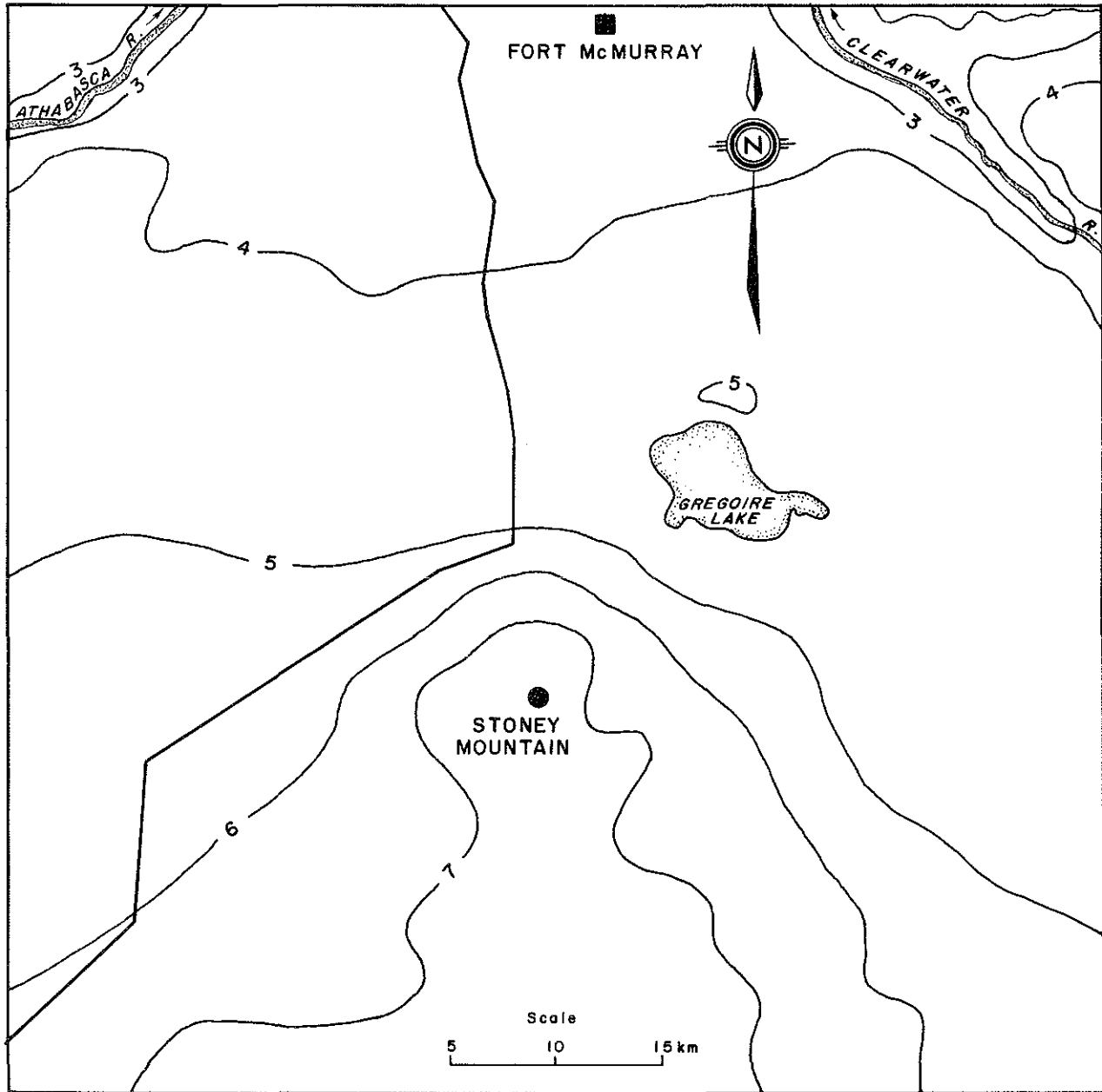


Figure 2. Area for which topographic effects on winds are computed by the Stoney Mountain model showing smoothed terrain heights in hundreds on m.

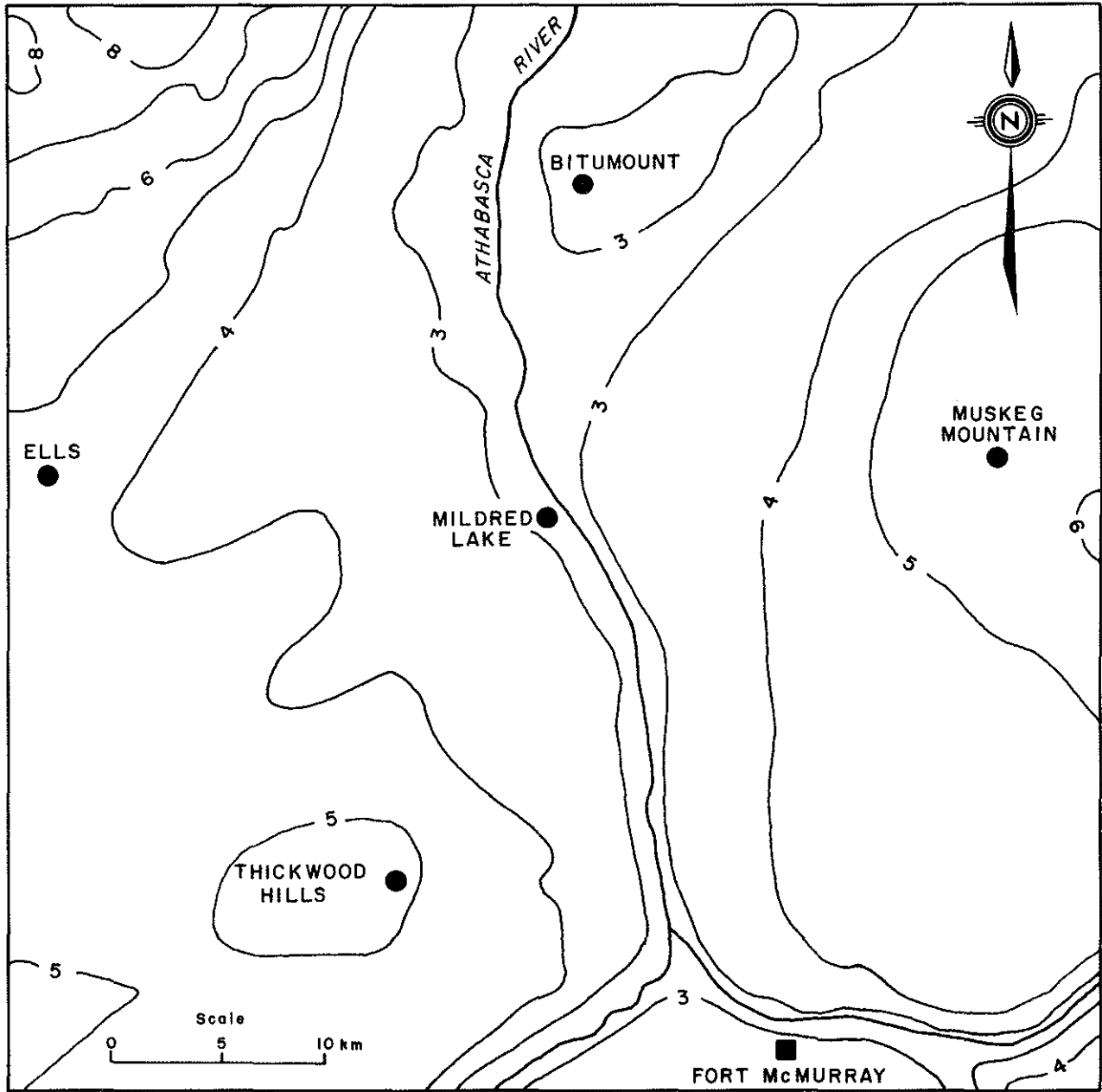


Figure 3. Area for which topographic effects on winds are computed by the Mildred Lake model.

2. THE STONEY MOUNTAIN MODEL

2.1 DESCRIPTION OF THE MODEL

This model is a modified version of the model designed by Danard (1977). Topographical data required for each grid square are elevation and fraction covered with water (or ice). Meteorological input data at the reference station (Fort McMurray) are surface and 850-mb temperatures, and sea-level and 850-mb geostrophic winds (obtained from AES charts).

It is assumed that, at some height H above the surface (assumed to coincide with the thermal boundary layer height), the mesoscale pressure field is unaffected by the underlying surface. If $p(H)$ is assumed constant, it may be shown from the hydrostatic equation that the rate of change of surface pressure p_s with time t is

$$\frac{\partial \ln p_s}{\partial t} = - \frac{g}{R \theta_s T_s} \int_0^H \frac{\partial \theta}{\partial t} dz \quad (1)$$

where g is acceleration of gravity, R is gas constant, θ_s is surface potential temperature, T_s is surface temperature, and z is height above the earth's surface. The first law of thermodynamics applied at the earth's surface may be written

$$\frac{\partial \theta_s}{\partial t} = - \vec{V} \cdot \nabla \theta_s + K_t \nabla^2 \theta_s + Q \quad (2)$$

Here, \vec{V} is the surface wind, ∇ is the horizontal gradient operator on the earth's surface, K_t is the horizontal thermal diffusivity, and Q is the diabatic rate of change of θ_s (to be discussed later). The influence of atmospheric stability on orographic channeling is included in the advection term $-\vec{V} \cdot \nabla \theta_s$ in Equation 2. The diffusion term represents the effects of subgrid scale mixing and also helps to control computational instability. The equation linking $\partial \theta / \partial t$ to $\partial \theta_s / \partial t$ will be discussed later.

The surface or anemometer level wind, which is the variable of greatest interest, is found from the equation of motion

$$\frac{\partial \vec{V}}{\partial t} = -\vec{V} \cdot \nabla \vec{V} - (g\nabla Z_s + RT_s \nabla \ln p_s) - f \vec{k} \times \vec{V} + \vec{F} + K_m \nabla^2 \vec{V} \quad (3)$$

The second term on the right (in parentheses) is the horizontal pressure gradient force at the earth's surface in "sigma" coordinates (Phillips 1957). The next three terms represent, respectively, Coriolis force, surface friction (to be discussed later) and horizontal mixing. The terrain height above sea-level is denoted by Z_s , and K_m is the horizontal momentum diffusivity. In sigma coordinates, the surfaces $\sigma = p/p_s =$ constant are coordinate surfaces. The earth's surface, where the wind, temperature, and pressure are predicted by the model, is the coordinate surface $\sigma = 1$. Sigma coordinates are especially suited to varying terrain, where the use of (x, y, p) or (x, y, z) coordinates would be awkward. In particular, in sigma coordinates, the pressure gradient force is expressed in terms of surface variables. There is no need to reduce pressures to sea-level or any other fixed level.

Equations 1 to 3 are written in finite difference form.

Starting from given initial values, they give new values of θ_s , $\ln p_s$, and \vec{V} . After a number of timesteps, fields of these variables will evolve which represent the modifying influences of topography. As used here, topographical influences include purely orographic effects in addition to influences of exchanges of heat and momentum with the earth's surface. Initial surface winds are computed assuming a balance between pressure gradient, Coriolis forces, and surface frictional forces (second, third, and fourth terms on the right side of Equation 3.)

Initial surface temperatures T_i and pressures are computed as follows. This is the state when, by definition, no mesoscale thermal or pressure gradients exist. The 850-mb temperature gradient is set equal to the value computed from the thermal wind equation and the vertical variation in geostrophic wind between sea-level and 850 mb. The 850-mb height and temperature at any point in the region may then be calculated

using the values at the reference station and the gradients of 850-mb height and temperature. The initial lapse rate γ near the earth's surface is assumed horizontally uniform and is obtained from the daily mean surface temperature \bar{T} at the reference station and the 850-mb temperature there. The surface temperature at any location is computed from the 850-mb height and temperature (which vary spatially) and the lapse rate. The hydrostatic equation is then integrated from the 850-mb level to the surface to give the surface pressure. In the cases studied in this report, \bar{T} is the average of the temperatures 6 h in the future and 6 h ago. Operationally, it would be the mean of the present temperature and the temperature 12 h ago (which is also used by AES to reduce pressures to sea-level).

Let

$$\Delta T = T_o - T_i \quad (4)$$

where T_o is a prescribed final air temperature. Over land, we set

$$\Delta T = T_r - \bar{T}$$

where T_r is the actual surface temperature at the reference station. ΔT is the same for all land points. Since at the reference station, $T_i = \bar{T}$, we have $T_o = T_r$ there. Over water, T_o is the water temperature or the surface temperature which would limit the mixing height (see Equation 7) to 750 m, whichever is higher. Note that $\Delta T > 0$ indicates heating and $\Delta T < 0$ means cooling. The rate of temperature change for use in Equation 2 is

$$Q = \frac{\theta_s}{T_s} \frac{\Delta T}{\tau} \quad (5)$$

where τ is the time interval over which the heating is added. The factor θ_s/T_s converts $\partial T_s/\partial t$ to $\partial \theta_s/\partial t$. For use in equation 1, one sets

$$\frac{\partial \theta}{\partial t} = \frac{\partial \theta_s}{\partial t} \left(\frac{H-z}{H} \right) \quad (6)$$

Thus, the model starts with a surface temperature which, by assumption, corresponds to the state when no mesoscale pressure gradients exist. The model then modifies the temperature during a time τ to a specified final value. This procedure produces pressure gradients which drive thermal circulations. If one were interested only in orographic effects, one would set $T_o = T_i$ or $Q = 0$.

H is the height of the first significant discontinuity in lapse rate. This is the top of the nocturnal inversion or the base of the convection-limiting inversion (see Figures 26 to 31 for examples). By assumption (Equation 1), $\partial p/\partial t = 0$ at this level. From the pressure tendency equation, this implies that the mass divergence above $z = H$ equals the upward mass flux at this level. The latter is largely determined by the divergence of the surface wind.

For $\Delta T > 0$, one computes H from the simple mixing height formula

$$H = \frac{\Delta T}{\gamma_d - \gamma} \quad (7)$$

For $\Delta T \leq 0$, one uses

$$H = 1.2 V_g / \left(\frac{g}{T} \frac{\Delta \theta}{H} \right)^{\frac{1}{2}} \quad (8)$$

where

$$\Delta \theta = \frac{\theta}{T} [-\Delta T + H(\gamma_d - \gamma)] \quad (9)$$

is the increase in θ from 0 to H . The quantity $\Delta \theta/H$ in (8) is a finite difference expression for $\partial \theta/\partial z$. The constant (1.2) in Equation 8 was obtained empirically from observed boundary layer heights given by minisonde data at Mildred Lake (see Section 3.2). This is close to the value of 1.3 that Laikhtman (1961) originally suggested although Hanna (1969) later proposed modifying it to 0.75. Equation 8 implies that the bulk Richardson number is 1.4.

If the assumptions of Ekman theory are accepted as valid (e.g., Haltiner and Martin 1957: 233-236), it may be shown that \vec{F} (needed in Equation 3) is directed at an angle of $3\pi/4$ radians to the right of \vec{V} . According to Deardorff (1972), the component of \vec{F} in the opposite direction to \vec{V} is cCV^2/h , where C is the drag coefficient and h is the momentum boundary layer height. The parameter c is 2.8 for stable and neutral case, and decreases to 1.0 for extreme instability. Here we set $c = 2.8$ for $\Delta T < 0$ and let c decrease linearly to 1.0 as ΔT increases from 0 to 10°C . For $\Delta T \geq 10^\circ\text{C}$, $c = 1.0$. The magnitude of \vec{F} is thus assumed to be

$$F = \frac{\sqrt{2} c C V^2}{h} \quad (10)$$

The value of h is calculated from

$$h = \begin{cases} H & \text{for } \Delta T < 0 \\ H + H_\ell & \text{for } \Delta T \geq 0 \end{cases} \quad (11)$$

where H_ℓ is the solution of Equation 8 for $\Delta T = 0$.

From the balance of forces for the initial surface winds, one obtains the two equations

$$\sqrt{2} F V_g \sin \epsilon = F \quad (12a)$$

$$\sqrt{2} f V_g \cos \epsilon = \sqrt{2} f V + F \quad (12b)$$

where V_g is the geostrophic wind speed, and ϵ is the angle between the surface geostrophic wind and the surface wind. Equation 10 is substituted into Equations 12a and b and the latter are solved iteratively for the initial ϵ and V .

The drag coefficient over land decreases with height (reflecting greater exposure) in accordance with

$$C = 6 \times 10^{-2} - 8.05 \times 10^{-5} Z_s \quad (13)$$

for Z_s in m. Lower and upper bounds for C are 10^{-2} and 3.6×10^{-2} (corresponding to $Z_s = 621$ and 282 m, respectively). Equation 13 was determined empirically to reduce systematic errors in the Mildred Lake model study (see Section 3). If C were constant, speeds at the lower stations would be overestimated compared to the higher stations. Over water, the drag coefficient increases with speed according to

$$C = 0.61 \times 10^{-3} + 4.4 \times 10^{-5} V_g \quad (14)$$

for V_g in m/s. Equation 14 was adapted from Smith (1980), replacing his V by $0.7 V_g$. Over ice, C is assigned the value 2×10^{-3} (e.g., Banke and Smith, 1971). The drag coefficient for each grid square is a weighted average in proportion to the fraction of area covered by the different types of surfaces. The timestep is 40 s. K_m and K_t are both assigned the value of $2 \times 10^4 \text{ m}^2 \cdot \text{s}^{-1}$. In Equation 7, τ is set equal to 8×10^2 s (20 timesteps). The total adjustment time is 1.6×10^3 s (40 timesteps).

2.2 VERIFICATION OF RESULTS

The Stoney Mountain version has been run for 10 cases in 1977 and 1978. The cases were chosen to provide a variety of synoptic conditions and wind directions for different seasons (see Table 1 and Figures 3 to 12). Figures 13 to 22 show computed winds. Sheltering to the lee of Stoney Mountain is particularly noticeable in Figure 22 and to a less extent in Figure 15. Results are summarized in Tables 2 to 4.

Tables 2 and 3 give reported (3 h running averages) and model-computed winds at Fort McMurray and Stoney Mountain. Winds at Stoney Mountain (and other AOSERP stations) are reported to 16 parts of the compass. In results presented here they are converted to degrees and then rounded to the nearest 10 degrees. Most of the time the results agree fairly closely. For Fort McMurray, the largest differences occur in Case 3 for direction and in Case 10 for speed. Differences

are even smaller for Stoney Mountain. For both stations, the average reported and computed speeds (last lines of Tables 2 and 3) agree to the nearest km/h.

Table 4 gives median absolute differences in vector, speed, and angle between computed and reported winds. The median has the simple interpretation that 50% of the absolute values are less than the values given. Thus, 50% of the time the difference in angle is less than 9° in magnitude, which is small. The median speed difference, 2.8 km/h, is a small fraction of the reported mean speed.

Table 1. Cases to which the Stoney Mountain model was applied.

Case	Time	Geostrophic direction
1	1400 GMT 17 Oct 77	W
2	1809 GMT 17 Oct 77	W
3	1411 GMT 23 Oct 77	SW
4	0000 GMT 24 Oct 77	SW
5	1200 GMT 8 Feb 78	SE
6	0000 GMT 9 Feb 78	S
7	0000 GMT 11 May 78	N
8	1200 GMT 25 Jul 78	NW
9	0000 GMT 26 Jul 78	NW
10	0000 GMT 26 Aug 78	SE

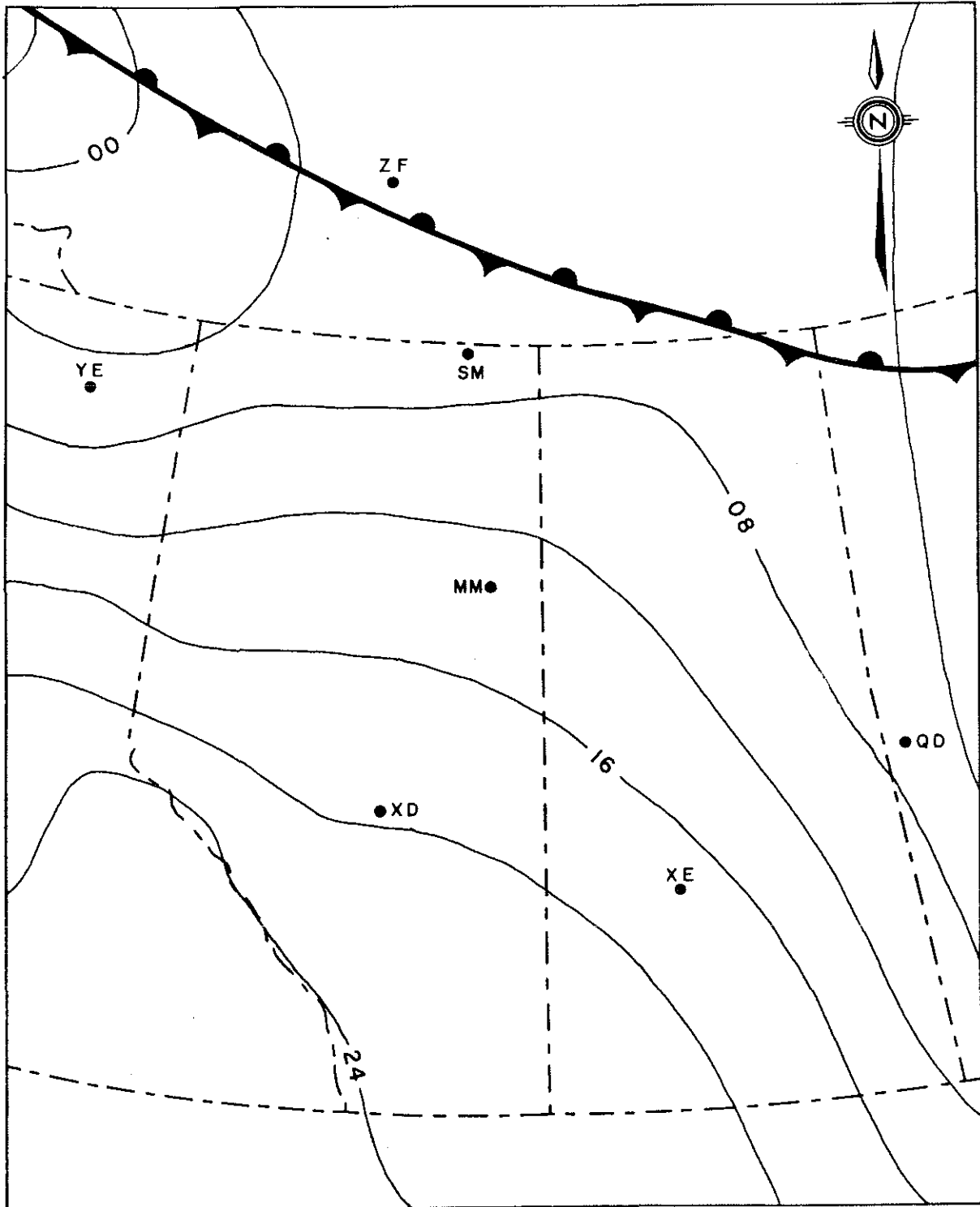


Figure 4. Sea-level pressure (mb) for 1200 GMT 17 October 77.

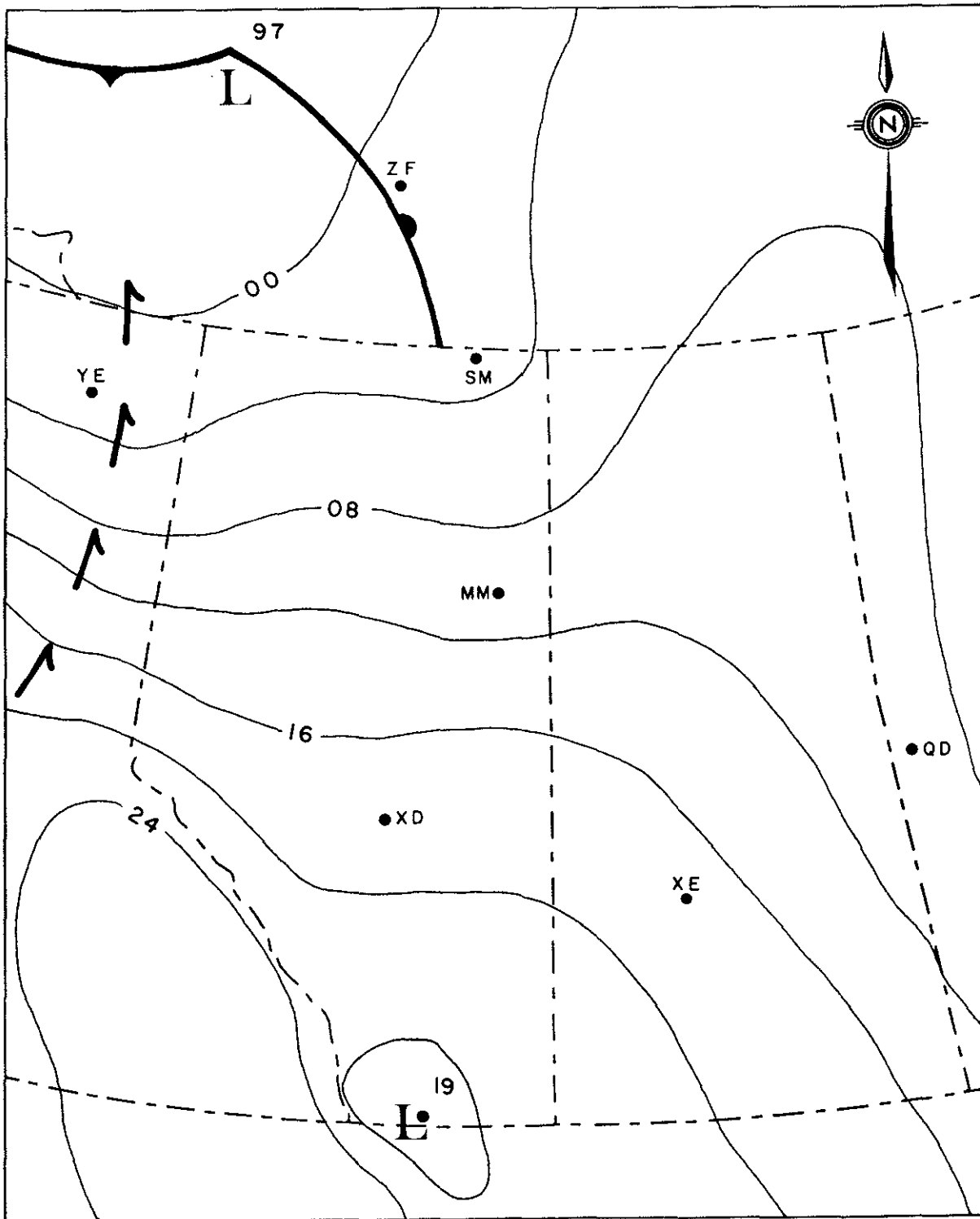


Figure 5. Sea-level pressure (mb) for 1800 GMT 17 October 77.

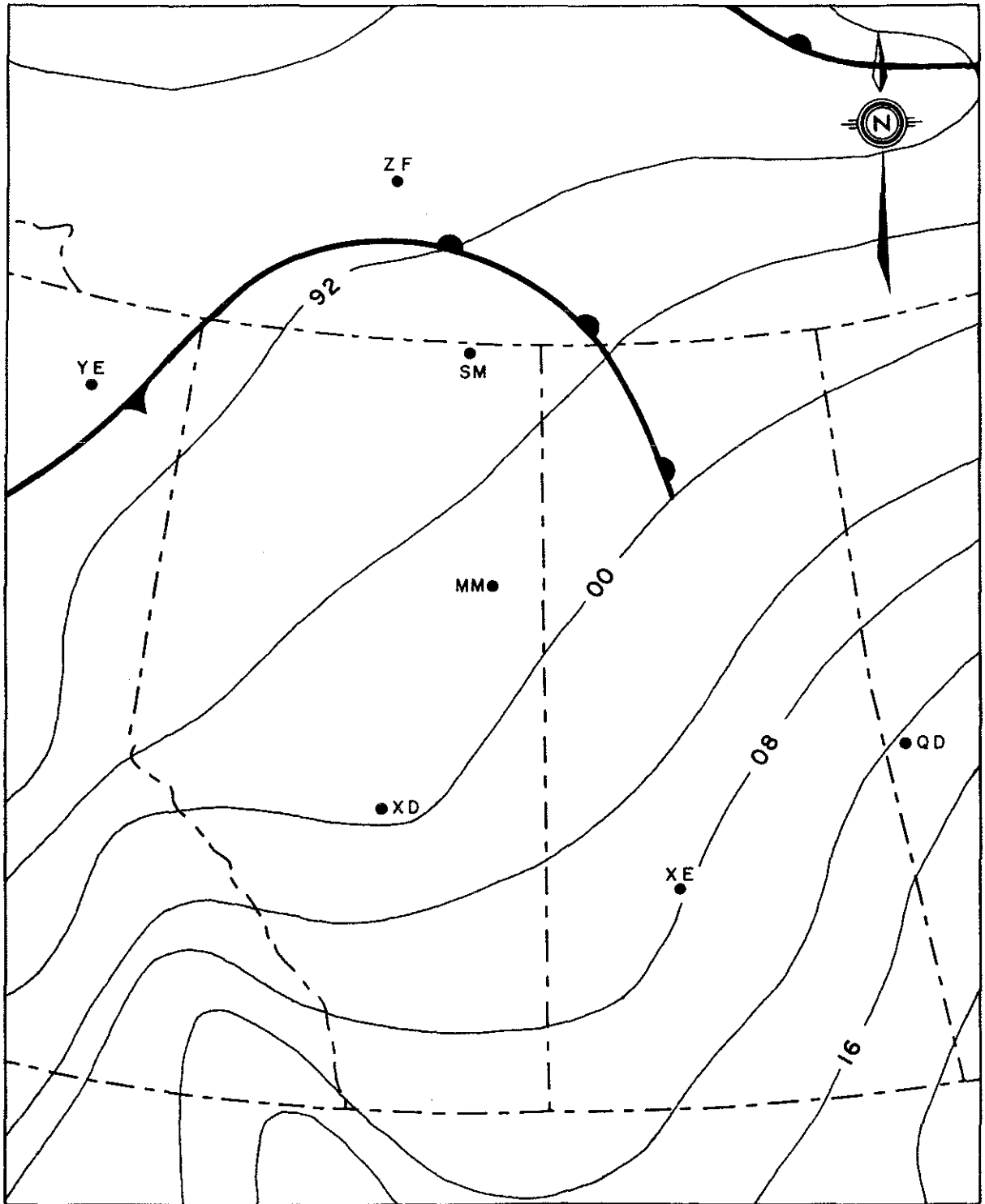


Figure 6. Sea-level pressure (mb) for 1200 GMT 23 October 77.

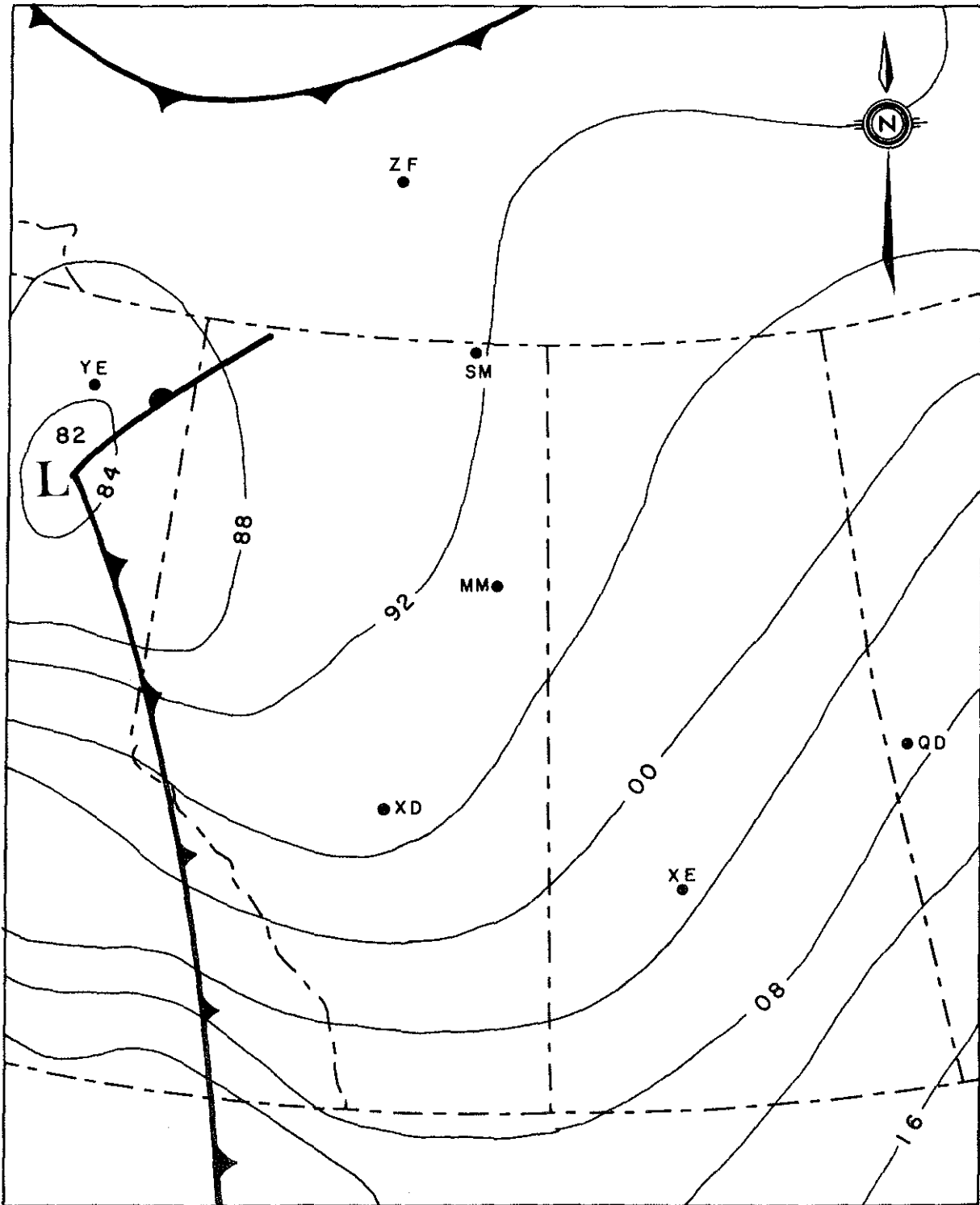


Figure 7. Sea-level pressure (mb) for 1800 GMT 23 October 77.

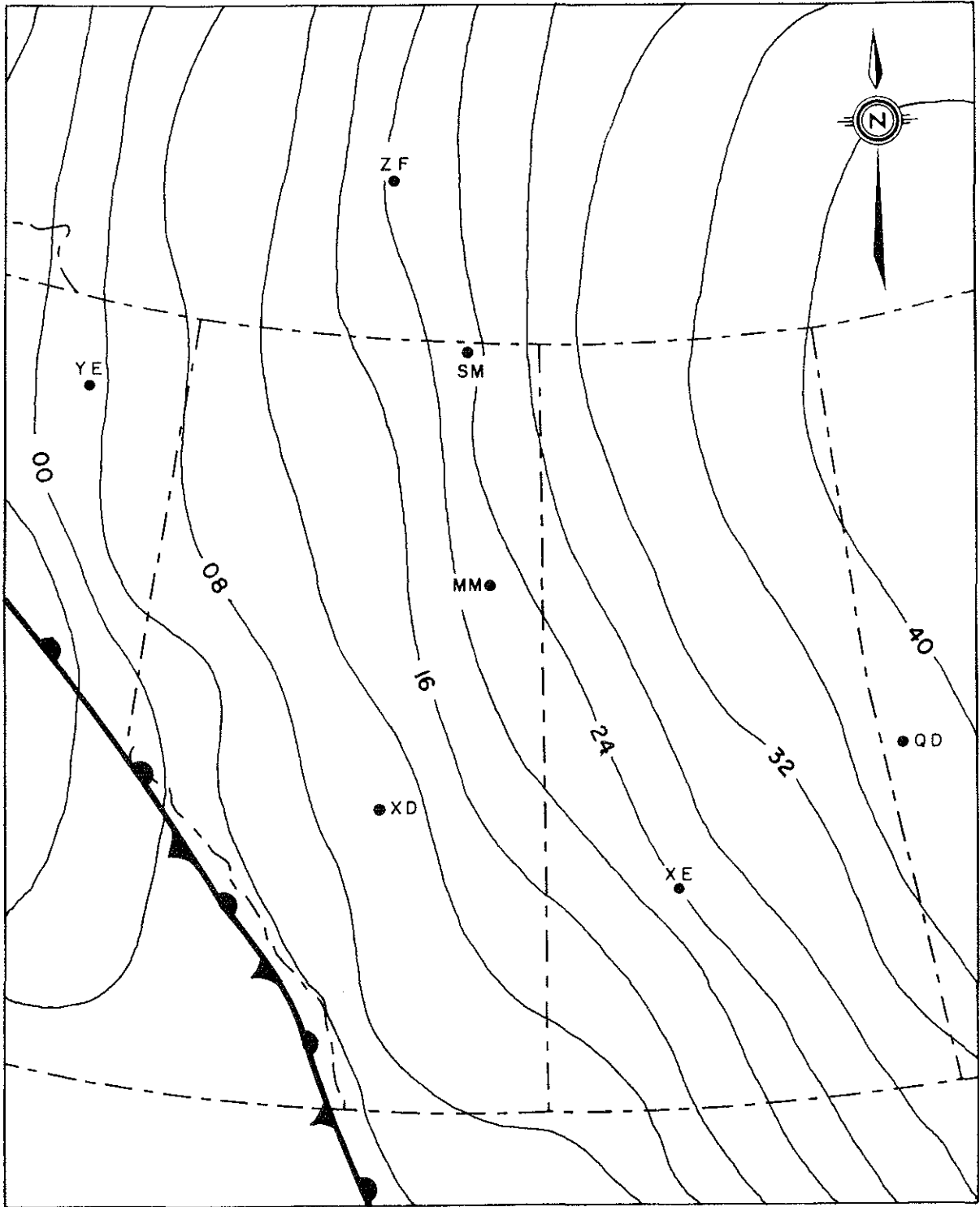


Figure 8. Sea-level pressure (mb) for 1200 GMT 8 February 78.

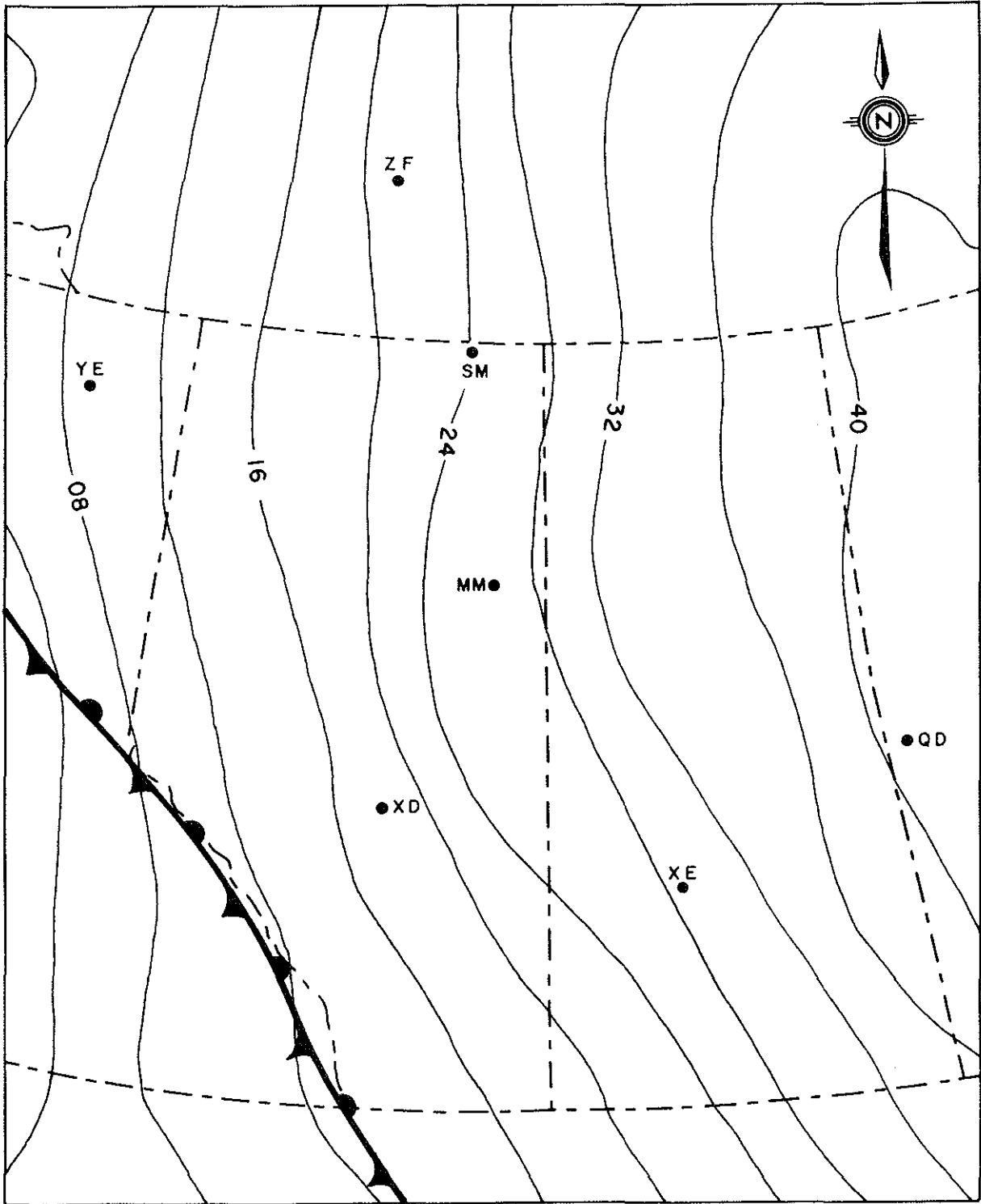


Figure 9. Sea-level pressure (mb) for 0000 GMT 9 February 78.

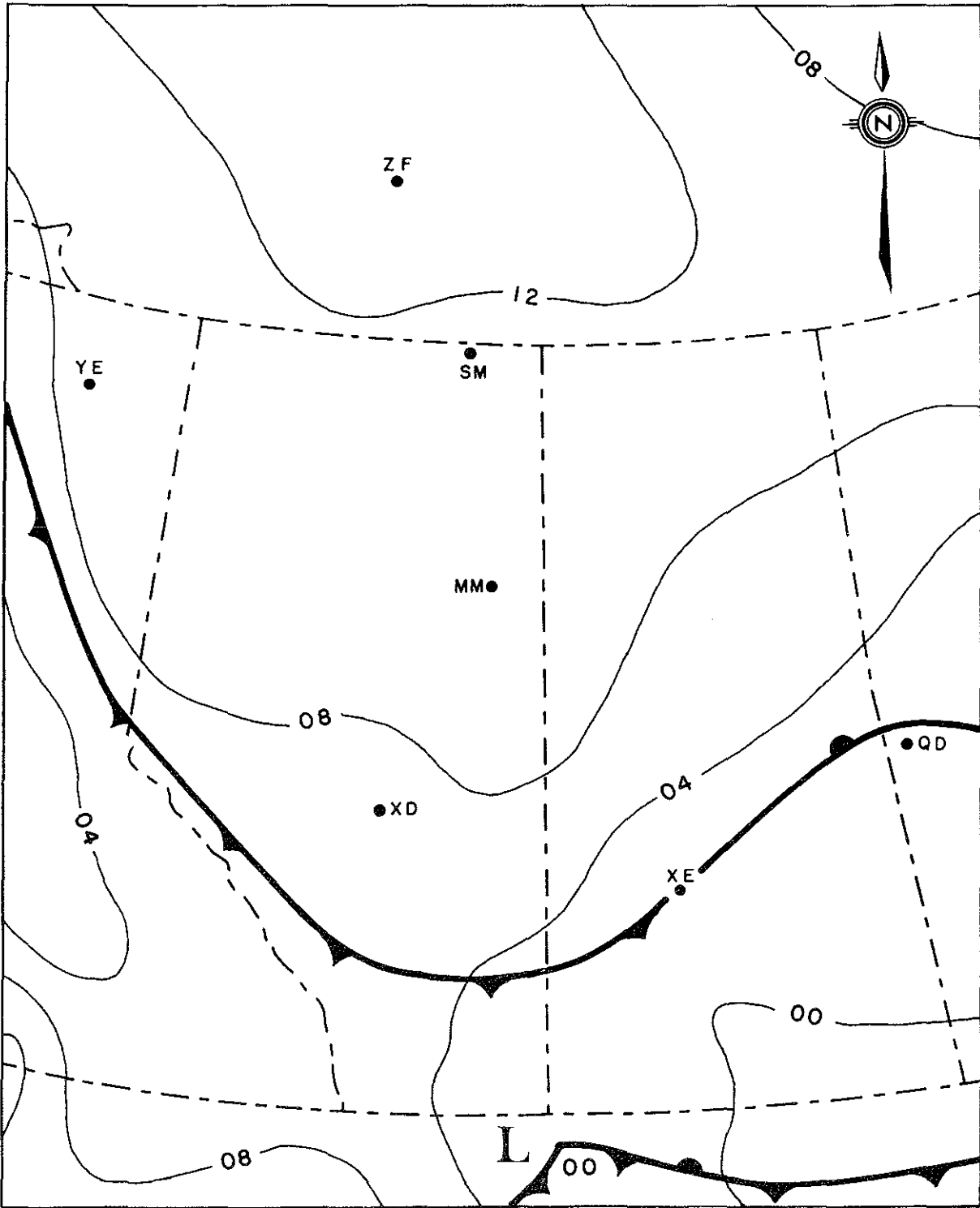


Figure 10. Sea-level pressure (mb) for 0000 GMT 11 May 78.

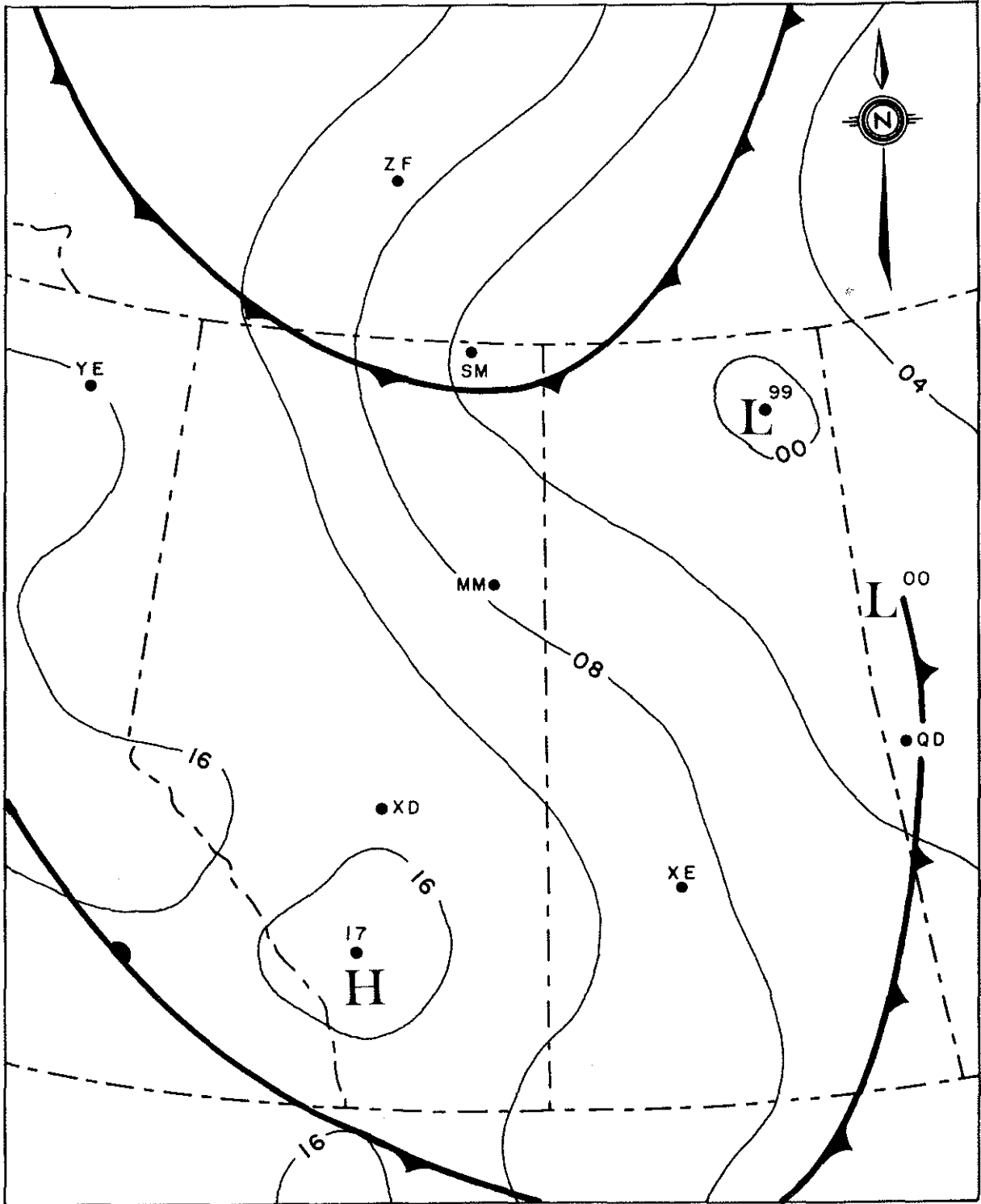


Figure 11. Sea-level pressure (mb) for 1200 GMT 23 July 78.

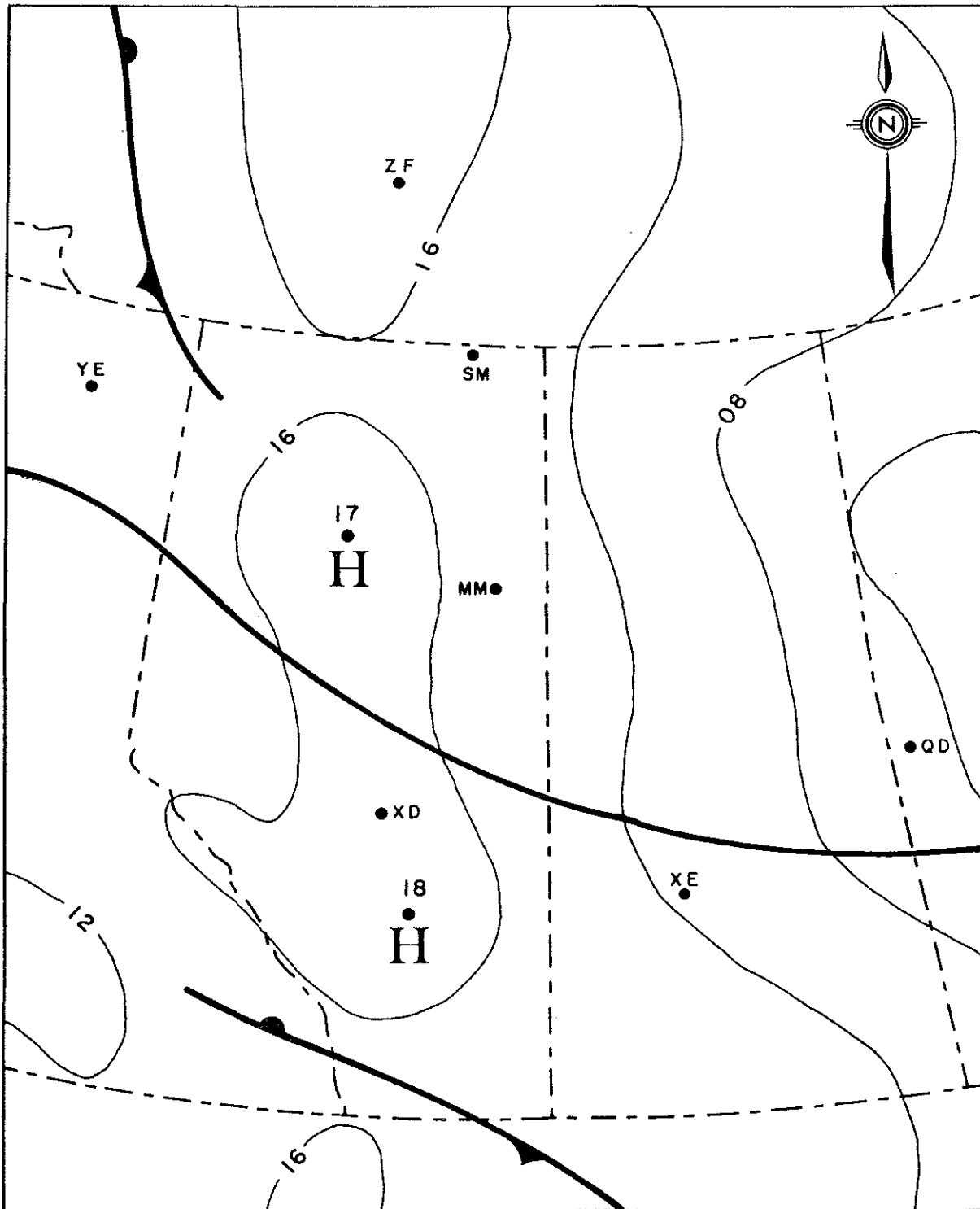


Figure 12. Sea-level pressure (mb) for 0000 GMT 26 July 78.

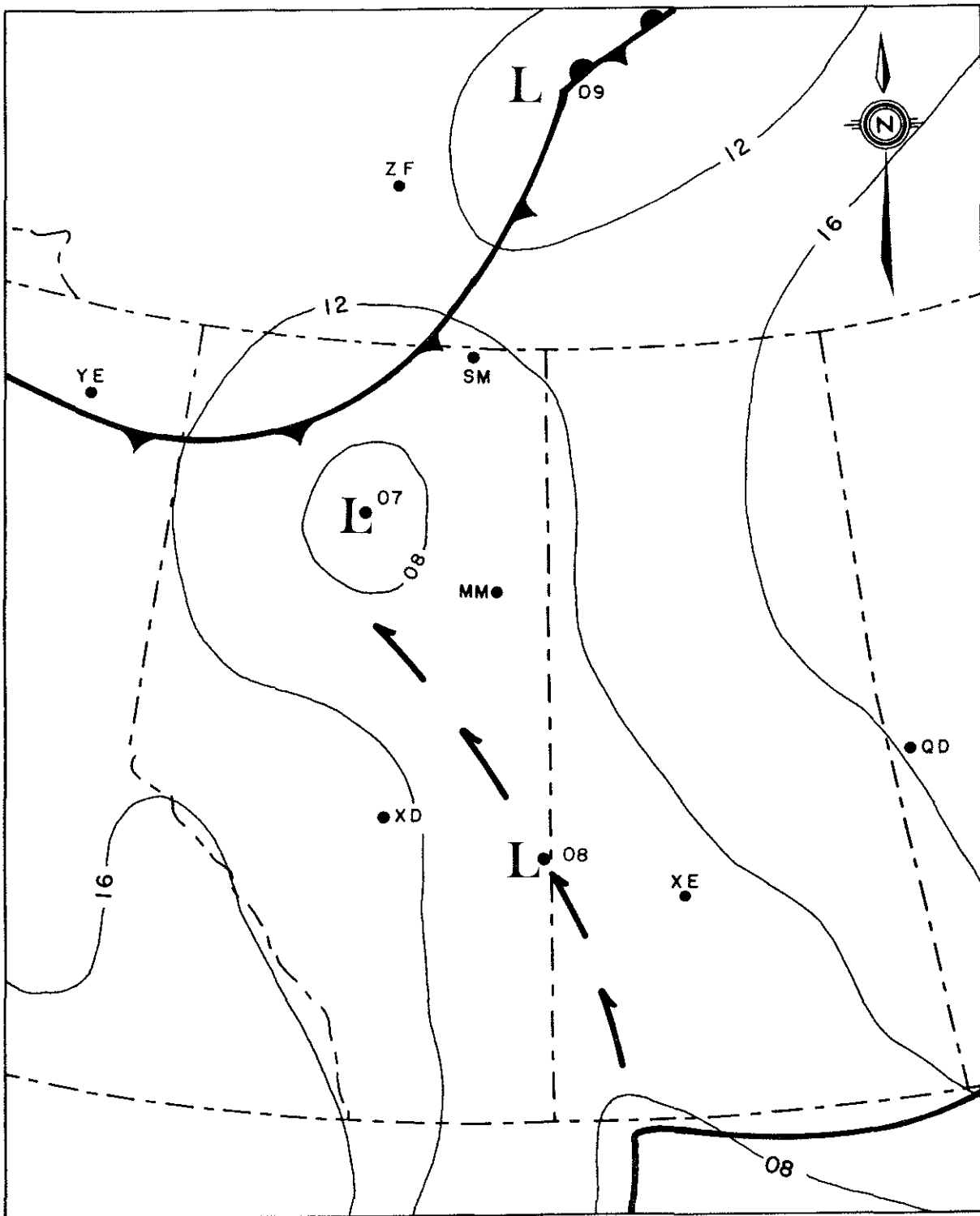


Figure 13. Sea-level pressure (mb) for 0000 GMT 26 August 78.

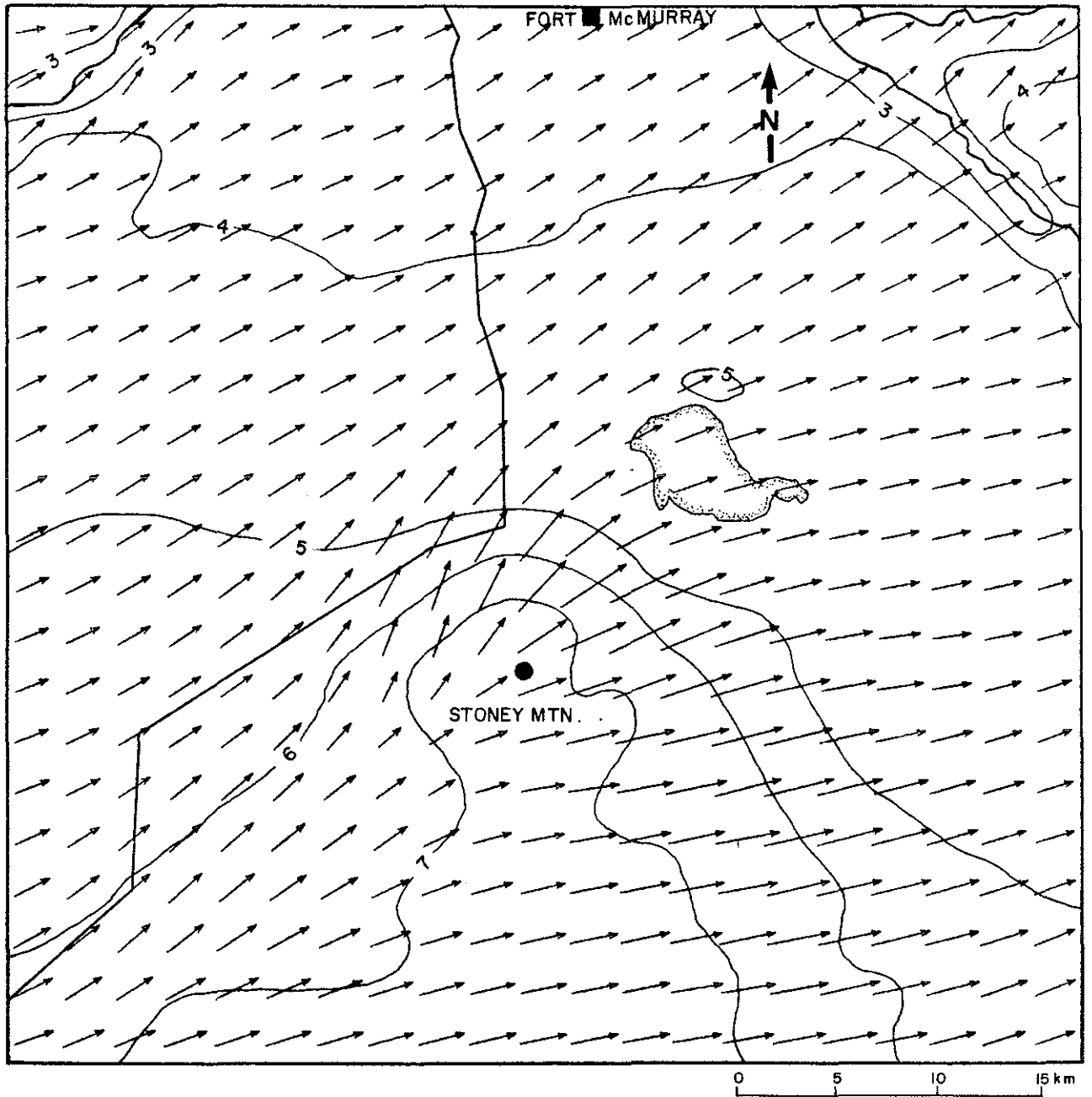


Figure 14. Winds computed by the Stoney Mountain model for Case 1 (1400 GMT 17 October 77). A vector of 1 cm length represents a wind of 20 km/h.

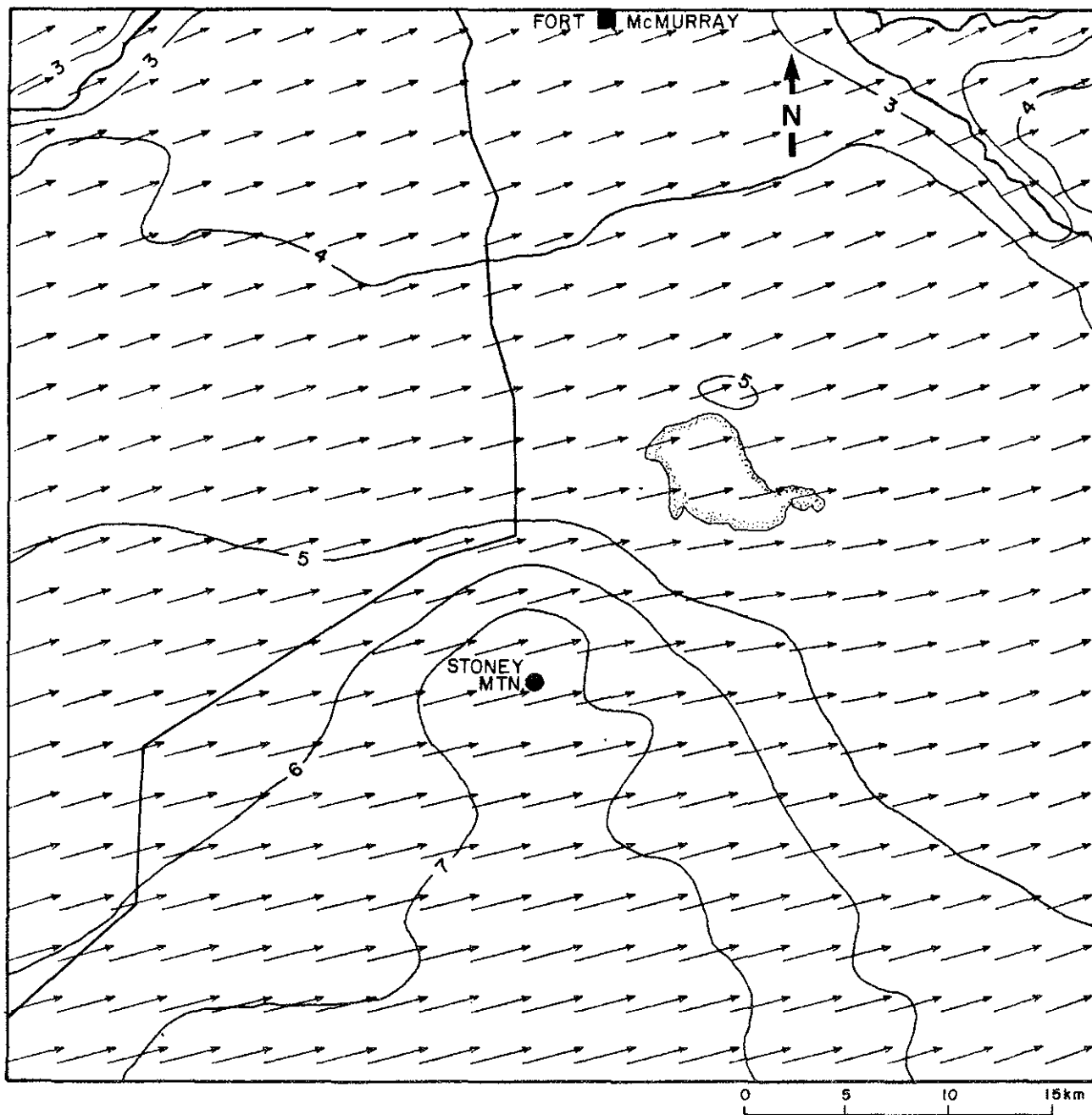


Figure 15. Winds computed by the Stoney Mountain model for Case 2 (1809 GMT 17 October 77). A vector of 1 cm length represents a wind of 20 km/h.

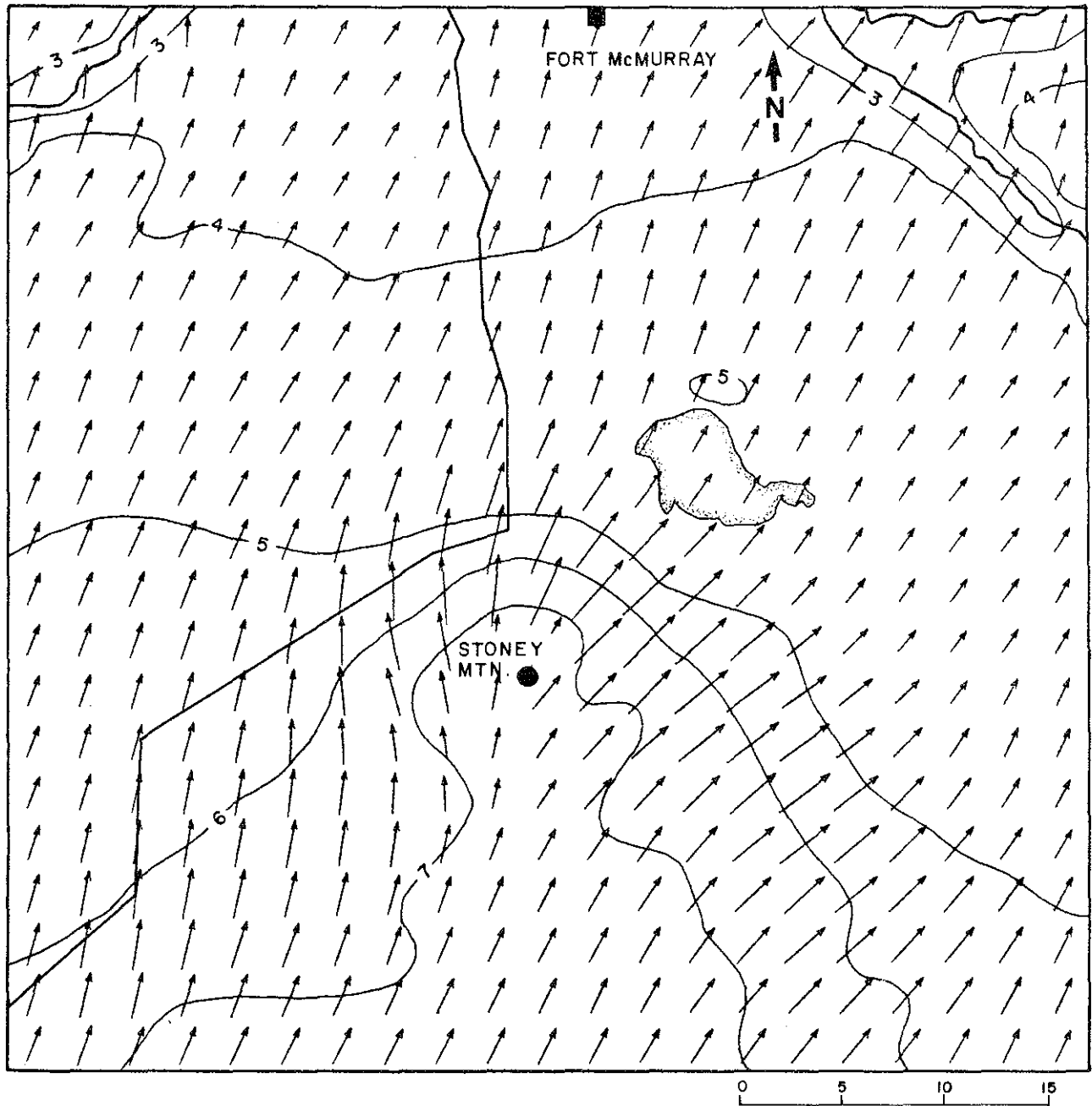


Figure 16. Winds computed by the Stoney Mountain model for Case 3 (1411 GMT 23 October 77). A vector of 1 cm length represents a wind of 20 km/h.

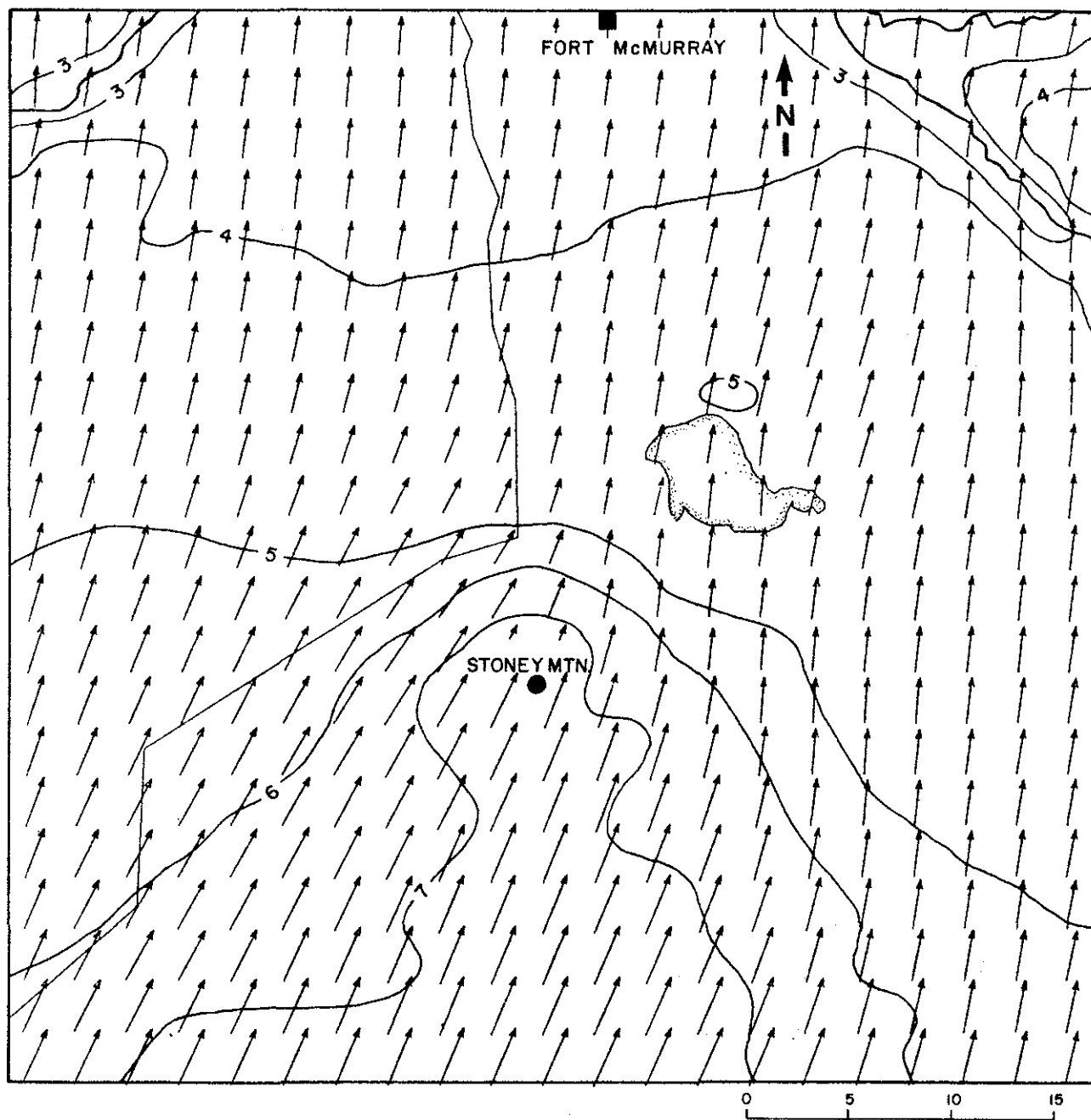


Figure 17. Winds computed by the Stoney Mountain model for Case 4 (0000 GMT 24 October 77). A vector of 1 cm length represents a wind of 25 km/h.

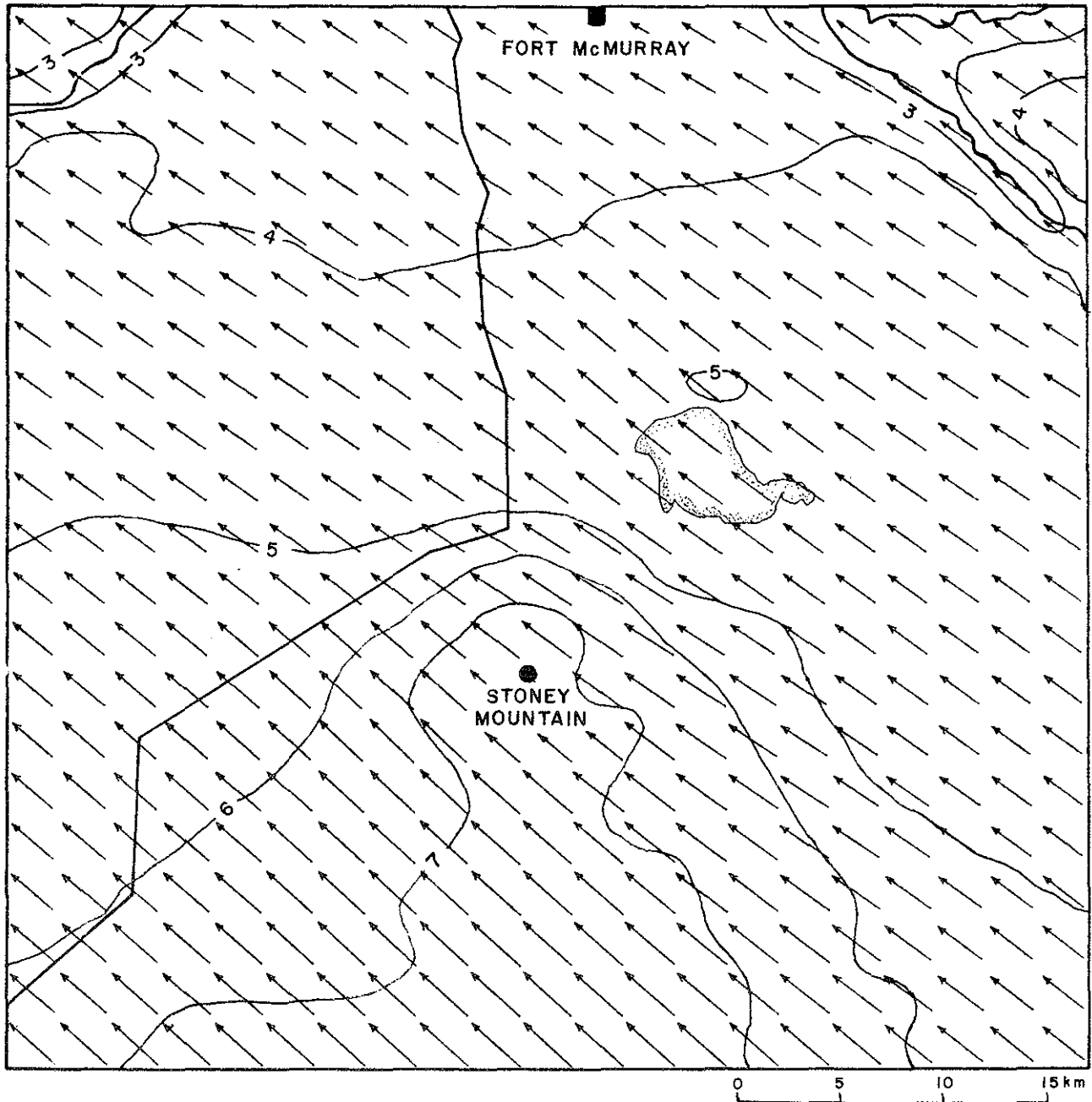


Figure 18. Winds computed by the Stoney Mountain model for Case 5 (1200 GMT 8 February 78). A vector of 1 cm length represents a wind of 35 km/h.

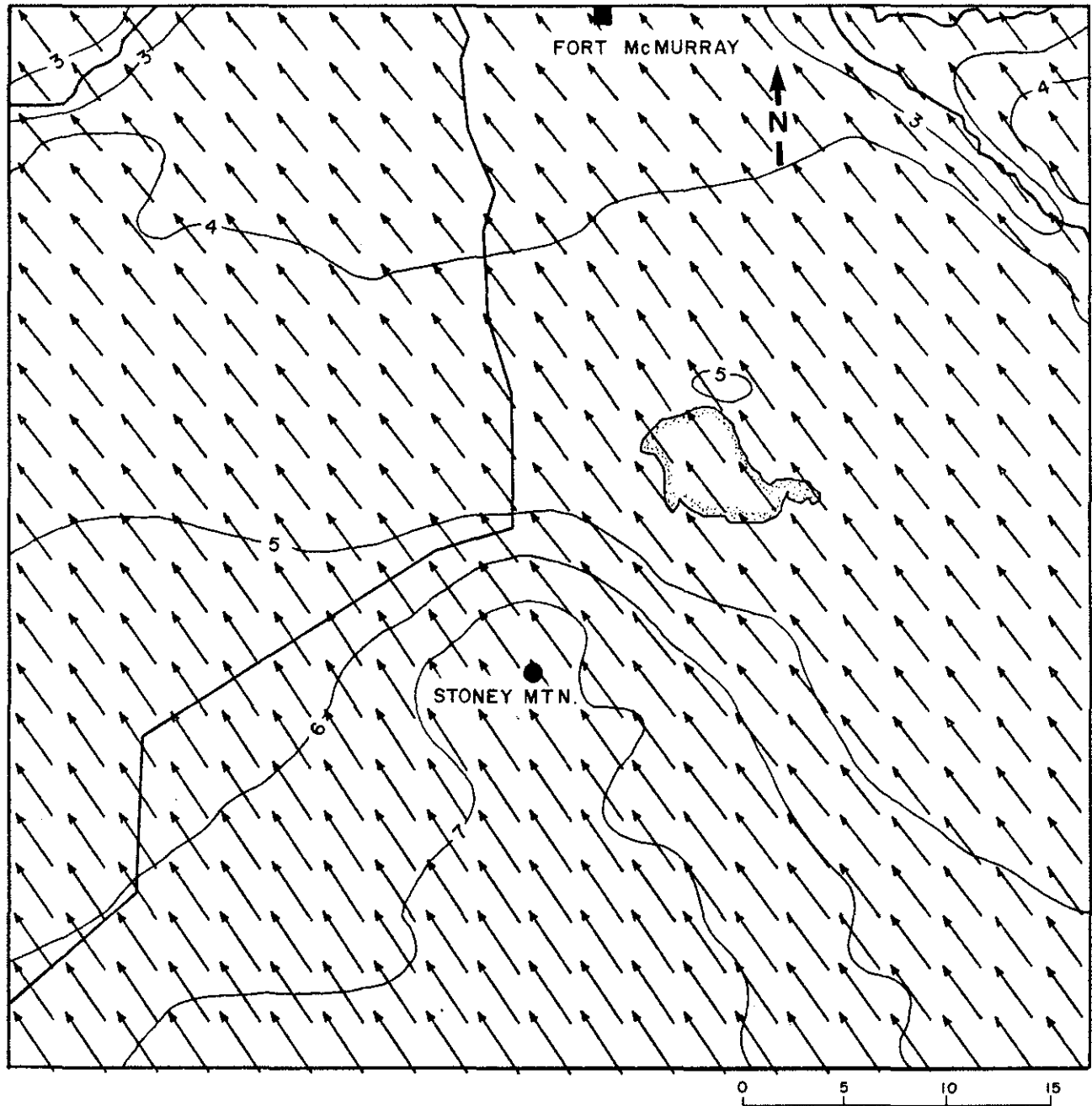
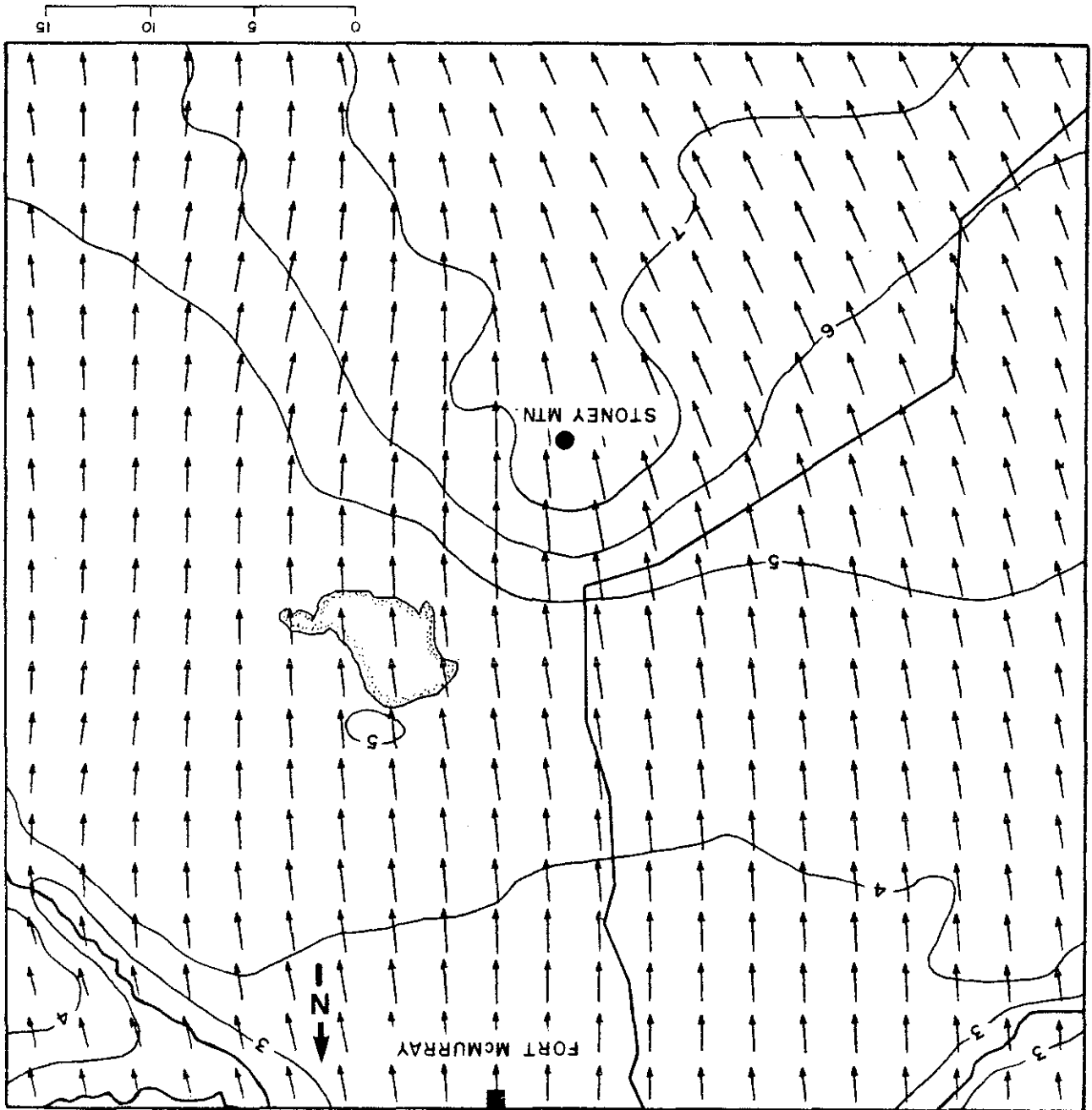


Figure 19. Winds computed by the Stoney Mountain model for Case 6 (0000 GMT 9 February 78). A vector of 1 cm length represents a wind of 25 km/h.

Figure 20. Winds computed by the Stoney Mountain model for Case 7 (0000 GMT 11 May 78). A vector of 1 cm length represents a wind of 20 km/h.



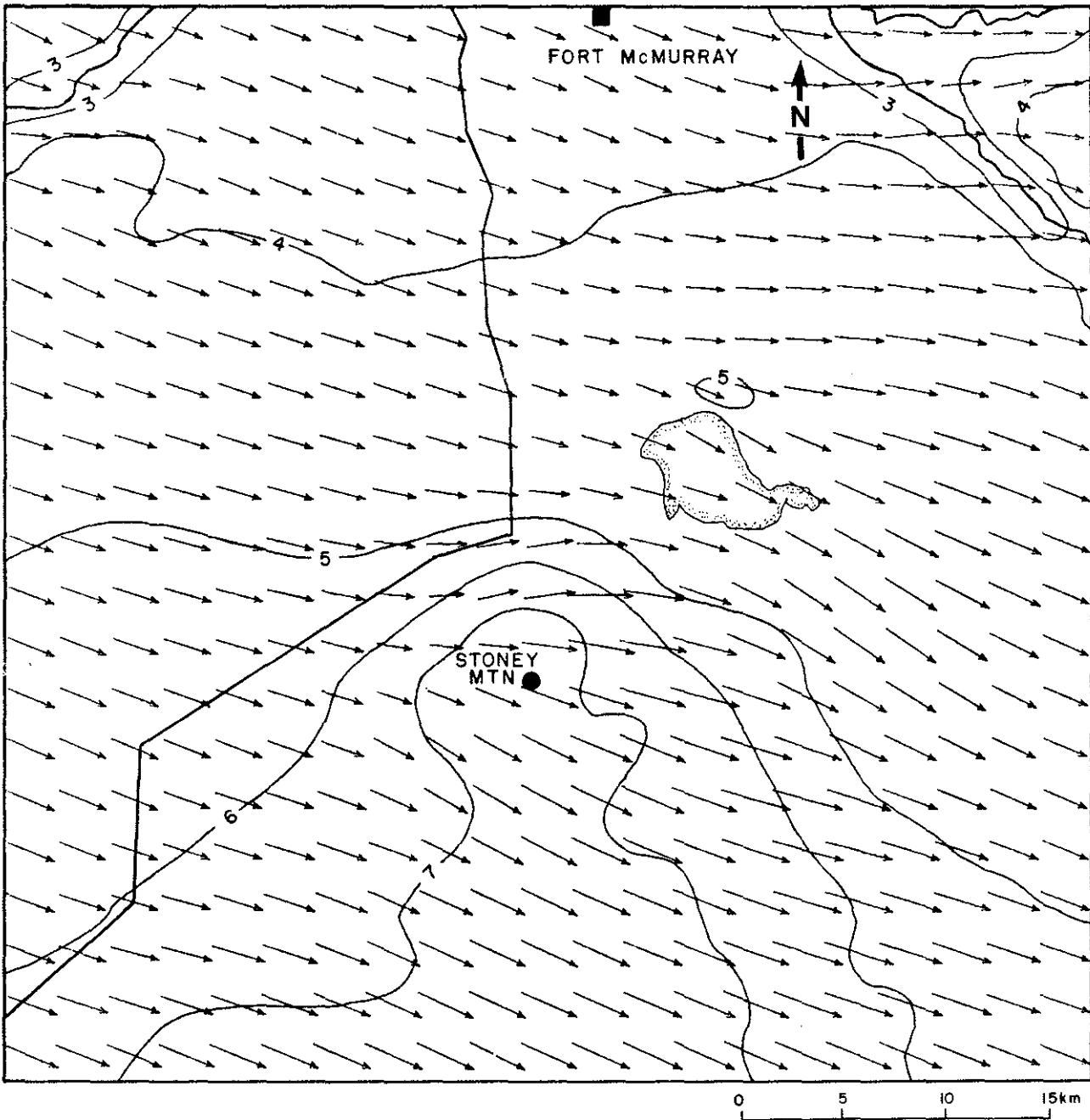


Figure 21. Winds computed by the Stoney Mountain model for Case 8 (1200 GMT 25 July 78). A vector of 1 cm represents wind of 20 km/h.

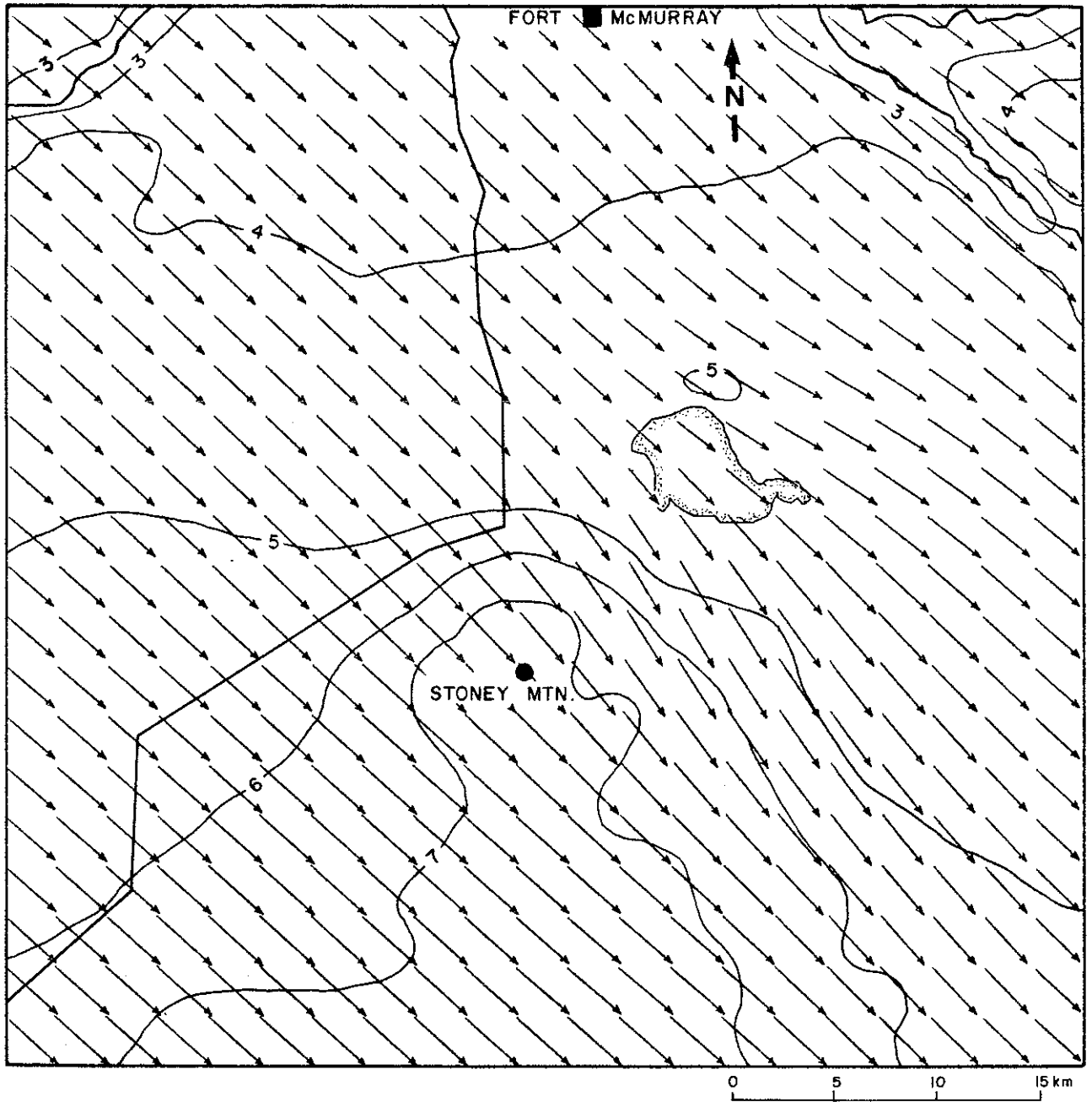


Figure 22. Winds computed by the Stoney Mountain model for Case 9 (0000 GMT 26 July 78). A vector of 1 cm length represents a wind of 20 km/h.

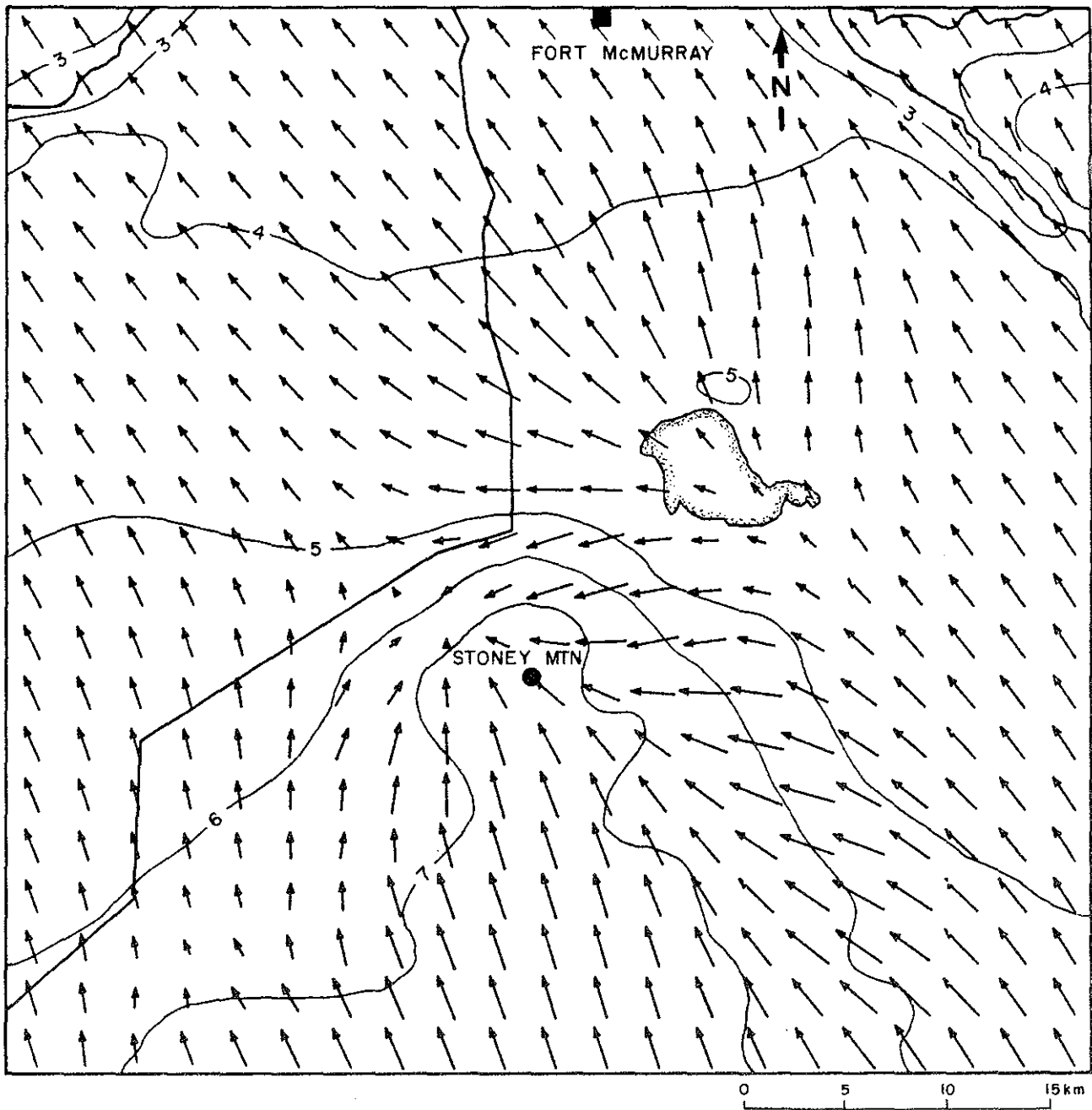


Figure 23. Winds computed by the Stoney Mountain model for Case 10 (0000 GMT 26 August 78). A vector of 1 cm length represents a wind of 30 km/h.

Table 2. Reported and Stoney Mountain model computed winds at Fort McMurray (km/h and degrees). See Table 1 for times of cases.

Case	Reported		Computed	
	Speed	Angle	Speed	Angle
1	6	240	9	240
2	15	260	11	250
3	7	120	8	200
4	8	170	13	190
5	16	130	20	120
6	16	140	17	140
7	11	330	11	360
8	15	300	11	290
9	15	010	15	310
10	23	130	15	140
Average	13		13	

Table 3. Reported and Stoney Mountain model computed winds at Stoney Mountain (km/h and degrees). See Table 1 for times of cases.

Case	Reported		Computed	
	Speed	Angle	Speed	Angle
1	15	240	15	240
2	22	250	17	260
3	14	210	14	210
4	18	200	22	200
5	31	130	33	130
6	29	110	27	150
7	12	340	14	350
8	22	260	16	290
9	20	330	21	320
10	10	120	16	130
Average	20		20	

Table 4. Median of the absolute value of the vector, speed, and angle differences between Stoney Mountain model computed and reported winds for both Fort McMurray and Stoney Mountain (km/h and degrees).

Vector	Speed	Angle
4.7	2.8	9

3. THE MILDRED LAKE MODEL

3.1 DESCRIPTION OF THE MODEL

This version is similar to the Stoney Mountain model (see Section 2.1) except for changes noted below. Meteorological input data needed are 850- and 700-mb heights at Mildred Lake (obtained from AES charts), winds, and temperatures measured by minisondes at Mildred Lake, and surface temperatures from the MAPS stations and Fort McMurray Airport.

The initial surface temperature T_i needed in Equation 4 is set equal to the daily mean temperature \bar{T} , obtained by fitting the equation

$$\bar{T} = a_0 + a_1x + a_2y + a_3z \quad (15)$$

to observed data at the six stations in Figure 2 (there must be at least four stations reporting). The final temperature T_0 over land (see Equation 4) is obtained by fitting the equation

$$T_0 = b_0 + b_1x + b_2y + b_3z \quad (16)$$

to observed present temperatures at the six stations. To avoid the possibility of unrealistic up- or downslope winds, we ensure that $|\Delta T| \leq 5^\circ\text{C}$ in Equation 5. In the Mildred Lake model, ΔT varies spatially; in the Stoney Mountain version it does not.

The 800-mb temperature at any point is obtained from the value at the reference point (Mildred Lake) and the isobaric temperature gradient inferred from the thermal wind equation and the vertical variation in winds above the momentum boundary layer measured by the minisonds. That is

$$\begin{aligned} \frac{\partial T}{\partial x} &= \frac{fT}{g} \frac{\partial v}{\partial z} \\ \frac{\partial T}{\partial y} &= - \frac{fT}{g} \frac{\partial u}{\partial z} \end{aligned} \quad (17)$$

The 800-mb height is obtained from the height at the reference point and the slope of the isobaric surface calculated assuming that the 800-mb wind is geostrophic. Initial surface pressures are calculated by integrating the hydrostatic equation down from 800 mb.

Thermal and momentum boundary layer heights are obtained directly from minisonde data (see Section 3.2). In Equation 5, τ is assigned the value of 1.6×10^3 s (40 timesteps). The total adjustment time is 3.2×10^3 s (80 timesteps).

3.2 PREPARATION OF INPUT DATA

The Mildred Lake model was applied to the six cases described in Table 5 and Figures 23 to 25. As in the Stoney Mountain application, the cases were chosen to provide a variety of directions and synoptic conditions. Note that Cases 4 to 6 are for the same times as Cases 1 to 3 in Table 1. In Table 5, the "geostrophic" direction is inferred by downward extrapolation of free atmosphere winds.

Temperature profiles, wind hodographs, and wind profiles are shown in Figures 26-31, 32-37 and 38-43, respectively. Since the raw winds provided by the minisondes were very noisy, it was necessary first to smooth the wind components and heights four times using the operator

$$u_k = 0.25 u_{k-1} + 0.5 u_k + 0.25 u_{k+1}$$

where the subscript indicates level in the vertical. It is the smoothed profiles which are plotted.

The height of the 800-mb surface at Mildred Lake is calculated by interpolation between the 850- and 700-mb values (obtained from AES charts) on a plot of z versus $\ln p$. Wind components and temperature at Mildred Lake for 800 mb are obtained from the minisonde profiles there. The heights of the 850, 800, and 700 mb surfaces are indicated as Z85, Z80 and Z70, respectively, in Figures 26 to 31 for temperatures and Figures 38 to 43 for the wind components. ZREF is the ground elevation.

The free atmosphere lapse rate is calculated from the temperature profiles. Temperatures at two heights that best estimate the lapse rate above the thermal boundary layer are extracted. In Figure 26, the

heights are shown as ZTL and ZTU, with corresponding temperatures of TL and TU, respectively. Note that ZTL, the lower height, must be greater than or equal to H, the thermal boundary layer height. H is the top of the nocturnal inversion (Figures 26, 29 and 31) or the base of the convection-limiting inversion (Figures 27, 28 and 30).

Figures 32 to 37 show wind hodographs. The top of the momentum boundary layer h is the level where the wind stops veering with height (e.g., Figures 32 and 33) and/or the vertical wind shear becomes small (e.g., Figure 34).

In order to calculate the wind shear at 800 mb needed for the thermal wind equation (17), winds at two heights ZWL and ZWU are needed (Figure 38). The corresponding wind components are U_L , V_L , and U_U and V_U , respectively. Since these winds are assumed geostrophic, the lower level (ZWL) must be greater than or equal to the height of the momentum boundary layer h . The 800-mb winds are obtained from a 5-point vertical running average centred on that level.

Table 5. Cases to which the Mildred Lake model was applied.

Case	Time	Geostrophic direction
1	1550 GMT 27 Jan 77	N
2	2100 GMT 23 Mar 77	E
3	1435 GMT 12 Jul 77	NE
4	1400 GMT 17 Oct 77	SW
5	1809 GMT 17 Oct 77	SW
6	1411 GMT 23 Oct 77	S

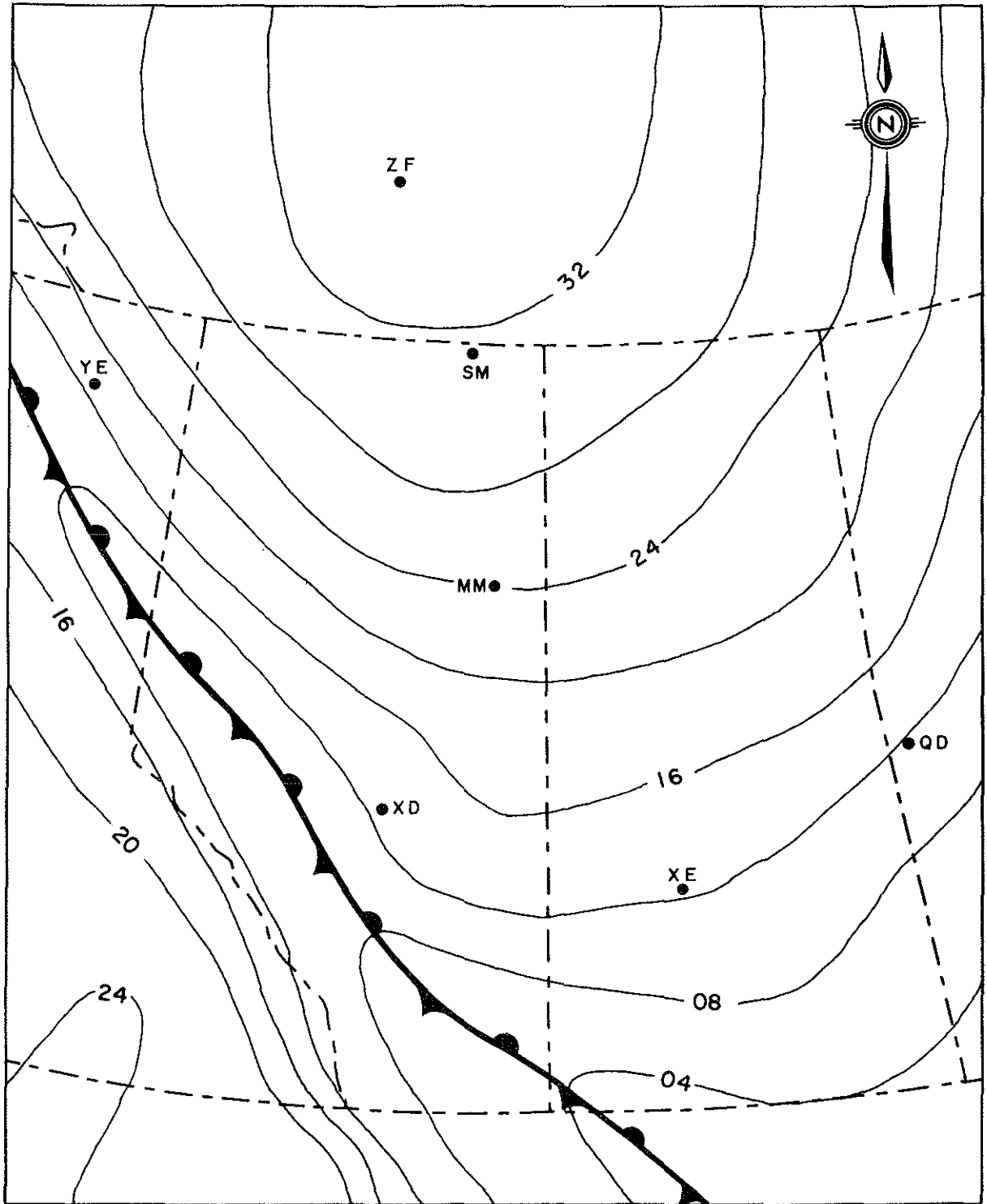


Figure 24. Sea-level pressure (mb) for 1200 GMT 27 January 77.

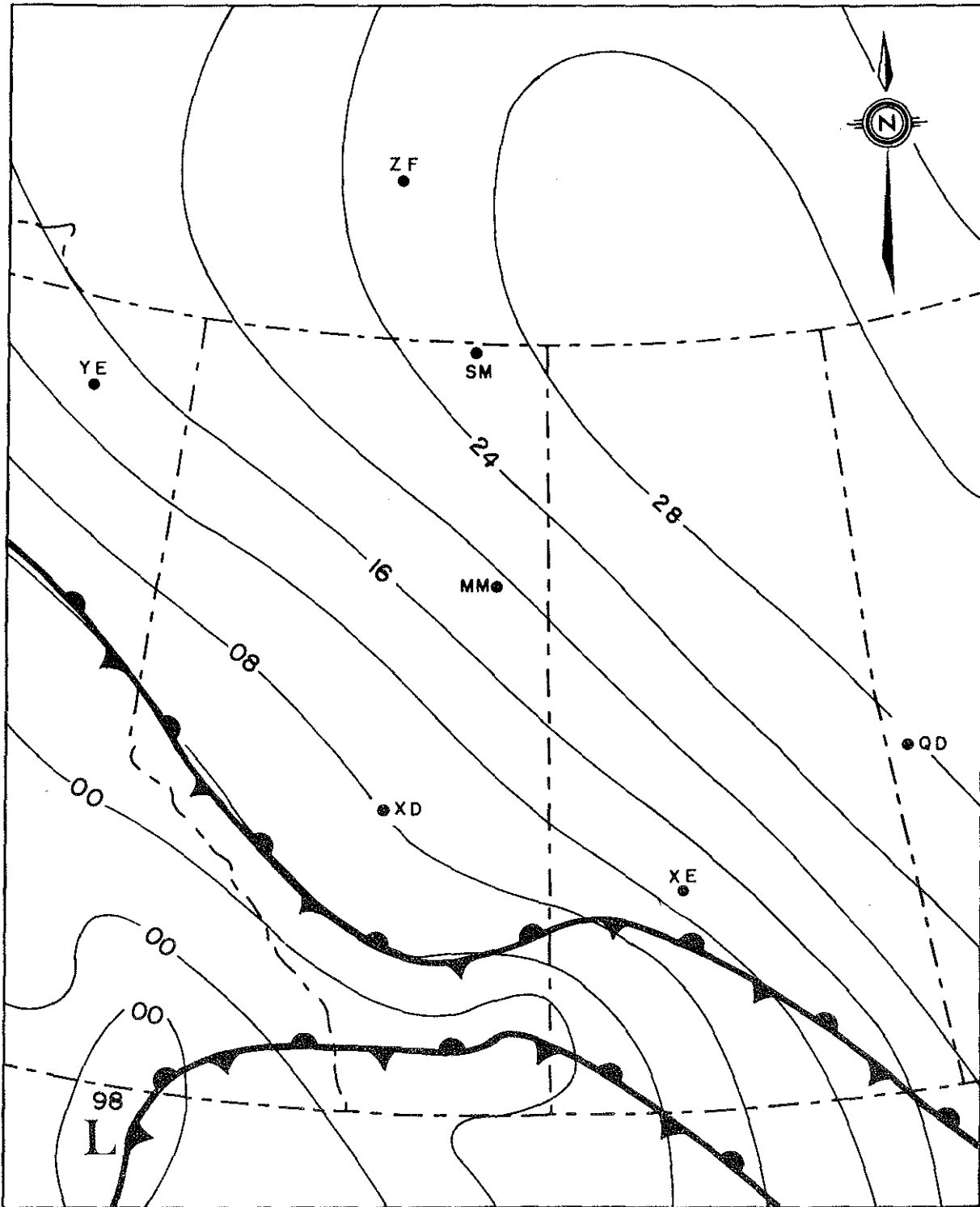


Figure 25. Sea-level pressure (mb) for 1800 GMT 23 March 77.

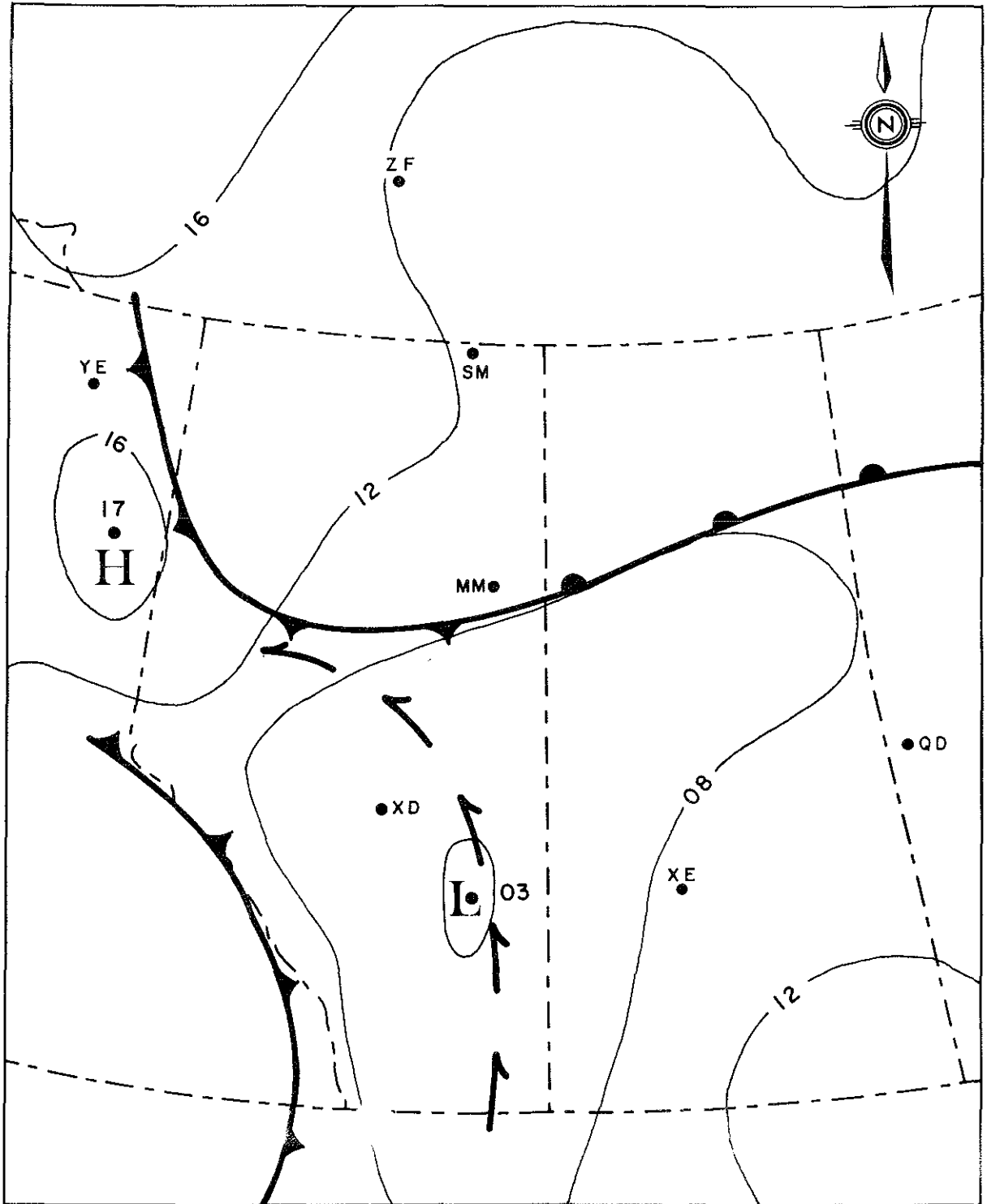


Figure 26. Sea-level pressure (mb) for 1200 GMT 12 July 77.

GCOS / JAN 27, 1977 / 0850 MST / 227M

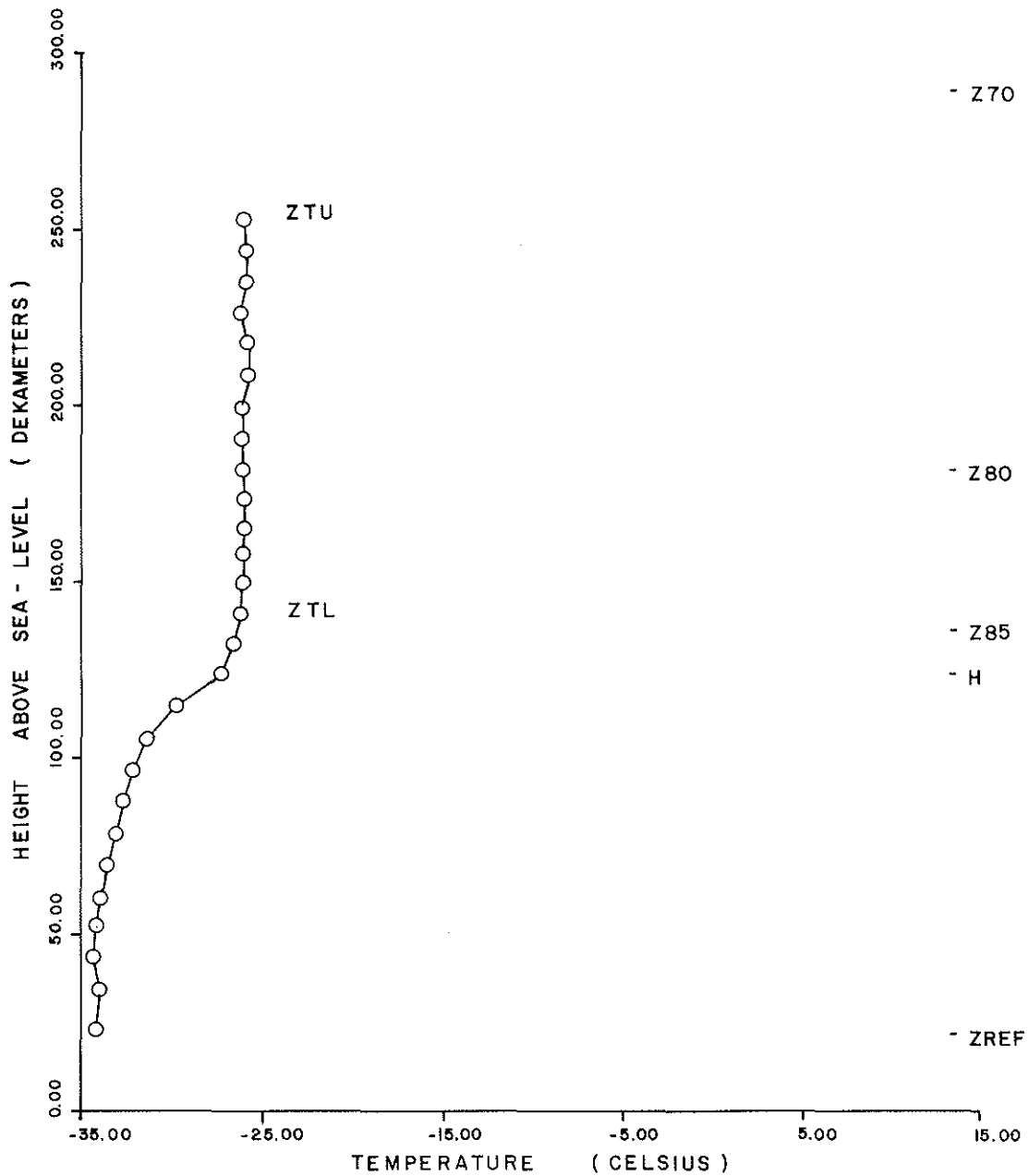


Figure 27. Temperature profile at Mildred Lake for 1550 GMT 27 January 1977. H is the estimated top of the thermal boundary layer.

SYNCRUDE STRIP / MAR 23, 1977 / 1400 MST / 320.6M

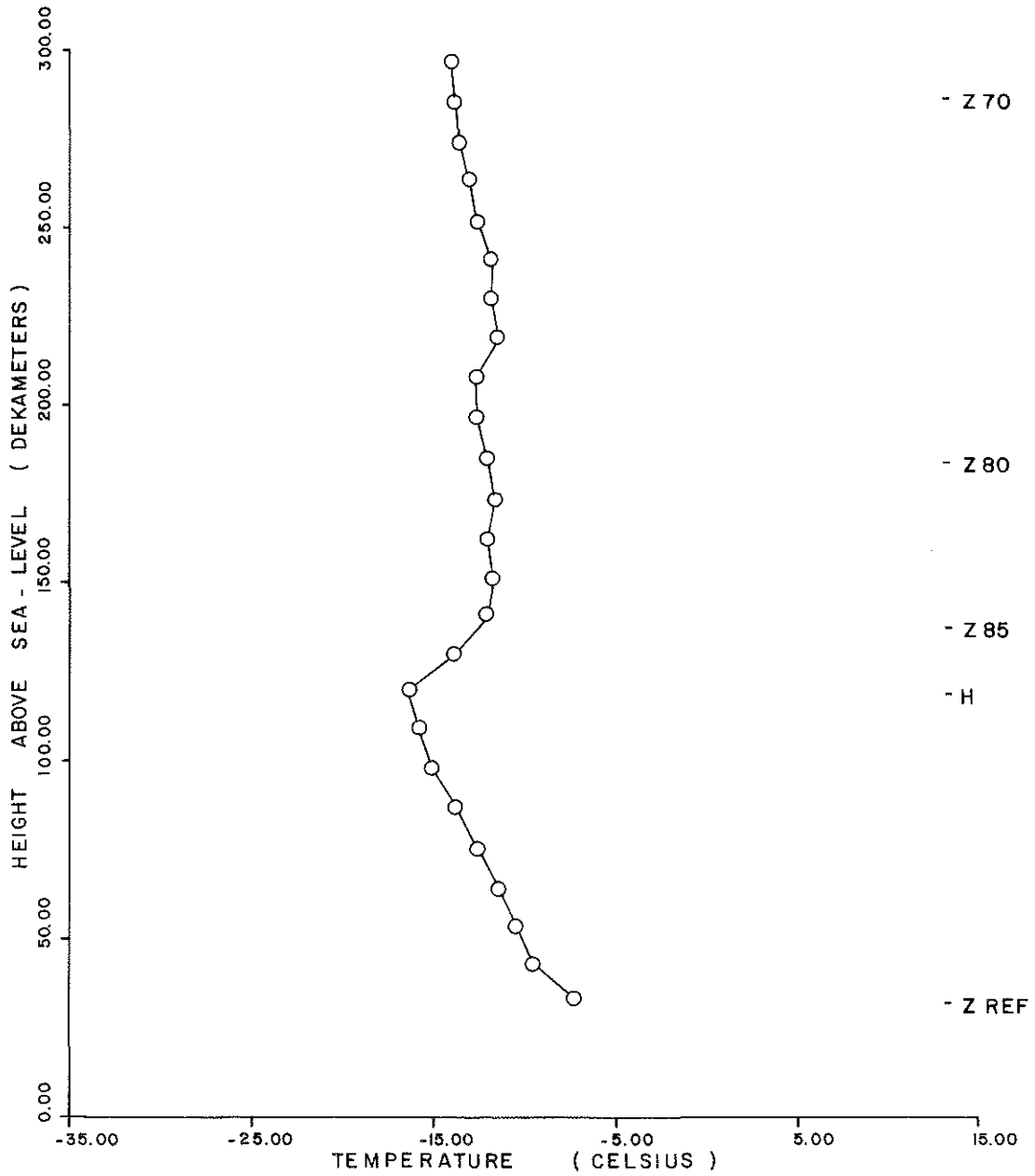


Figure 28. Temperature profile at Mildred Lake for 2100 GMT 23 March 1977.

SYNCRUDE STRIP / JUL 12, 1977 / 0735 MST / 320.0M

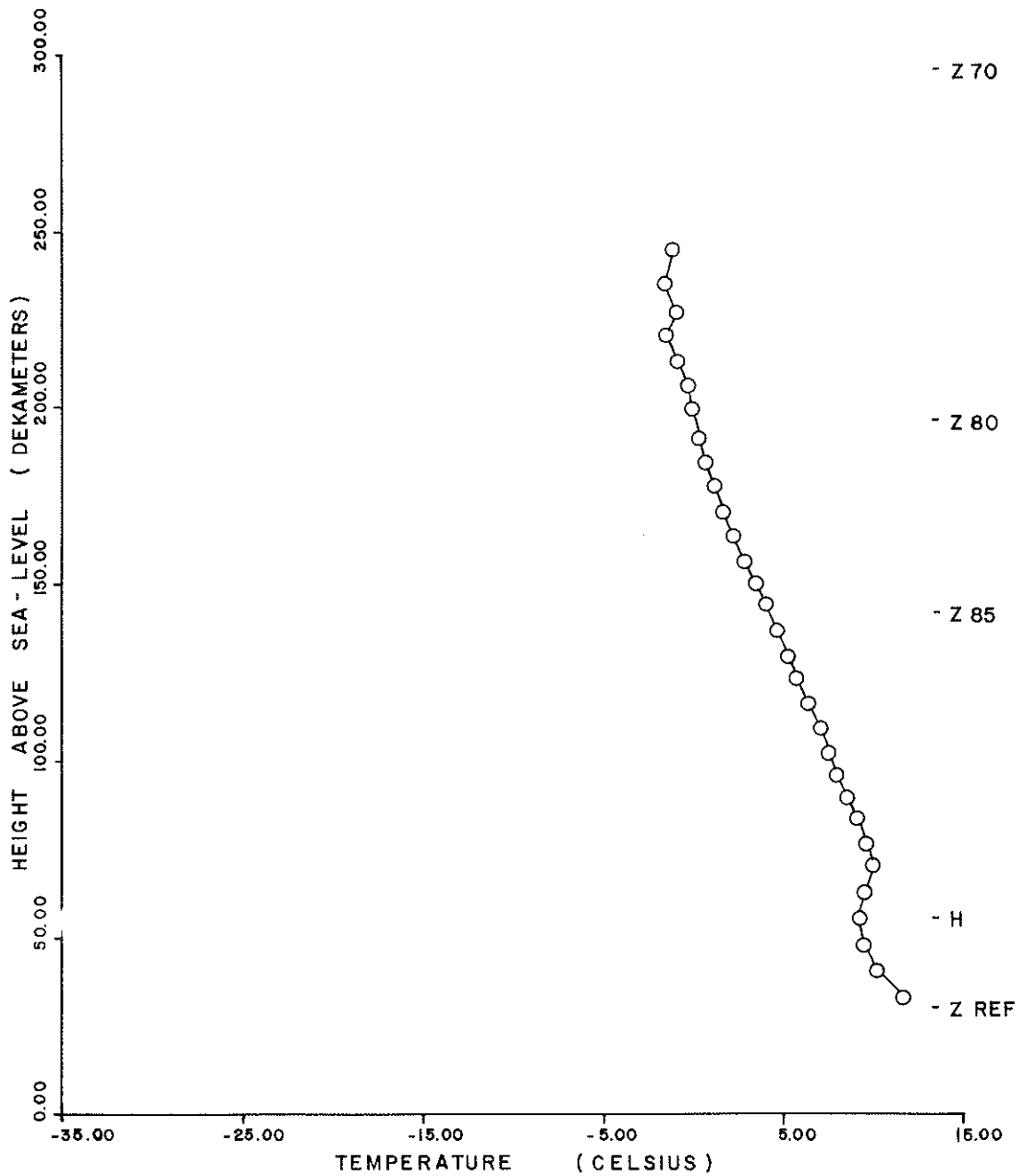


Figure 29. Temperature profile at Mildred Lake for 1435 GMT 12 July 1977.

SYNCRUDE STRIP / OCT 17, 1977 / 0700 MST / 320.0M

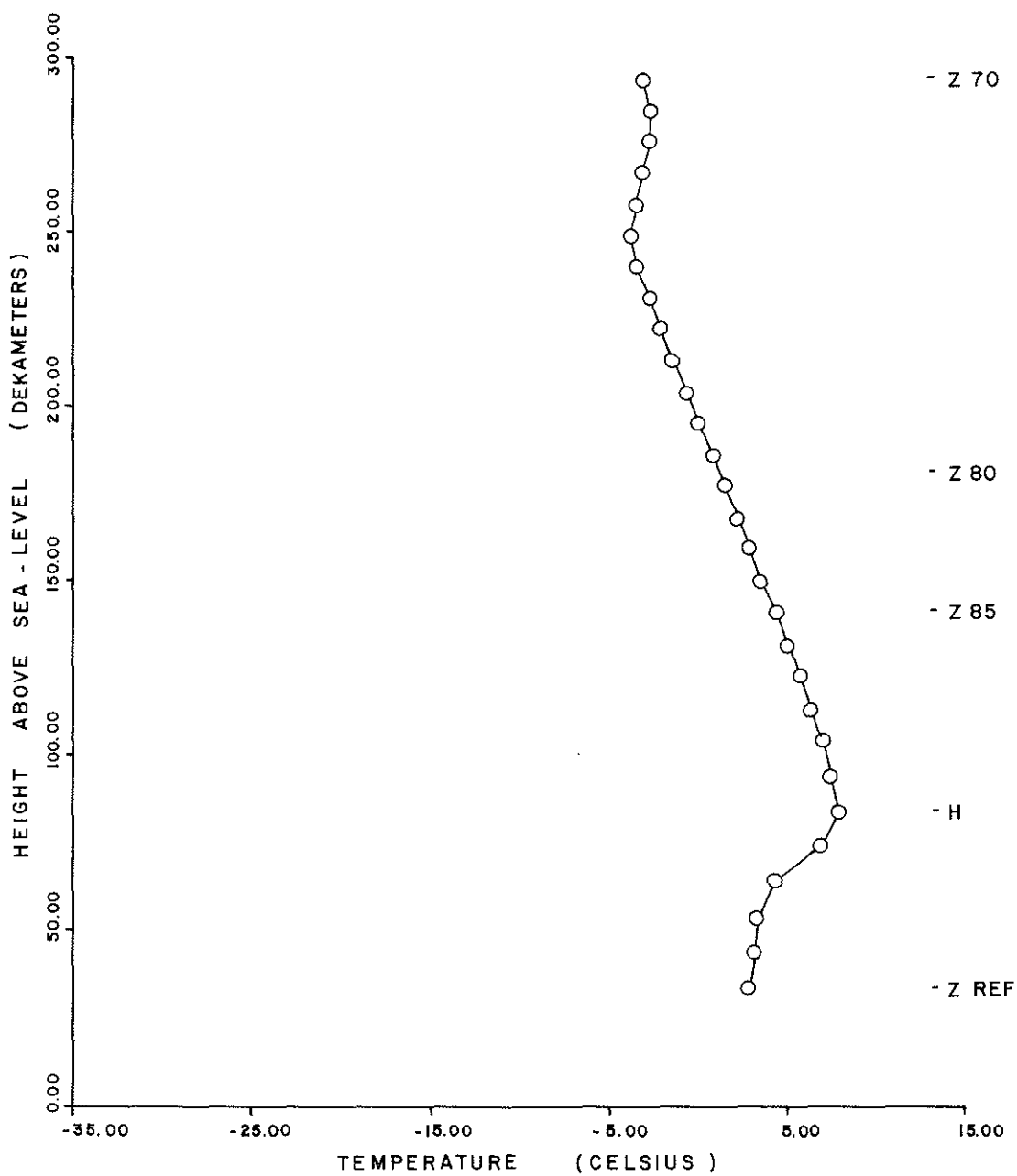


Figure 30. Temperature profile at Mildred Lake for 1400 GMT 17 October 1977.

SYNCRUDE STRIP / OCT 17, 1977 / 1109 MST / 320.0M

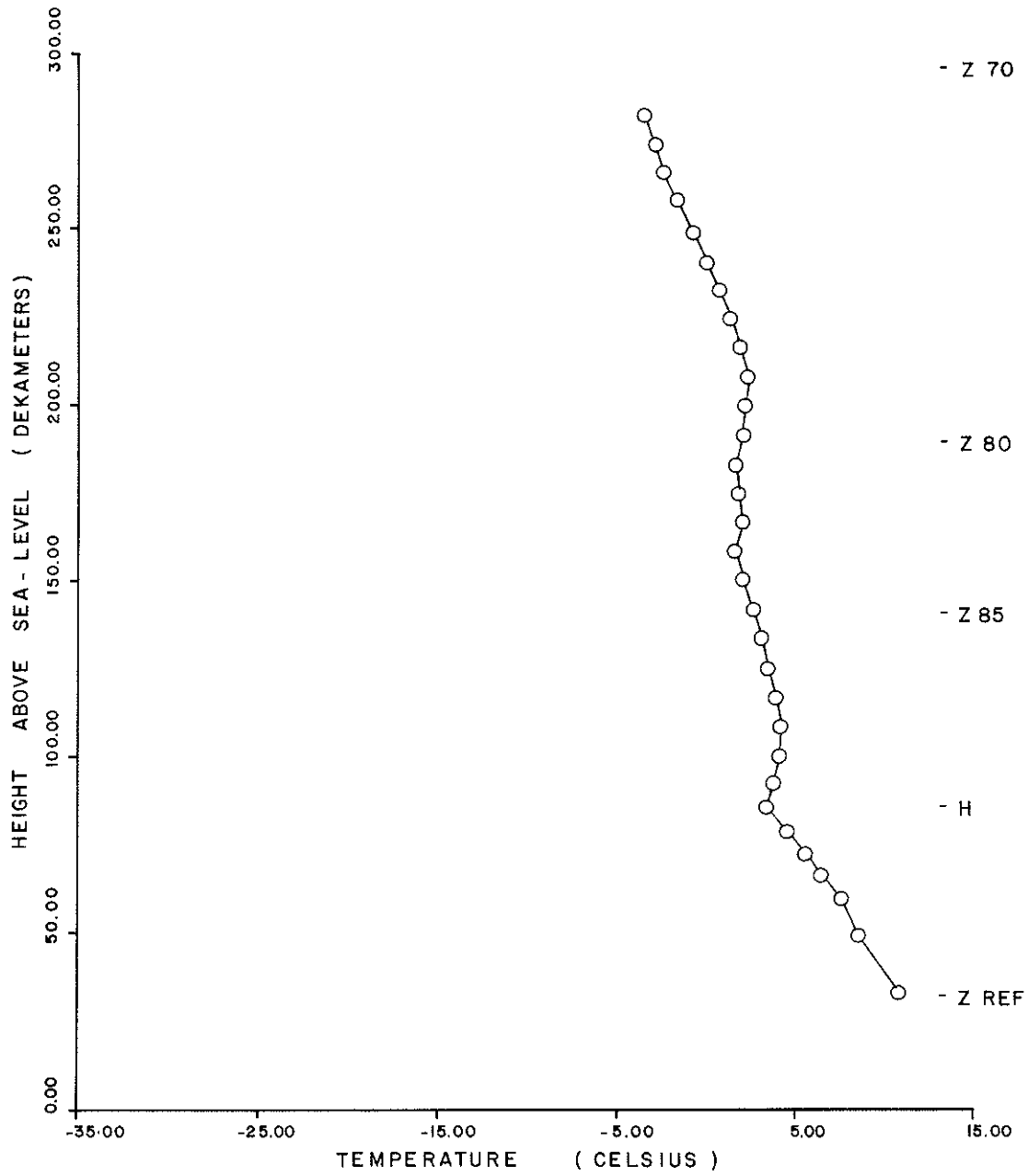


Figure 31. Temperature profile at Mildred Lake for 1309 GMT 17 October 1977.

SYNCRUDE AIRSTRIP / OCT 23, 1977 / 0711 MST / 320.0M

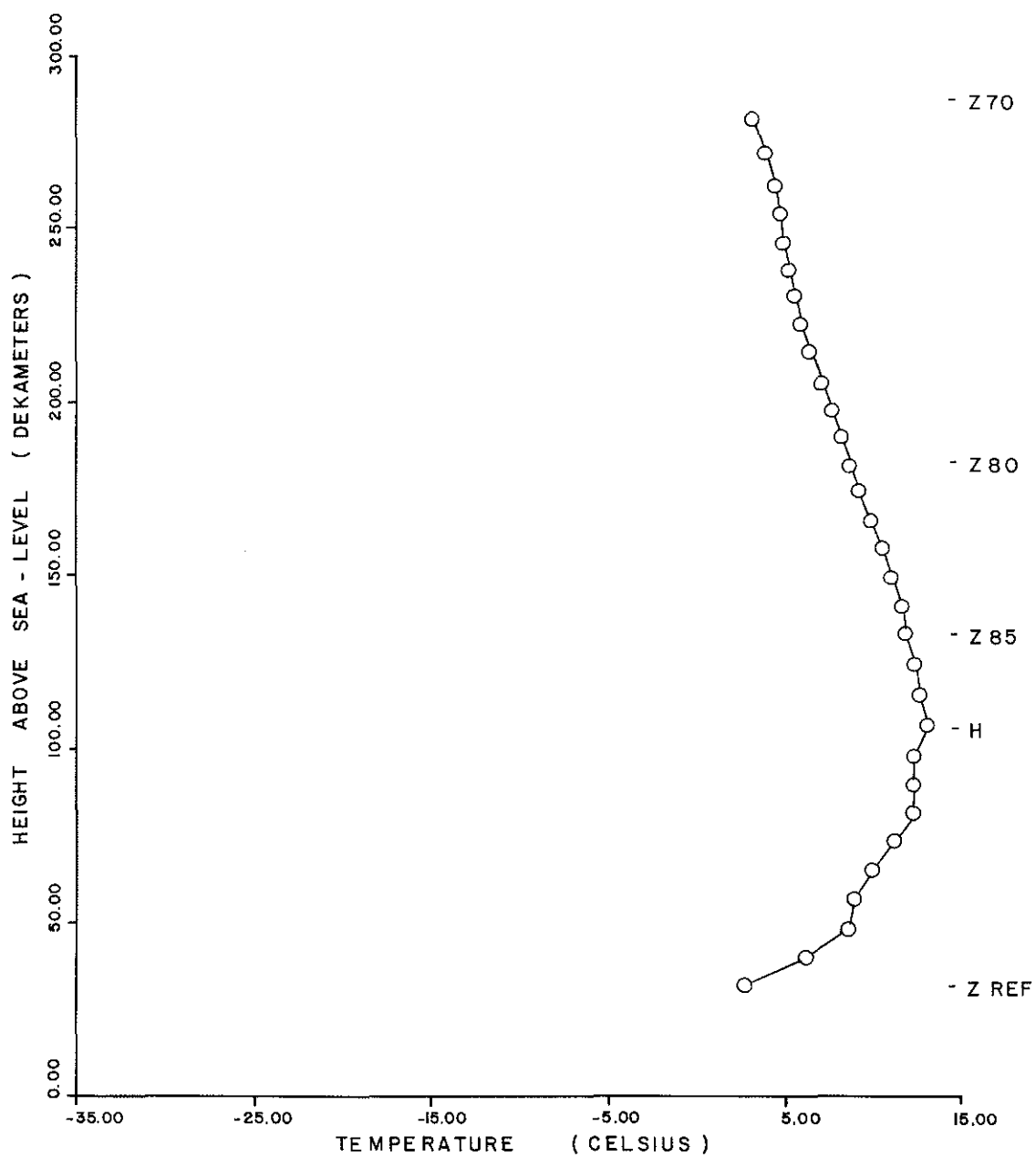


Figure 32. Temperature profile at Mildred Lake for 1411 GMT 23 October 1977.

GCOS/JAN 27, 1977/0850 MST / 227M.

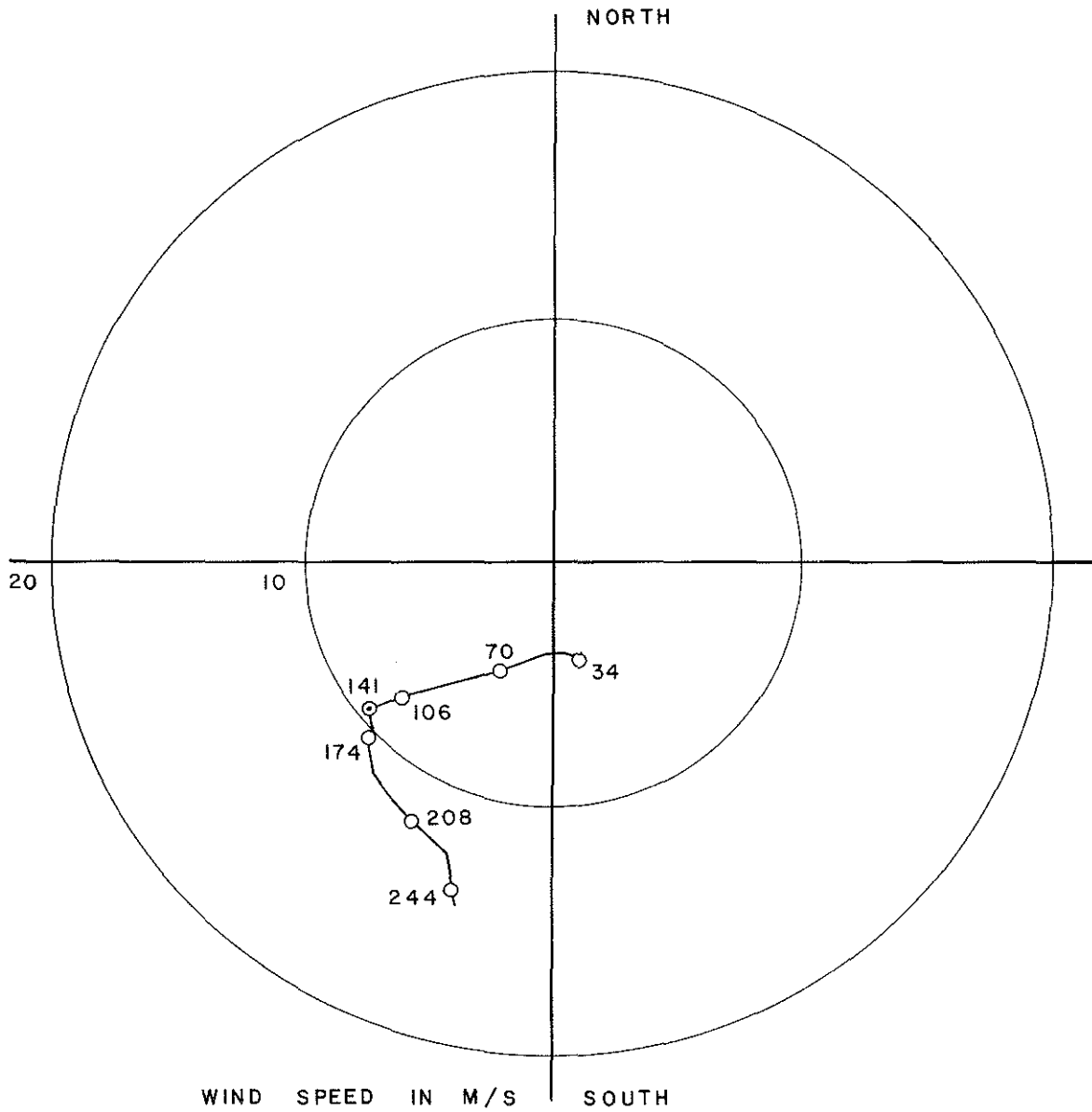


Figure 33. Wind hodograph at Mildred Lake for 1550 GMT 27 January 1977. Numbers represent Heights above sea-level in dekameters. The dot is the estimated top of the momentum boundary layer (h).

SYNCRUDE STRIP/MAR 23, 1977/1400 MST/320.6M

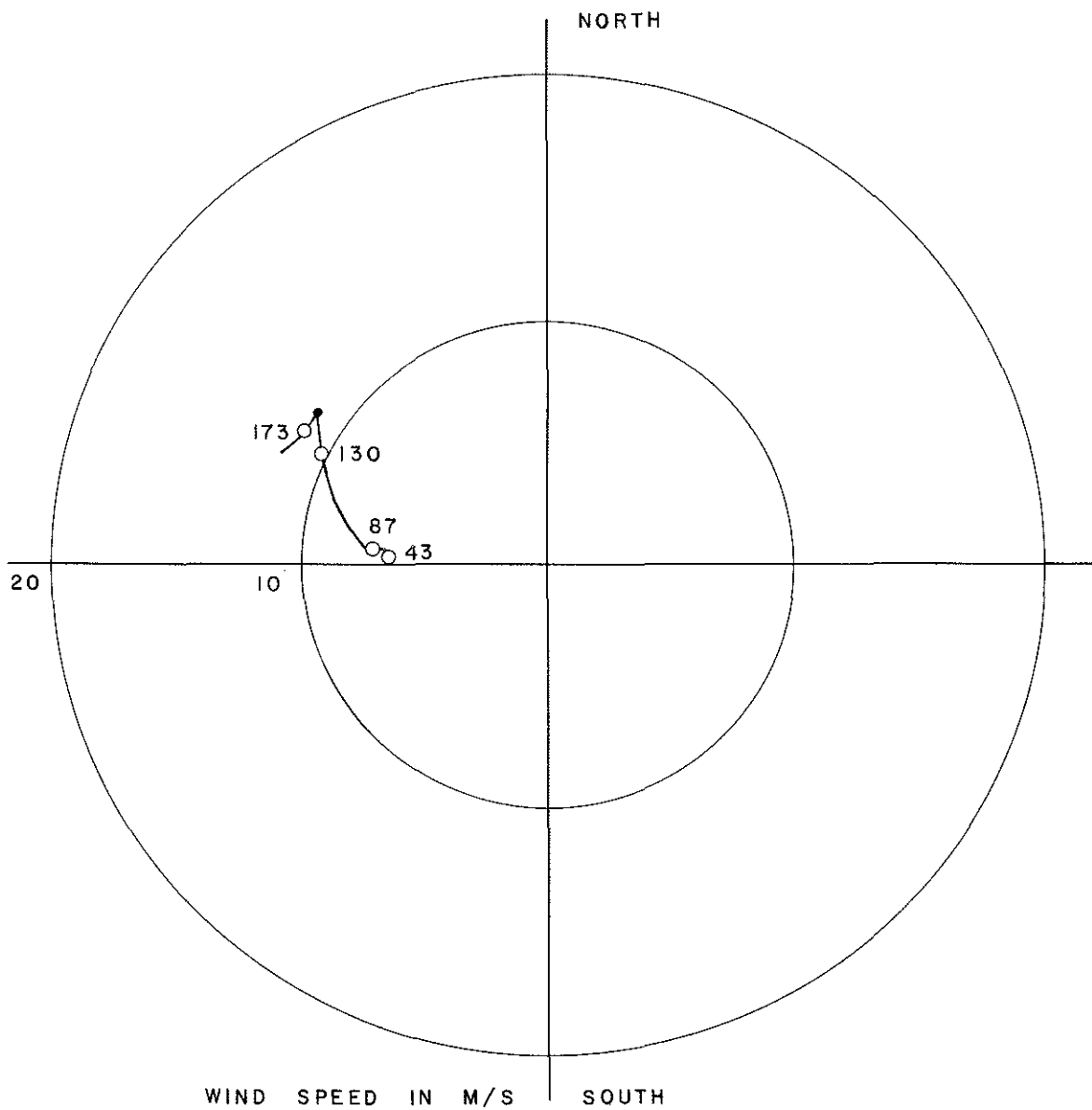


Figure 34. Wind hodograph at Mildred Lake for 2100 GMT 23 March 1977.

SYNCRUDE STRIP / JUL 12, 1977 / 0735 MST / 320.0M

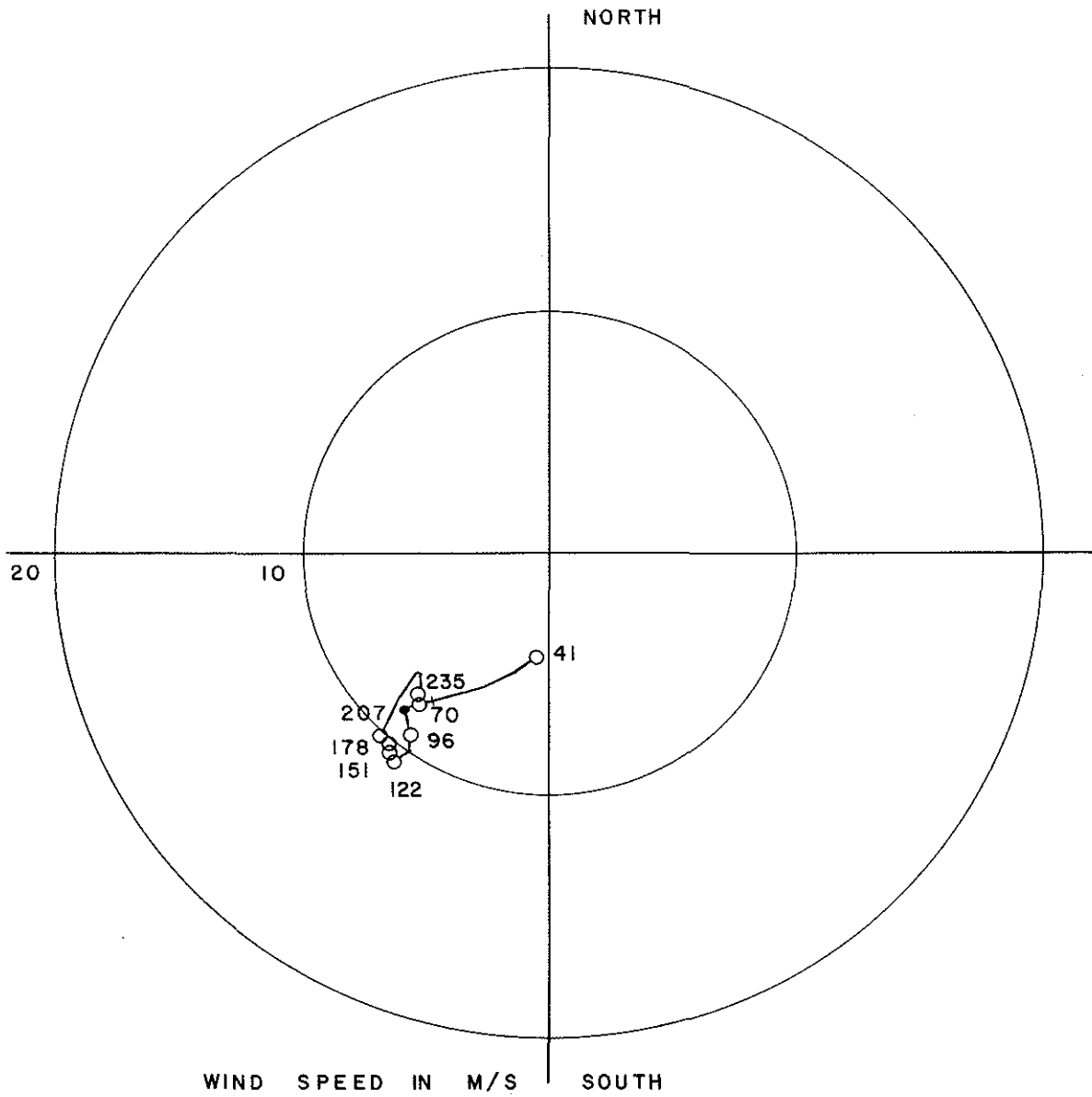


Figure 35. Wind hodograph at Mildred Lake for 1435 GMT 12 July 1977.

SYNCRUDE STRIP / OCT 17, 1977 / 0700 MST / 320.0M

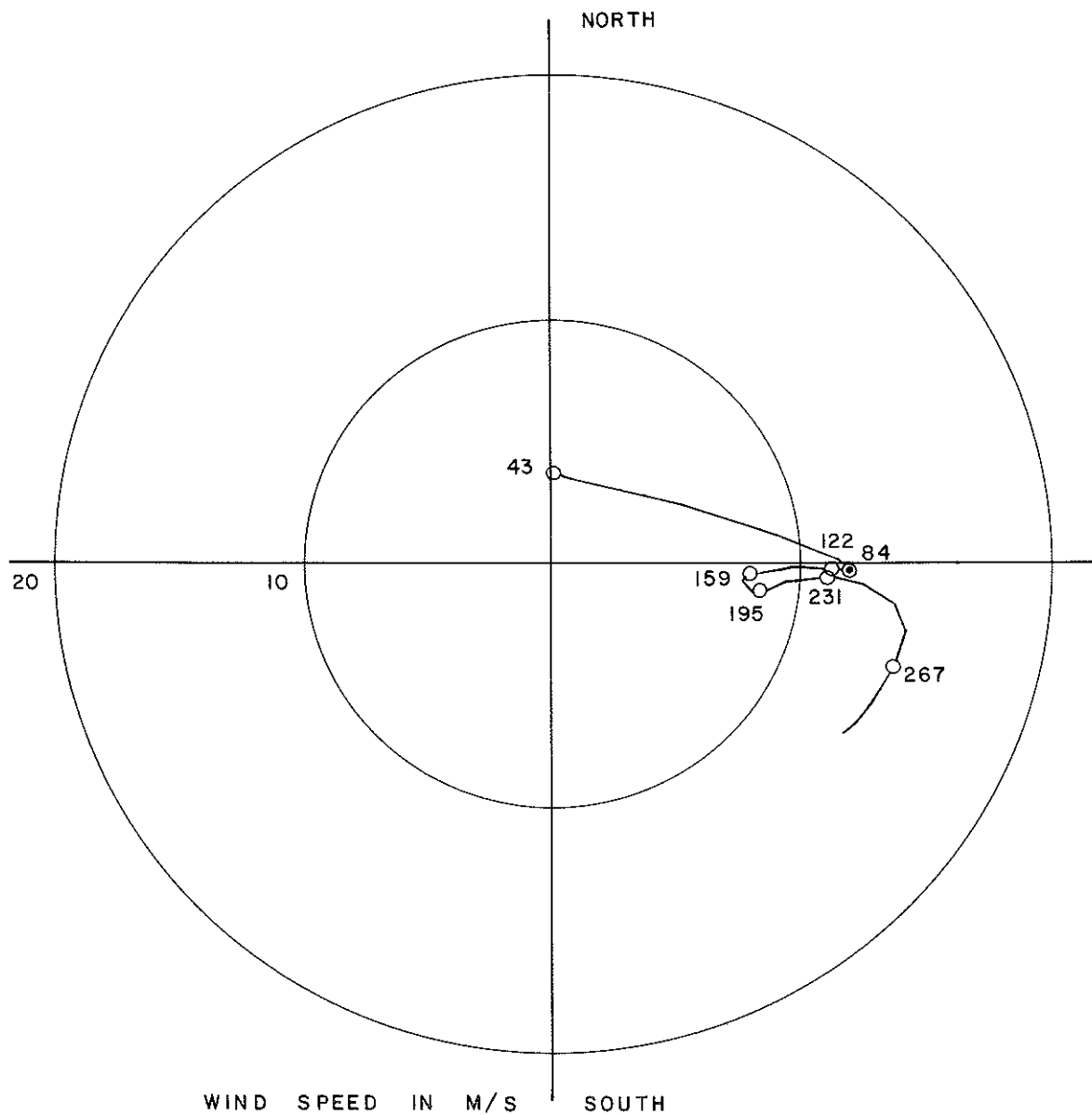


Figure 36. Wind hodograph at Mildred Lake for 1400 GMT 17 October 1977.

SYNCRUDE STRIP / OCT 17, 1977 / 1109 MST / 320.0M

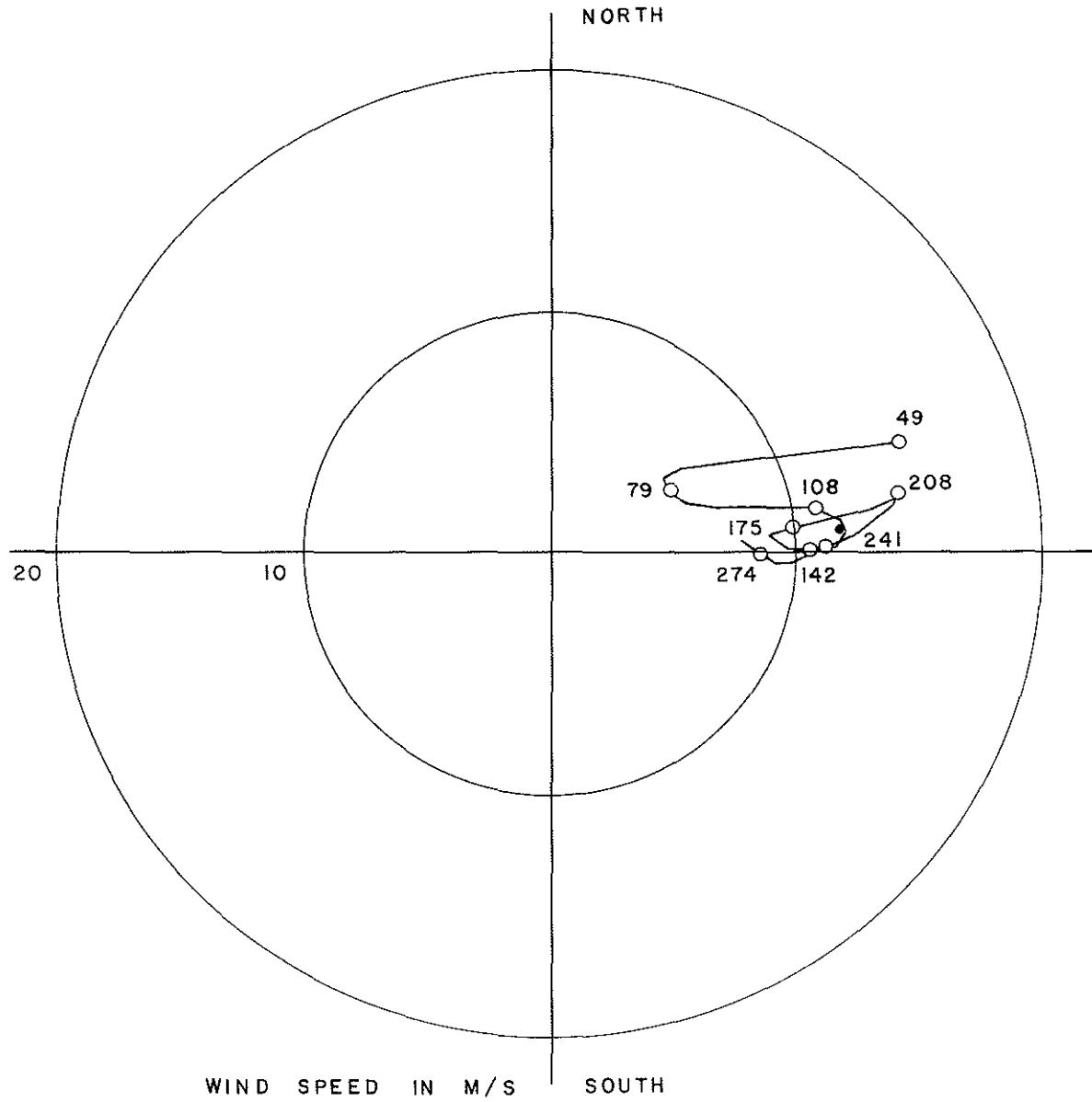


Figure 37. Wind hodograph at Mildred Lake for 1809 GMT
17 October 1977.

SYNCRUDE AIRSTRIP / OCT 23, 1977 / 0711 MST / 320.0M

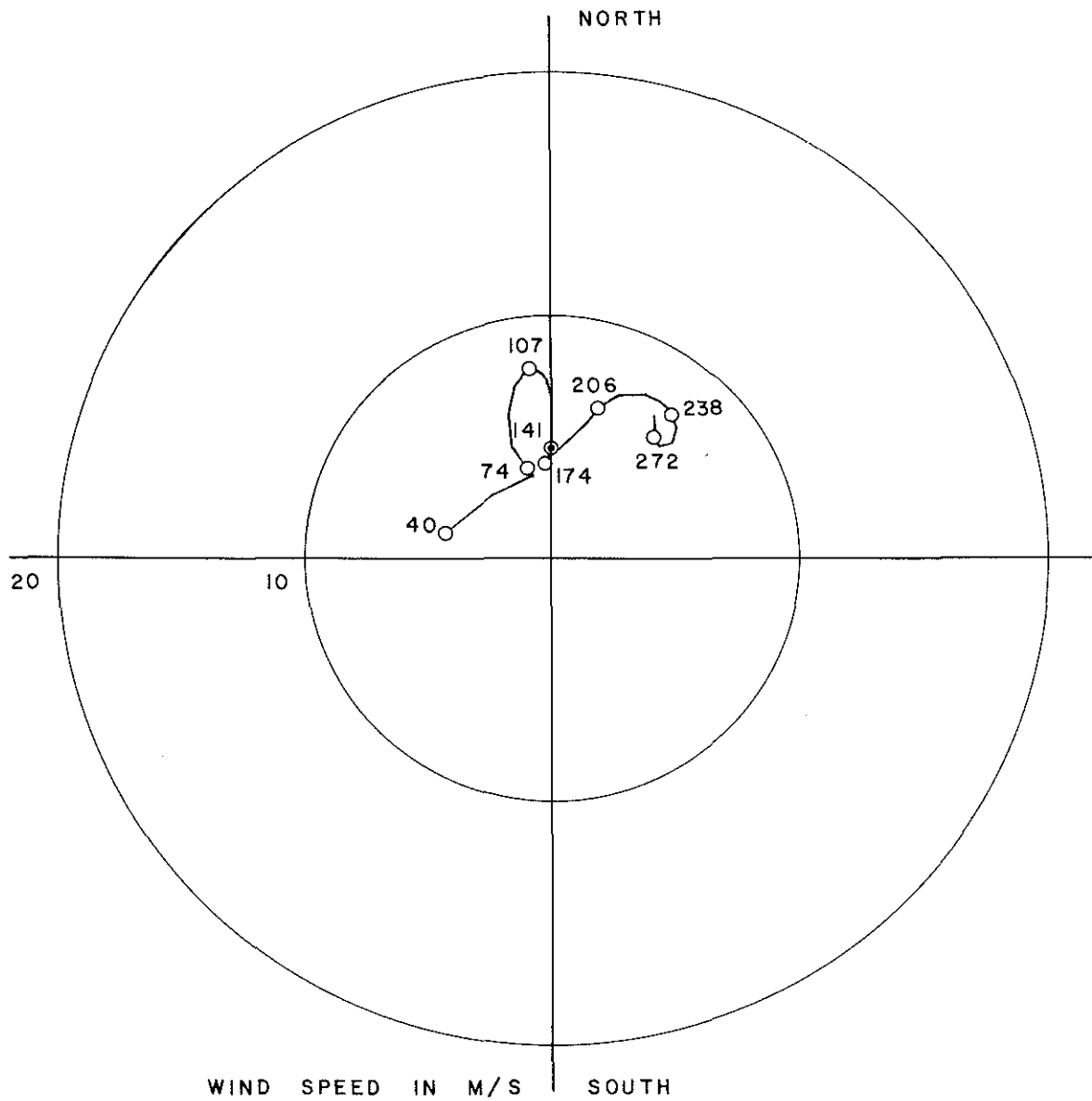


Figure 38. Wind hodograph at Mildred Lake for 1411 GMT 23 October 1977.

GCOS/JAN 27, 1977 / 0850 MST/227M

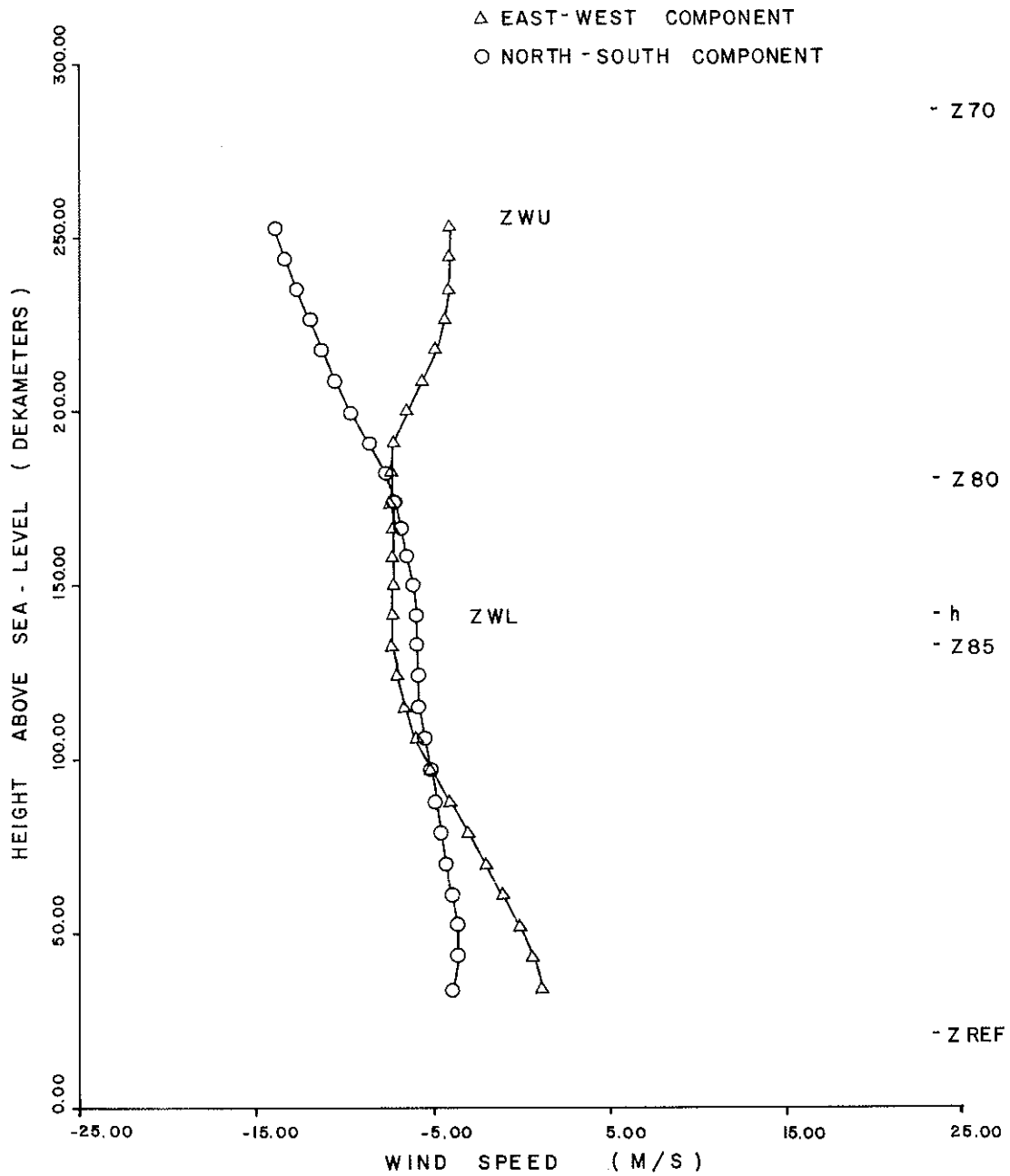


Figure 39. Profile of wind components at Mildred Lake for 1550 GMT 27 January 1977. h is the estimated top of the momentum boundary layer (see Figure 32).

SYNCRUDE STRIP / MAR 23, 1977 / 1400 MST / 320.6M

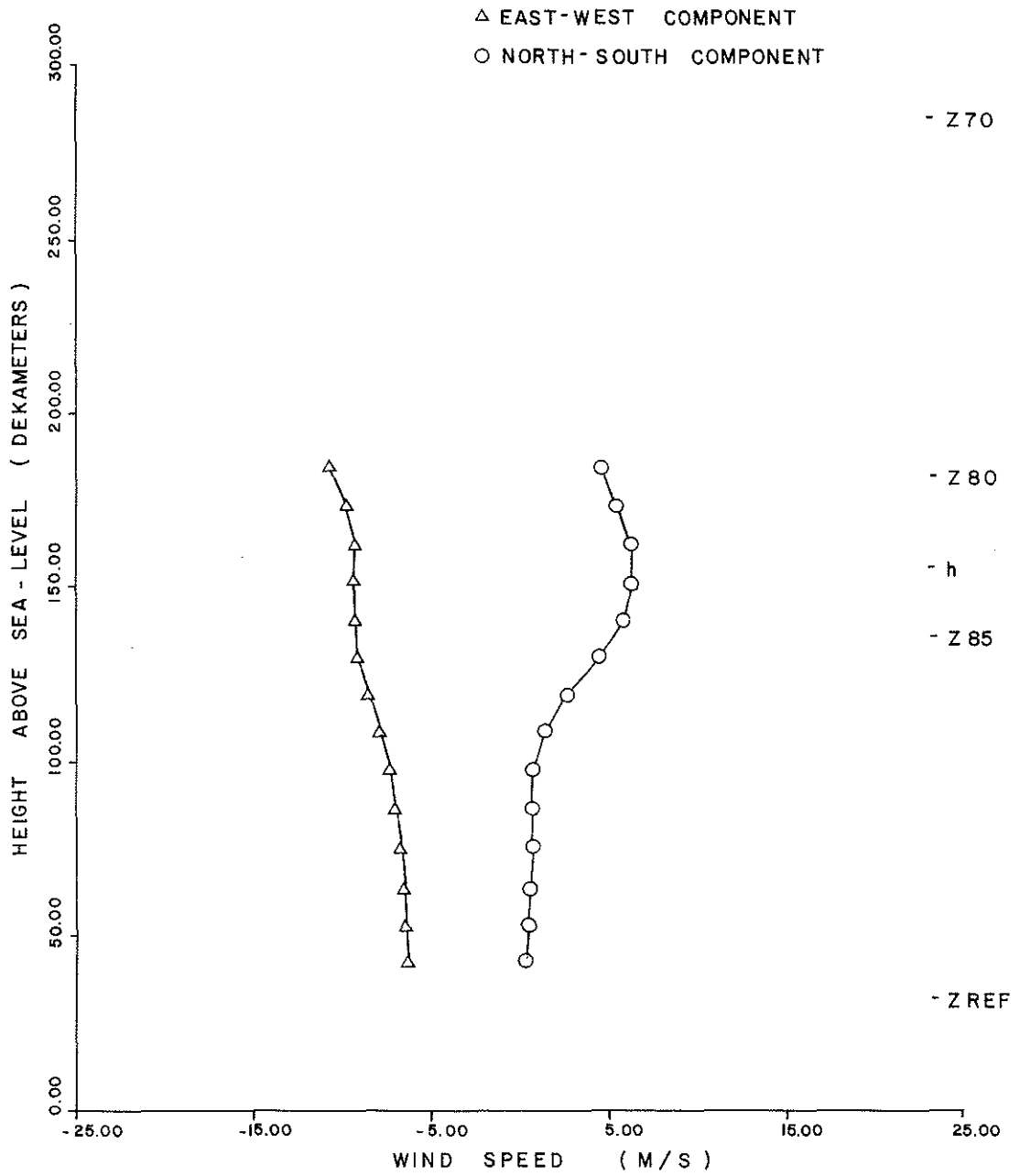


Figure 40. Profile of wind components at Mildred Lake for 2100 GMT 23 March 1977.

SYNCRUDE STRIP/JUL 12, 1977 / 0735 MST / 320.0M

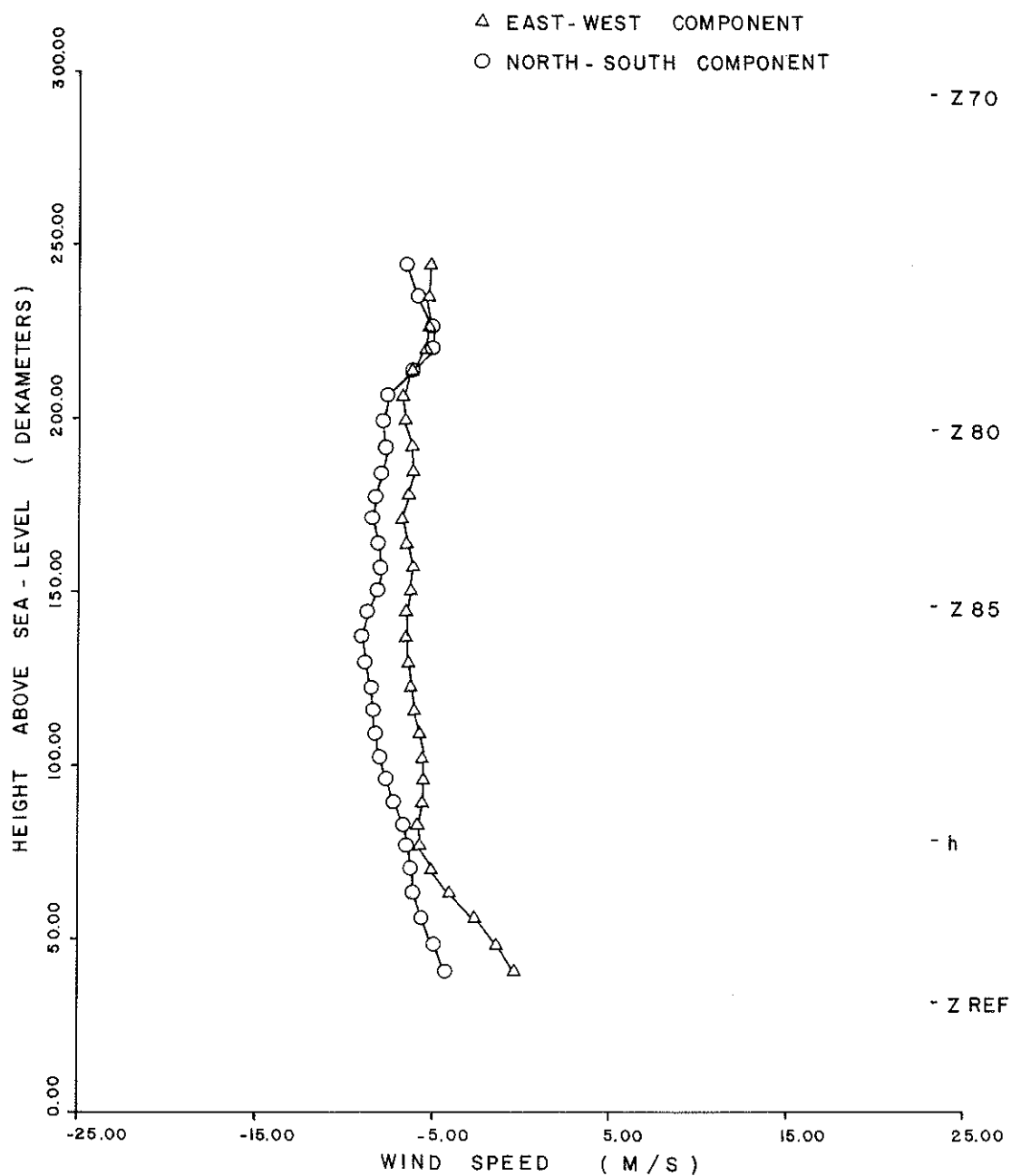


Figure 41. Profile of wind components at Mildred Lake for 1435 GMT 12 July 1977.

SYNCRUDE STRIP / OCT 17, 1977 / 07 00 MST / 320.0M

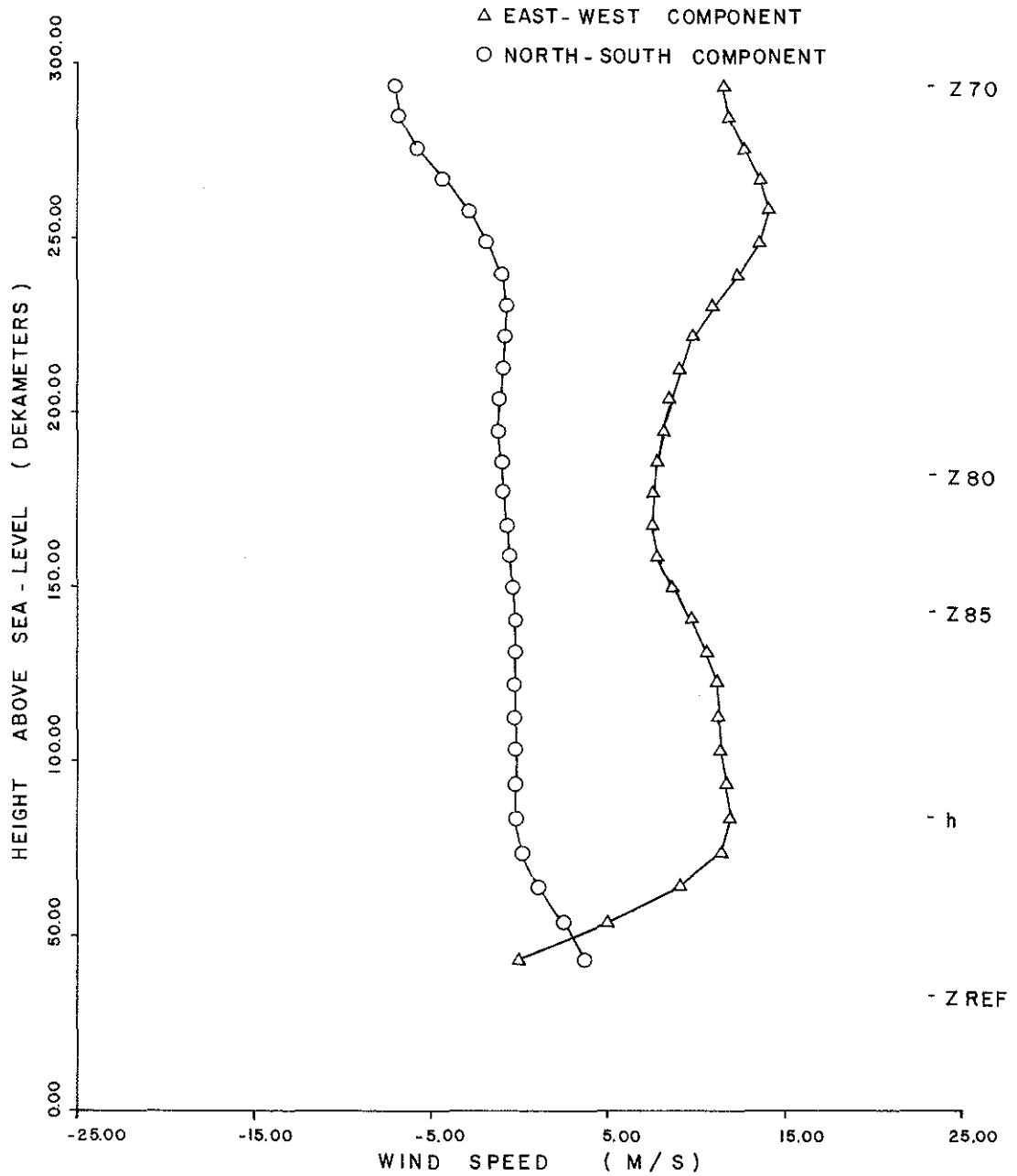


Figure 42. Profile of wind components at Mildred Lake for 1400 GMT 17 October 1977.

SYNCRUDE STRIP / OCT 17, 1977 / 1109 MST / 320.0M

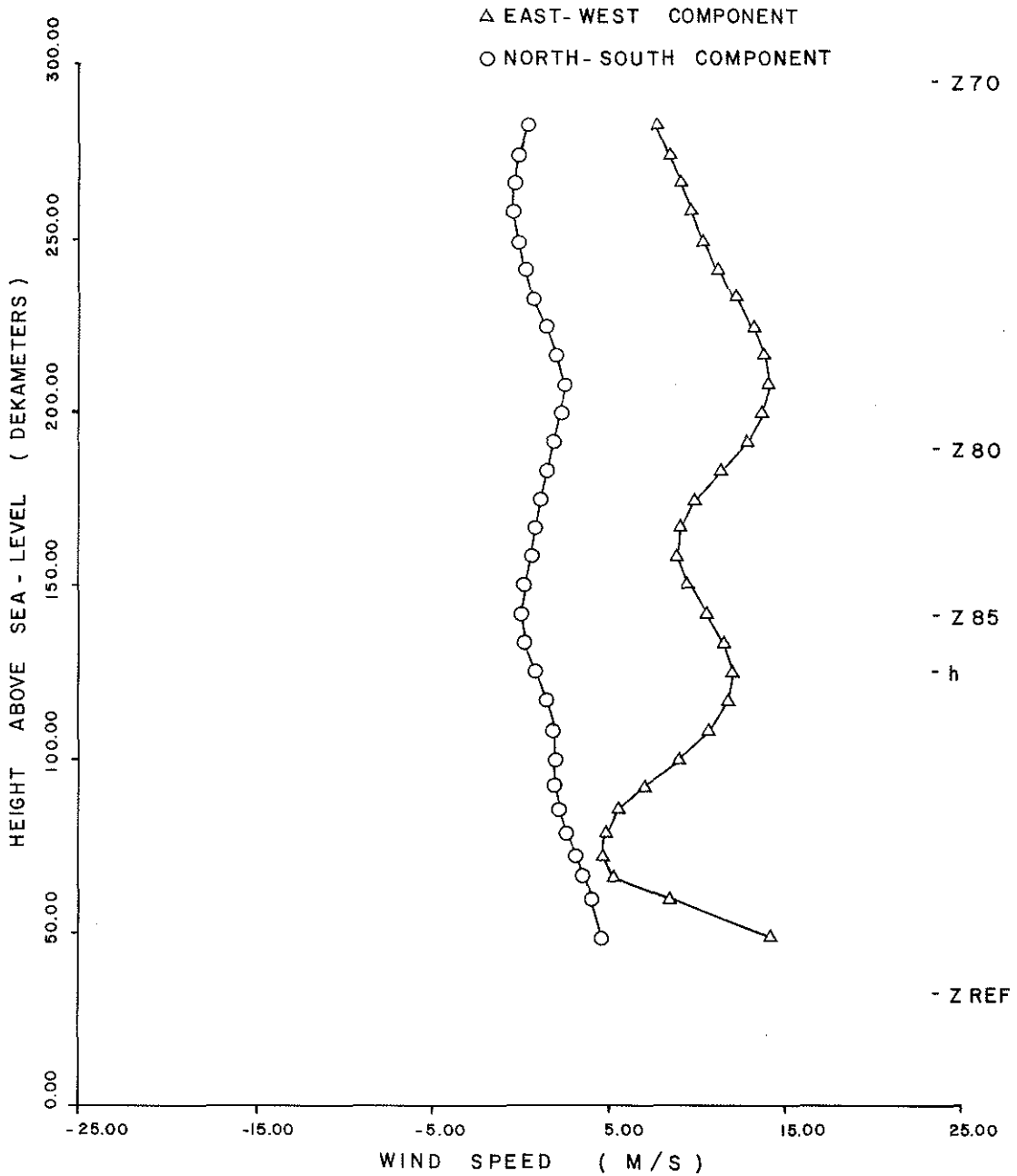


Figure 43. Profile of wind components at Mildred Lake for 1809 GMT 17 October 1977.

SYNCRUDE AIRSTRIP / OCT 23, 1977 / 0711 MST / 320.0M

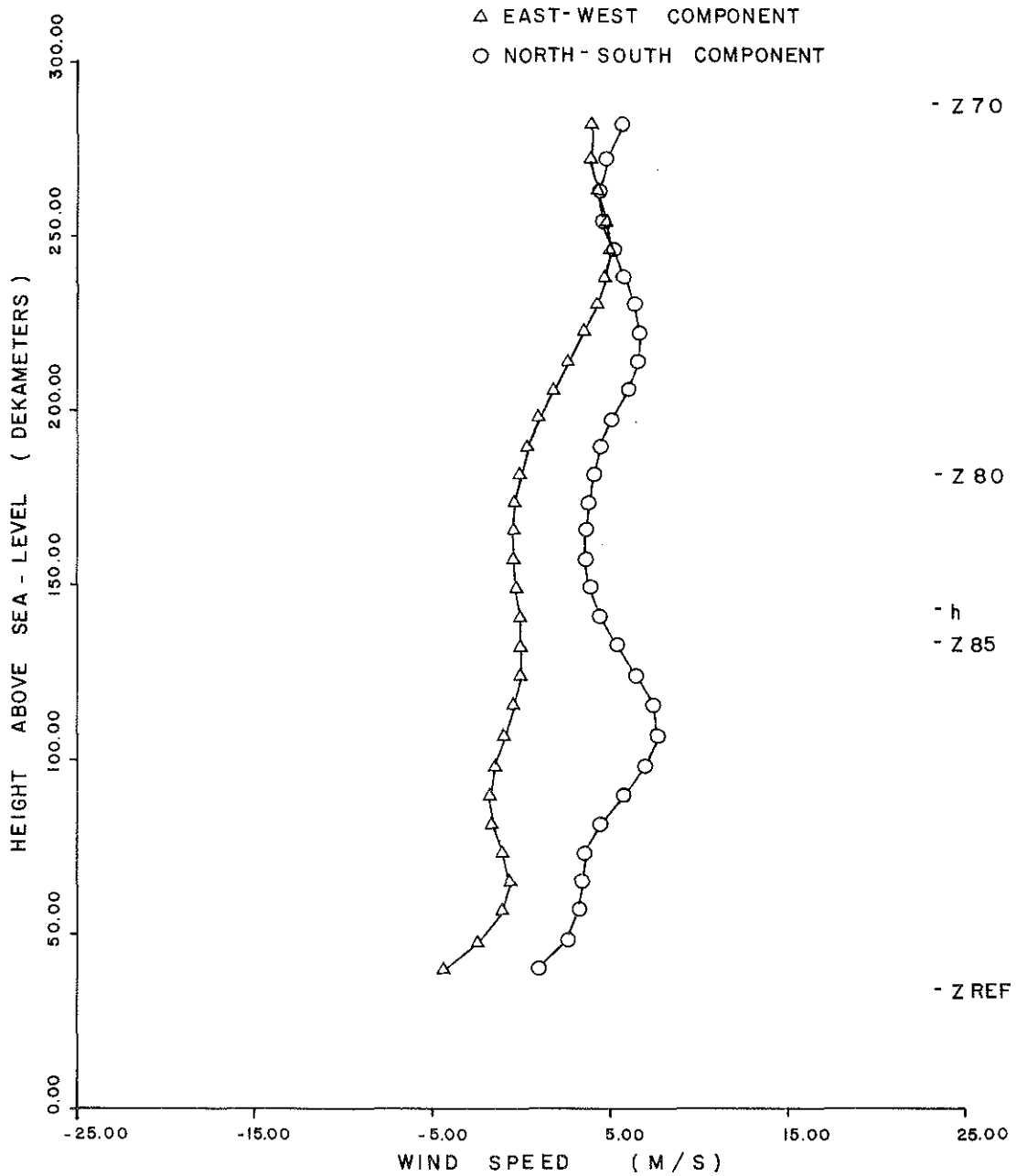


Figure 44. Profile of wind components at Mildred Lake for 1411 GMT 23 October 1977.

3.3 VERIFICATION OF RESULTS

Computed winds for the six cases studied are shown in Figures 44 to 49. In Figures 44 and 49 note that the cold air drainage winds reinforce the wind east of the Athabasca River and oppose the wind to the west. The reverse is true in Figure 47. Katabatic winds are also evident off the Birch Mountains in the northwest corner of the map in all cases with nocturnal inversions (Figures 44, 47, and 49). In the other three cases (Figures 45, 46, and 48), the Birch Mountains also affect the winds significantly. The channeling influences of the Athabasca River valley are not as great as might be expected although Figure 46 does show this effect south of Mildred Lake. Probably in most of the cases selected, thermal influences tend to be more important than purely orographic (adiabatic) effects.

The Mildred Lake model's performance is summarized in Tables 6 to 12. Tables 6 to 11 present reported and computed winds at the six stations. The average speeds (last line in the tables) are calculated for the same cases for both reported and computed winds. On the average, Thickwood Hills' speeds tend to be underestimated (Table 6) and Ells' overestimated (Table 10). It must be remembered, however, that the model's winds represent averages over 2.5 x 2.5 km grid squares, while reported winds are 1-min means for a point. The model cannot respond to local topographical effects about which it has no information.

Cases 4 to 6 in Table 11 for Fort McMurray may be compared to Cases 1 to 3 in Table 2 which are for the same times but using the Stoney Mountain model. The computed speeds are similar but there are differences in computed angles. The Mildred Lake model does better with Case 6 in Table 11 than the Stoney Mountain version does with Case 3 in Table 2. However, for the remaining two times, the Stoney Mountain model is superior.

Median absolute differences between computed and reported winds are presented in Table 12. Fiftieth percentiles for the magnitude of the speed and angle differences are 2.7 km/h and 19°, which are low values.

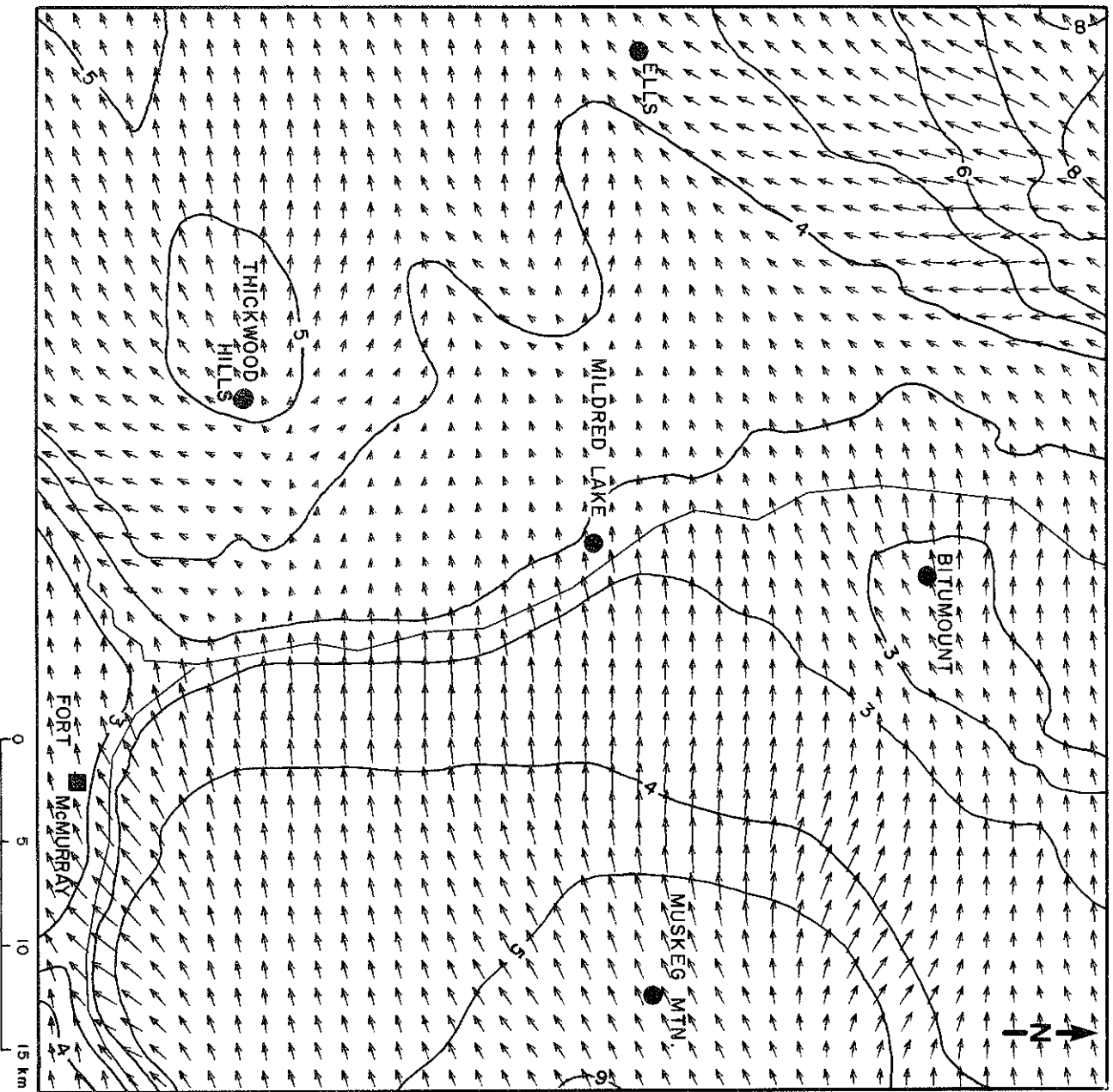


Figure 45. Winds computed by the Mildred Lake model for 1550 GMT 27 January 77. A vector of 1 cm length represents a wind of 70 km/h.

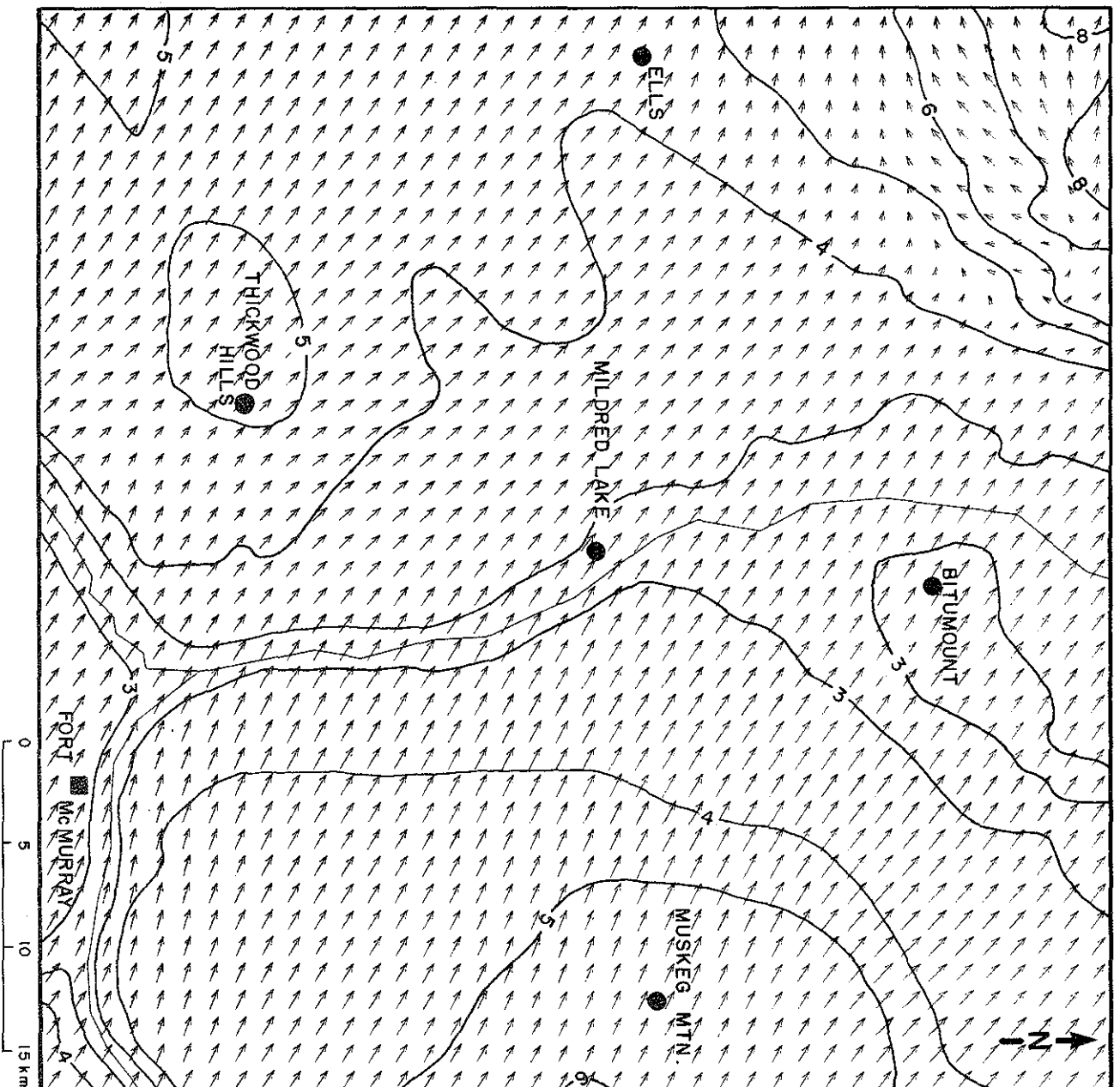


Figure 46. Winds computed by the Mildred Lake model for 2100 GMT 23 March 77. A vector of 1 cm length represents a wind of 65 km/h.

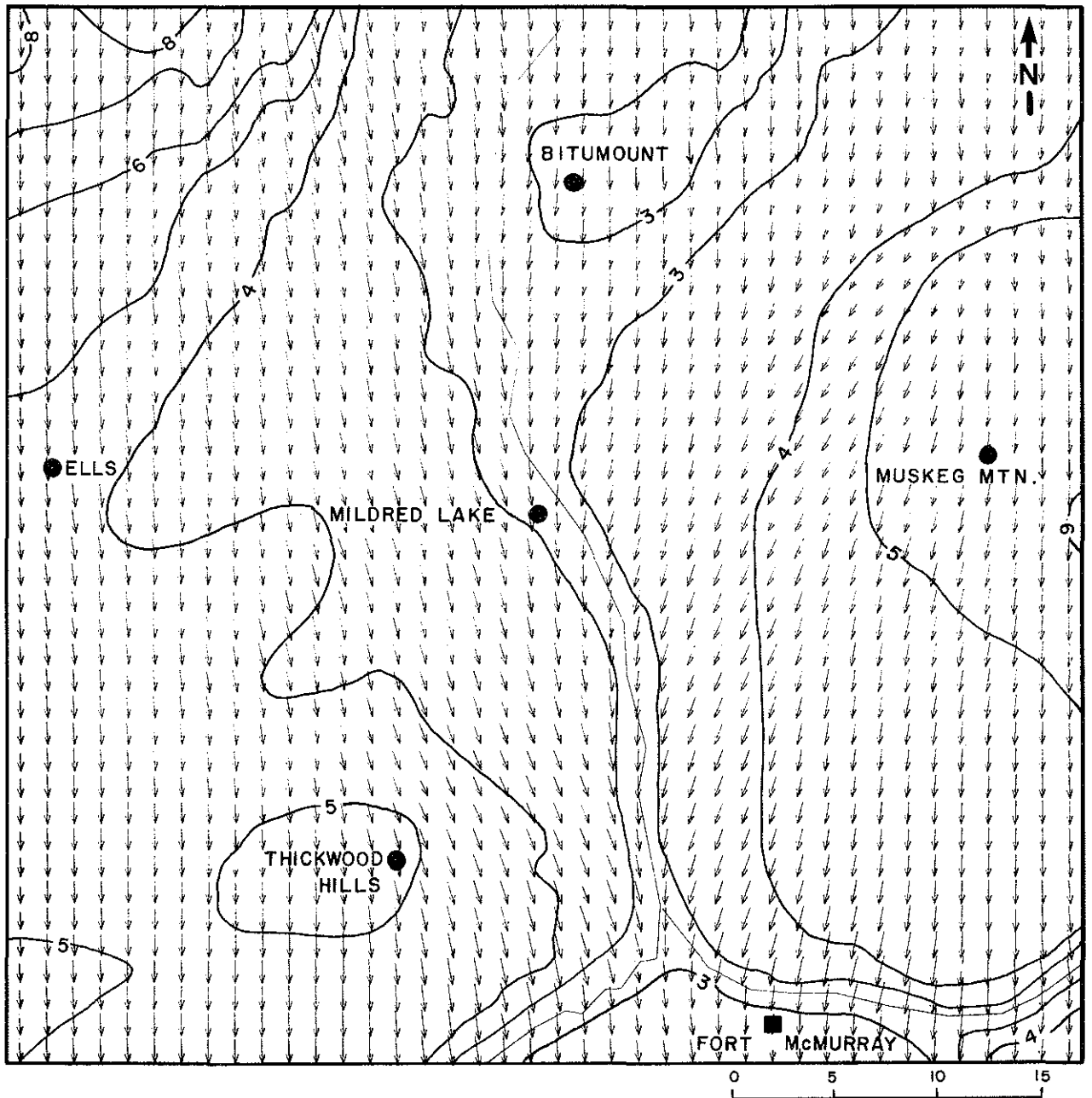


Figure 47. Winds computed by the Mildred Lake model for 14:35 GMT 12 July 77. A vector of 1 cm length represents a wind of 35 km/h.

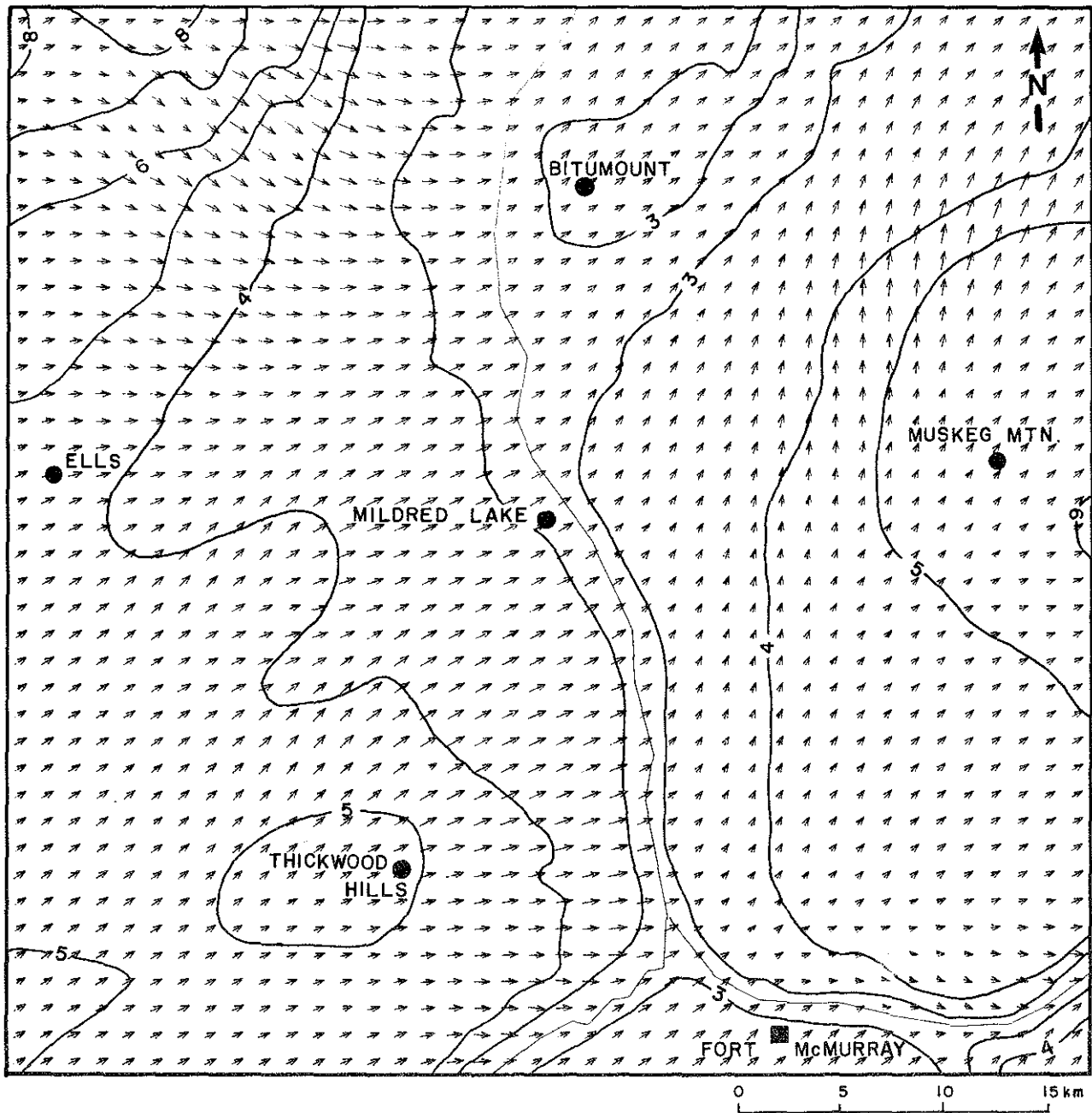


Figure 48. Winds computed by the Mildred Lake model for 1400 GMT 17 October 77. A vector of 1 cm length represents a wind of 65 km/h.

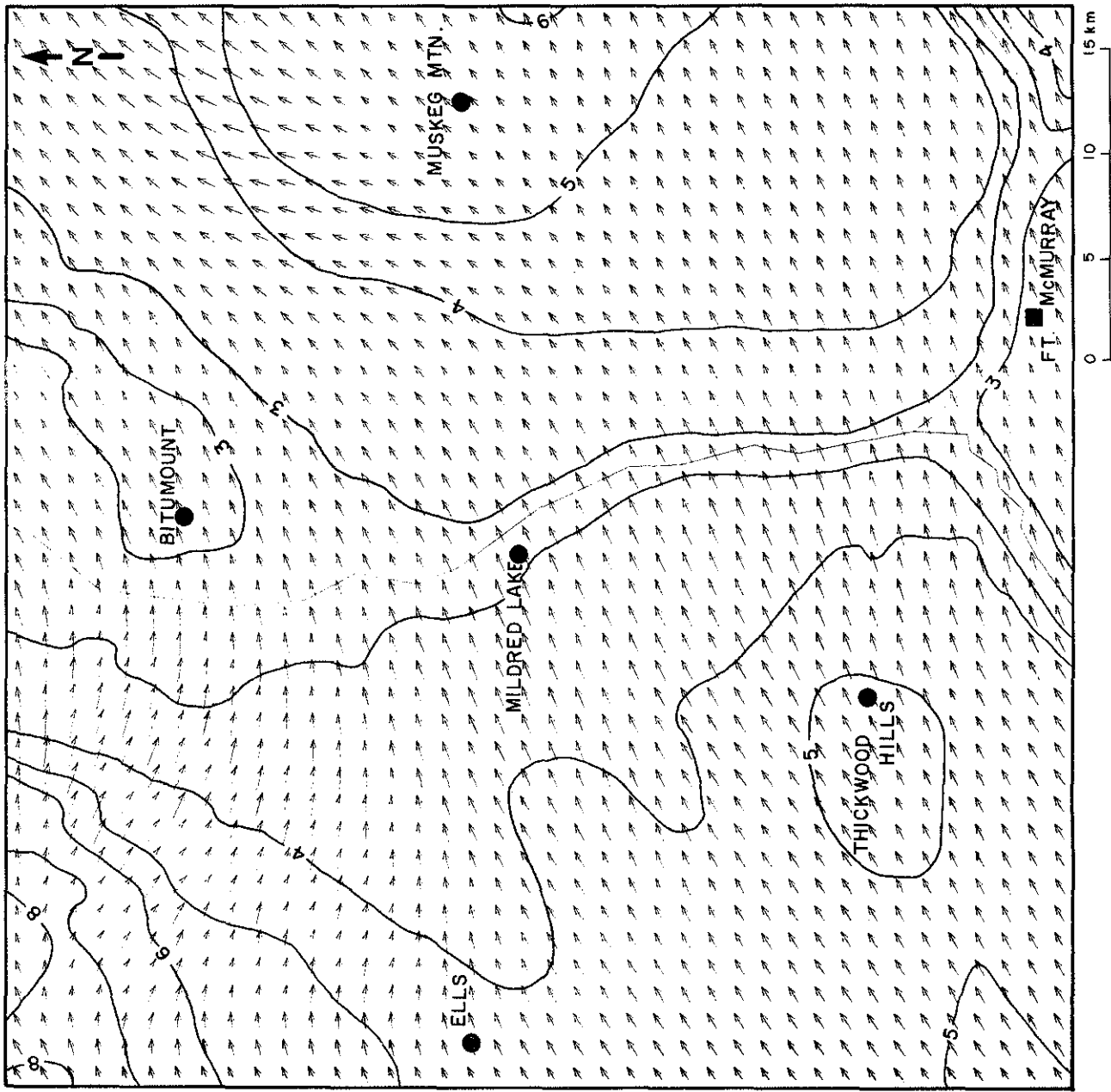


Figure 49. Winds computed by the Mildred Lake model for 1809 GMT 17 October 77. A vector of 1 cm length represents a wind of 60 km/h.

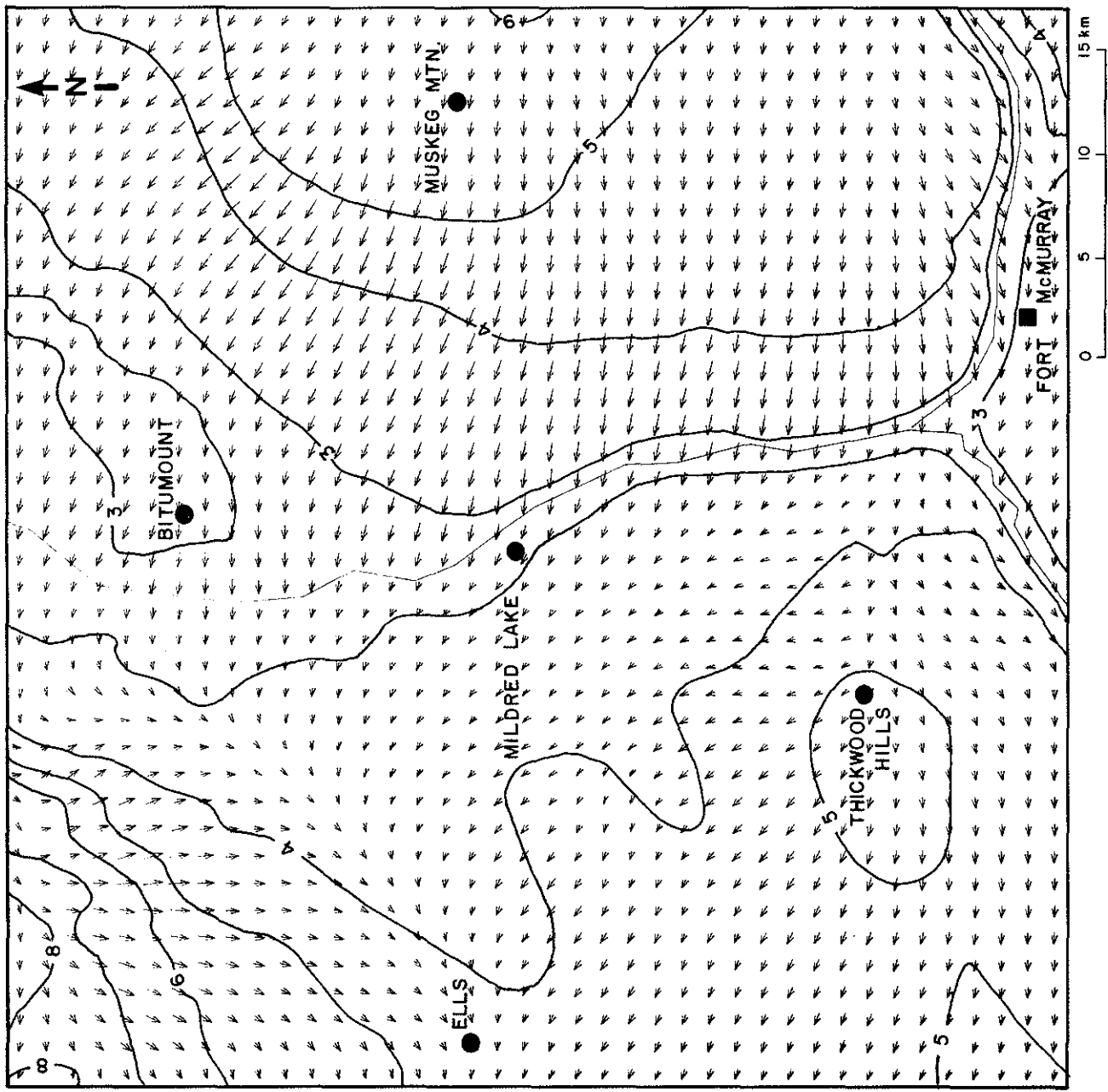


Figure 50. Winds computed by the Mildred Lake model for 1411 GMT 23 October 77. A vector of 1 cm length represents a wind of 65 km/h.

Table 6. Reported and Mildred Lake model computed winds at Thickwood Hills (km/h and degrees). See Table 5 for times of cases.

Case	Reported		Computed	
	Speed	Angle	Speed	Angle
1	*	360	18	340
2	30	110	16	060
3	*	*	8	350
4	12	*	10	240
5	13	*	14	230
6	8	180	8	200
Average	16		12	

* missing data

Table 7. Reported and Mildred Lake model computed winds at Mildred Lake (km/h and degrees). See Table 5 for times of cases.

Case	Reported		Computed	
	Speed	Angle	Speed	Angle
1	1	360	15	330
2	40	120	16	100
3	8	360	6	360
4	9	200	9	220
5	9	210	11	220
6	6	160	9	180
Average	12		11	

Table 8. Reported and Mildred Lake model computed winds at Muskeg Mountain (km/h and degrees). See Table 5 for times of cases.

Case	Reported		Computed	
	Speed	Angle	Speed	Angle
1	23	020	28	360
2	*	100	26	110
3	8	020	9	010
4	10	220	8	190
5	13	210	11	190
6	14	150	10	140
Average	13		15	

* missing data

Table 9. Reported and Mildred Lake model computed winds at Bitumont(km/h and degrees). See Table 5 for times of cases.

Case	Reported		Computed	
	Speed	Angle	Speed	Angle
1	0	*	14	360
2	8	110	16	090
3	9	010	6	010
4	8	210	5	190
5	9	210	8	210
6	6	200	6	120
Average	7		9	

* undefined

Table 10. Reported and Mildred Lake model computed winds at Ells (km/h and degrees). See Table 5 for times of cases.

Case	Reported		Computed	
	Speed	Angle	Speed	Angle
1	5	080	17	340
2	*	*	23	060
3	8	020	8	010
4	*	*	7	240
5	*	*	12	220
6	*	*	4	060
Average	7		12	

* missing data

Table 11. Reported and Mildred Lake model computed winds at Fort McMurray (km/h and degrees). See Table 5 for times of cases.

Case	Reported		Computed	
	Speed	Angle	Speed	Angle
1	6	350	17	350
2	21	130	18	090
3	4	030	6	020
4	6	240	8	210
5	15	260	10	220
6	7	120	8	140
Average	10		11	

Table 12. Median of the absolute value of the vector, speed, and angle differences between Mildred Lake model computed and reported winds for all stations (km/h and degrees).

Vector	Speed	Angle
4.1	2.7	19

4. MODEL SENSITIVITY AND APPLICATION TO OTHER AREAS

4.1 GENERAL GUIDELINES FOR NEW APPLICATIONS

Both the Stoney Mountain and Mildred Lake models are "tuned" in their present state. However, the Stoney Mountain model is designed for easy application elsewhere and some comments are in order concerning sensitivity of input parameters. The most critical quantities are the timestep, total adjustment time, and temperature change ΔT (used in Equation 5).

Timestep: Computational stability requires that the timestep (Δt) depend on the grid size (Δx). The following are approximate values:

Δx (km)	Δt (s)
1	20
2.5	40
5	75
10	150
20	200

Total adjustment time: This is approximately the time required for an air parcel moving with a characteristic speed (say, 10 m/s) to traverse a topographic control feature (e.g., width of a valley, mountain, or lake), or the model domain, whichever is less.

Surface, upper air, and water temperatures: It is important that ΔT (see Equation 4) not be excessively large or unrealistic thermal circulations will arise. As a safeguard, ΔT is constrained not to exceed 5°C in magnitude (in the Mildred Lake model), although this is rarely invoked since T_i is set equal to the daily mean temperature \bar{T} .

Geostrophic winds: These should be evaluated over a distance of the order of 500 km.

Planetary boundary layer heights: These are not too crucial. The pressure change in Equation 1 is directly proportional to H and the frictional force per unit mass in Equation 10 to c/h .

Terrain heights: These should be carefully calculated since it is the ready availability of small scale height variations which the model takes advantage of. In extremely rough terrain, it may be necessary to smooth the heights to reduce numerical instability but this should only be done as a last resort.

Water fraction of grid square: This is easily estimated from topographic maps. An accuracy to the nearest tenth is sufficient.

Drag coefficients: There is considerable variability of published values in the literature. It is often possible to make realistic assumptions such as Equation 13 to reduce systematic errors in winds. In the first version of the Mildred Lake model, the drag coefficient was constant with height and speeds at the lower elevations were over-estimated.

Eddy diffusivities: These values are not too critical although they should be in the range of 10^3 to $2 \times 10^4 \text{ m}^2 \cdot \text{s}^{-1}$. Excessively large values cause spurious cooling (and katabatic winds) over the highest terrain. In general, they should be reduced as the grid size decreases.

4.2 SENSITIVITY TESTS

In order to determine the sensitivity to changes in input data, the ten Stoney Mountain model cases were re-run perturbing, in turn, sea-level geostrophic wind angle (VGSLA) by 20° , sea-level pressure difference from which geostrophic wind is computed (DELP) by 2 mb, and 850 mb, initial and final temperatures (T85, TBAR and TREF) by 2°C each. The 850-mb geostrophic direction and speed were unchanged

so that the perturbation in surface geostrophic wind was less than at sea-level, particularly at higher elevations.

Results at Fort McMurray and Stoney Mountain are shown in Tables 13 to 16. The only significant speed changes in Table 13 and 14 occur when DELP is perturbed. Similarly, the direction is modified appreciably in Tables 15 and 16 only when VGSLA is perturbed. A meteorologist is normally aware when the geostrophic wind is dubious. Thus the model is not overly sensitive to uncertainties in input data. This conclusion could also have been obtained from Table 4, since small errors would not otherwise have been possible.

Table 13. Sensitivity of wind speed (km/h) to changes in input data, computed at Fort McMurray by the Stoney Mountain model.

Case	Perturbation					
	None	VGSLA 20 ^o	DELP 2 mb	T85 2 C	TBAR 2 C	TREF 2 C
1	9	9	11	9	10	9
2	11	11	13	10	10	13
3	8	8	9	8	9	8
4	13	14	16	13	13	15
5	21	20	24	20	19	23
6	17	17	20	17	15	19
7	11	11	18	9	10	15
8	11	11	17	11	11	13
9	15	15	20	14	14	19
10	15	15	20	13	19	18
Average	13	13	16	12	13	15

Table 14. Sensitivity of wind speed (km/h) to changes in input data, computed at Stoney Mountain by the Stoney Mountain model.

Case	Perturbation					
	None	VGSLA 20 ^o	DELP 2 mb	T85 2 C	TBAR 2 C	TREF 2 C
1	15	14	17	14	15	15
2	17	17	20	16	16	20
3	14	14	15	14	15	14
4	22	23	25	21	20	25
5	33	33	38	32	31	37
6	27	26	30	26	25	30
7	14	13	20	12	12	19
8	16	15	24	16	16	18
9	21	20	26	20	18	25
10	16	14	26	17	20	20
Average	19	18	24	18	18	22

Table 15. Sensitivity of wind angle ($^{\circ}$) to changes in input data, computed at Fort McMurray by the Stoney Mountain model.

Case	Perturbation					
	None	VGSLA 20 $^{\circ}$	DELP 2 mb	T85 2 C	TBAR 2 C	TREF 2 C
1	238	252	241	238	233	245
2	249	265	248	249	245	256
3	199	211	199	199	199	200
4	185	204	184	184	182	188
5	121	137	122	120	123	120
6	141	158	142	141	139	140
7	358	013	360	355	356	003
8	294	312	297	294	287	299
9	315	331	314	314	310	320
10	142	162	142	136	149	146

Table 16. Sensitivity of wind angle ($^{\circ}$) to changes in input data, computed at Stoney Mountain by the Stoney Mountain model.

Case	Perturbation					
	None	VGSLA 20 $^{\circ}$	DELP 2 mb	T85 2 C	TBAR 2 C	TREF 2 C
1	239	246	244	238	233	246
2	256	266	256	255	248	265
3	205	212	206	205	204	206
4	204	216	202	203	200	207
5	128	140	130	128	129	129
6	146	158	147	145	149	146
7	350	002	359	347	349	356
8	287	300	294	285	281	295
9	317	332	316	315	310	327
10	126	156	152	141	152	139

5. CONCLUSIONS AND RECOMMENDATIONS

This report has been concerned with the application of mesoscale wind model to northeastern Alberta. Two versions have been designed. In the Stoney Mountain model, the geostrophic wind is obtained directly from AES charts. In the Mildred Lake version, geostrophic winds are inferred by downward extrapolation of free-atmosphere winds. In the Stoney Mountain model, semi-empirical formulas are used to obtain boundary layer heights. In the Mildred Lake version, they are observed directly from upper air winds and temperatures measured by minisondes.

By comparing Tables 4 and 12, one might be tempted to conclude that the Stoney Mountain model is just as good as the Mildred Lake version. If this were true, a possible reason may be sensitivity to errors in minisonde winds. This could be alleviated by further smoothing these winds. However, the cases studied by the two models were not the same. Moreover, the free-atmosphere winds contain effects such as centripetal and isallobaric accelerations. These influence surface winds and are not readily obtainable from AES charts. Thus, the Mildred Lake model should in principle be superior to the Stoney Mountain version.

The model probably works best when orographic effects are important (variable terrain and/or moderate or strong winds). Less satisfactory performance is likely when thermal circulations are dominant.

The use of Monin-Obukhov similarity theory could improve the inclusion of effects of stability on the drag coefficient and angle between the surface and frictional force per unit mass. However, it would be necessary to solve the surface heat balance equation. Prognostic equations for the boundary layer heights could also be employed.

6. REFERENCES CITED

- Banke, E.G. and S.D. Smith. 1971. Wind stress over ice and over water in Beaufort Sea. *J. Geophys. Res.* 76, 7368-7374.
- Danard, M.B. 1977. A simple model for mesoscale effects of topography on surface winds. *Mon. Wea. Rev.* 105, 572-581.
- Danard, M.B., M. Gray, and G. Lyv. in prep. A mesoscale model for surface winds in the Alberta tar sands area. Prep. for Alberta Environment, Pollution Control and Research Management Divisions. March 1981.
- Deardorff, J.W. 1972. Parametization of the planetary boundary layer for use in general circulation models. *Mon. Wea. Rev.* 100, 93-106.
- Haltiner, G.J. and F.L. Martin. 1957. *Dynamical and physical meteorology*. McGraw-Hill. 470 pp.
- Hanna, S.R. 1969. The thickness of the planetary boundary layer. *Atmos. Environ.* 3, 519-536.
- Laikhtman, D.L. 1961. *Physics of the boundary layer of the atmosphere*. Israel program for Scientific Translations. Jerusalem, 1964, 200 pp.
- Phillips, N.A. 1957. A coordinate system having some special advantages for numerical forecasting. *J. Meteor.*, 14, 184-185.
- Smith, S.D. 1980. Wind stress and heat flux over the ocean in gale force winds. *J. Phys. Ocean.*, 10, 709-726.

7. LIST OF AOSERP RESEARCH REPORTS

1. AOSERP first annual report, 1975.
2. Walleye and goldeye fisheries investigations in the Peace-Athabasca Delta--1975.
3. Structure of a traditional baseline data system. 1976.
4. A preliminary vegetation survey of the AOSERP study area. 1976.
5. The evaluation of wastewaters from an oil sand extraction plant. 1976.
6. Housing for the north--the stackwall system; construction report--Mildred Lake tank and pump house. 1976.
7. A synopsis of the physical and biological limnology and fishery programs within the Alberta oil sands area. 1977.
8. The impact of saline waters upon freshwater biota (a literature review and bibliography). 1977.
9. A preliminary investigation into the magnitude of fog occurrence and associated problems oil sands area. 1977.
10. Development of a research design related to archaeological studies in the Athabasca oil sands area. 1977.
11. Life cycles of some common aquatic insects of the Athabasca River, Alberta. 1977.
12. Very high resolution meteorological satellite study of oil sands weather: "a feasibility study". 1977.
13. Plume dispersion measurements from an oil sands extraction plant, March 1976.
- 14.
15. A climatology of low-level air trajectories in the Alberta oil sands area. 1977.
16. The feasibility of a weather radar near Fort McMurray, Alberta. 1977.
17. A survey of baseline levels of contaminants in aquatic biota of the AOSERP study area. 1977.
18. Interim compilation of stream gauging data to December 1976 for AOSERP. 1977.
19. Calculations of annual averaged sulphur dioxide concentrations at ground level in the AOSERP study area. 1977.
20. Characterization of organic constituents in waters and wastewaters of the Athabasca oil sands mining area. 1978.

21. AOSERP second annual report, 1976-77.
22. AOSERP interim report covering the period April 1975 to November 1978.
23. Acute lethality of mine depressurization water to trout-perch and rainbow trout: Volume 1: 1979.
24. Air system winter field study in the AOSERP study area, February 1977.
25. Review of pollutant transformation processes relevant to the Alberta oil sands area. 1977.
26. Interim report on an intensive study of the fish fauna of the Muskeg River watershed of northeastern Alberta. 1977.
27. Meteorology and air quality winter field study in the AOSERP study area, March 1976.
28. Interim report on a soils inventory in the Athabasca oil sands area. 1978.
29. An inventory system for atmospheric emissions in the AOSERP study area. 1978.
30. Ambient air quality in the AOSERP study area, 1977.
31. Ecological habitat mapping of the AOSERP study area: Phase 1. 1978.
32. AOSERP third annual report, 1977-78.
33. Relationships between habitats, forages, and carrying capacity of moose range in northern Alberta. Part 1: moose preferences for habitat strata and forages. 1978.
34. Heavy metals in bottom sediments of the mainstem Athabasca River system in the AOSERP study area. 1978.
35. The effects of sedimentation on the aquatic biota. 1978.
36. Fall fisheries investigations in the Athabasca and Clearwater rivers upstream of Fort McMurray: Volume 1. 1978.
37. Community studies: Fort McMurray, Anzac, Fort MacKay. 1978.
38. Techniques for the control of small mammal damage to plants: a review. 1979.
39. The climatology of the AOSERP study area. 1979.
40. Mixing characteristics of the Athabasca River below Fort McMurray--winter conditions. 1979.
41. Acute and chronic toxicity of vanadium to fish. 1978.
42. Analysis of fur production records for registered traplines in the AOSERP study area, 1970-75.

43. A socio-economic evaluation of the recreational use of fish and wildlife resources in Alberta, with particular reference to the AOSERP study area. Vol. 1: summary and conclusions. 1979.
44. Interim report on symptomology and threshold levels of air pollutant injury to vegetation, 1975 to 1978.
45. Interim report on physiology and mechanisms of air-borne pollutant injury to vegetation, 1975 to 1978.
46. Interim report on ecological benchmarking and biomonitoring for detection of air-borne pollutant effects on vegetation and soils, 1975 to 1978.
47. A visibility bias model for aerial surveys of moose in the AOSERP study area. 1979.
48. Interim report on a hydrogeological investigation of the Muskeg River basin, Alberta. 1979.
49. The ecology of macrobenthic invertebrate communities in Harley Creek, northeastern Alberta.
50. Literature review on pollution deposition processes. 1979.
51. Interim compilation of 1976 suspended sediment data for the AOSERP study area. 1979.
52. Plume dispersion measurements from an oil sands extraction plant, June 1977.
53. Baseline states of organic constituents in the Athabasca River System upstream of Fort McMurray. 1979.
54. A preliminary study of chemical and microbial characteristics of the Athabasca River in the Athabasca oil sands area of northeastern Alberta. 1979.
55. Microbial populations in the Athabasca River. 1979.
56. The acute toxicity of saline groundwater and of vanadium to fish and aquatic invertebrates. 1979.
57. Ecological habitat mapping of the AOSERP study area (supplement): Phase I. 1979.
58. Interim report on ecological studies on the lower trophic levels of Muskeg rivers within the AOSERP study area. 1979.
59. Semi-aquatic mammals: annotated bibliography. 1979.
60. Synthesis of surface water hydrology. 1979.
61. An intensive study of the fish fauna of the Steepbank River watershed of northeastern Alberta. 1979.
62. Amphibians and reptiles in the AOSERP study area. 1979.

63. Analysis of AOSERP plume sigma data. 1979.
64. A review and assessment of the baseline data relevant to the impacts of oil sands developments on large mammals in the AOSERP study area. 1979.
65. A review and assessment of the baseline data relevant to the impacts of oil sands development on black bear in the AOSERP study area. 1979.
66. An assessment of the models LIRAQ and ADPIC for application to the Alberta oil sands area. 1979.
67. Aquatic biological investigations of the Muskeg River watershed. 1979.
68. Air system summer field study in the AOSERP study area, June 1977.
69. Native employment patterns in Alberta's Athabasca oil sands region. 1979.
70. An interim report on the insectivorous animals in the AOSERP study area.
71. Lake acidification potential in the AOSERP study area. 1979.
72. The ecology of five major species of small mammals in the AOSERP study area: a review. 1979.
73. Distribution, abundance, and habitat associations of beavers, muskrats, mink, and river otters in the AOSERP study area, northeastern Alberta. 1979.
74. Air quality modelling and user needs. 1979.
75. Interim report on a comparative study of benthic algal primary productivity in the AOSERP study area. 1979.
76. An intensive study of the fish fauna of the Muskeg River watershed of northeastern Alberta. 1979.
77. Overview of local economic development in the Athabasca oil sands region since 1961. 1979.
78. Habitat relationships and management of terrestrial birds in northeastern Alberta. 1979.
79. The multiple toxicity of vanadium, nickel, and phenol to fish. 1979.
80. History of the Athabasca oil sands region, 1890 to 1960's. Volume I: socio-economic developments. Volume II: oral history. 1980.
81. Species distribution and habitat relationships of waterfowl in northeastern Alberta. 1979.

82. Breeding distribution and behaviour of the White Pelican in the Athabasca oil sands area. 1979.
83. The distribution, foraging behaviour and allied activities of the White Pelican in the Athabasca oil sands area. 1979.
84. Investigations of the spring spawning fish populations in the Athabasca and Clearwater rivers upstream from Fort McMurray: Volume I. 1979.
85. An intensive surface water quality study of the Muskeg River watershed. Volume I: water chemistry. 1979.
86. An observational study of fog in the AOSERP study area. 1979.
87. Hydrogeological investigation of Muskeg River basin, Alberta. 1980.
88. Ecological studies of the aquatic invertebrates of the AOSERP study area of northeastern Alberta. 1980.
89. Fishery resources of the Athabasca River downstream of Fort McMurray, Alberta: Volume I. 1980.
90. A wintertime investigation of the deposition of pollutants around an isolated power plant in northern Alberta. 1980.
91. Characterization of stored peat in the Alberta oil sands area. 1980.
92. Fisheries and habitat investigations of tributary streams in the southern portion of the AOSERP study area. Volume I: summary and conclusions. 1980.
93. Fisheries and aquatic habitat investigations in the MacKay River watershed of northeastern Alberta. 1980.
94. A fisheries and water quality survey of ten lakes in the Richardson Tower area, northeastern Alberta. Volume I: methodology, summary, and discussion. 1980.
95. Evaluation of the effects of convection on plume behaviour in AOSERP study area. 1980.
96. Service delivery in the Athabasca oil sands region since 1961. 1980.
97. Differences in the composition of soils under open and canopy conditions at two sites close-in to the Great Canadian Oil Sands operation, Fort McMurray, Alberta. 1980.
98. Baseline condition of jack pine biomonitoring plots in the Athabasca oil sands area: 1976-1977.
99. Synecology and autecology of boreal forest vegetation in the AOSERP study area. 1980.

100. Baseline inventory of aquatic macrophyte species distributions in the AOSERP study area. 1980.
101. Woodland caribou population dynamics in northeastern Alberta. 1980.
102. Wolf population dynamics and prey relationships in northeastern Alberta.
103. Analysis of the leisure delivery system 1972-1979, with projections for future servicing requirements.
104. Review of requirements for air quality simulation models. 1980.
105. Approaches to the design of a biomonitoring program using arthropods as bioindicators for the AOSERP study area. 1980.
106. Meteorological factors affecting ambient SO₂ concentrations near an oil sands extraction plant. 1980.
107. Small mammal populations of northeastern Alberta. Volume I: populations in natural habitats. 1980.
108. Small mammal populations of northeastern Alberta. Volume II: populations in reclamation areas. 1980.
109. Symptomology and threshold levels of air pollutant injury to vegetation, 1979-1980.
110. Physiology and mechanisms of airborne pollutant injury to vegetation, 1979-1980.
111. Ecological benchmarking and biomonitoring for detection of airborne pollutant effects on vegetation and soils. 1980.
112. A study of human adjustment in Fort McMurray. Volume I: field study and results. 1980.
113. A laboratory study of long-term effects of mine depressurization groundwater on fish and invertebrates. 1980.
114. Aquatic biophysical inventory of major tributaries in the AOSERP study area. Volume I: summary report. 1980.
115. Report on an ecological survey of terrestrial insect communities in the AOSERP study area. 1980.
116. An assessment of benthic secondary production in the Muskeg River of northeastern Alberta. 1980.
117. Development of a chemically reactive plume model for application in the AOSERP study area. 1981.
118. Alberta Oil Sands Environmental Research Program, 1975-1980. A summary report. 1981.

119. Airshed management system for the Alberta oil sands.
Volume I: A Gaussian frequency distribution model. 1981.
120. Airshed management system for the Alberta oil sands.
Volume II: meteorological data.
121. The metabolism of selected organic compounds by micro-organisms in the Athabasca River.
122. Soils inventory of the AOSERP study area. in prep.
123. Circulation of water and sediment in the Athabasca delta area. 1981.
124. Airshed management system for the Alberta oil sands.
Volume III: validation and sensitivity studies.
125. The 1981 snowpack survey in the AOSERP study area. 1981.

This material is provided under educational reproduction permissions included in Alberta Environment's Copyright and Disclosure Statement, see terms at <http://www.environment.alberta.ca/copyright.html>. This Statement requires the following identification:

"The source of the materials is Alberta Environment <http://www.environment.gov.ab.ca/>. The use of these materials by the end user is done without any affiliation with or endorsement by the Government of Alberta. Reliance upon the end user's use of these materials is at the risk of the end user.